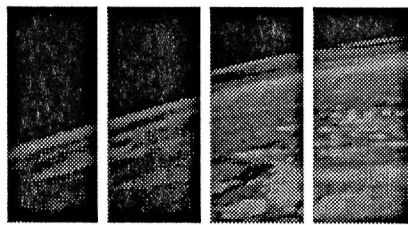
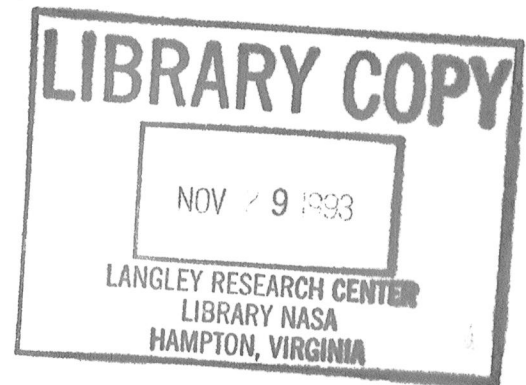


WORKSHOP ON ATMOSPHERIC TRANSPORT ON MARS



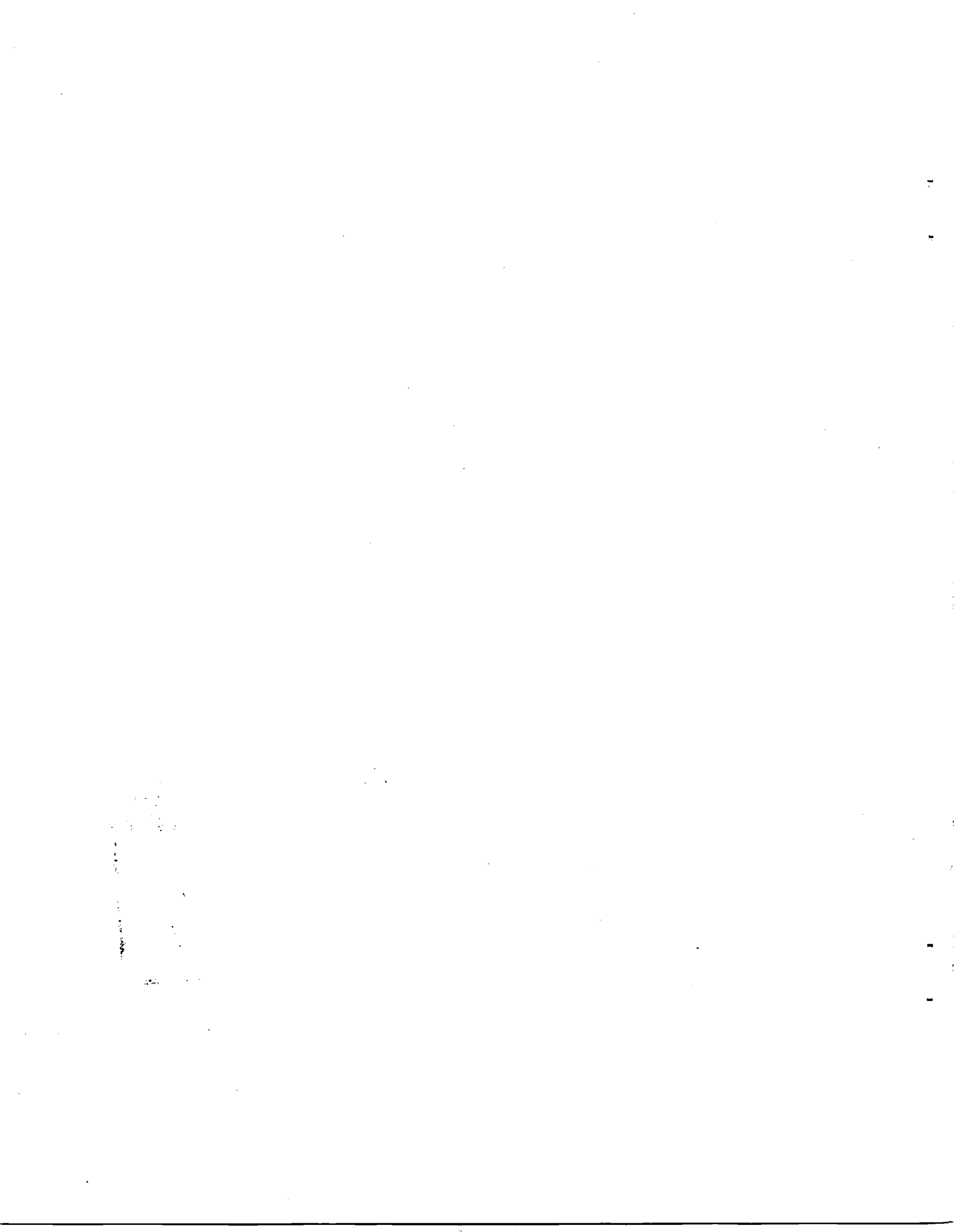
MSATT

Mars Surface and Atmosphere Through Time



LPI Technical Report Number 93-05

Lunar and Planetary Institute 3600 Bay Area Boulevard Houston TX 77058-1113
LPI/TR--93-05



DISPLAY 05/6/1

94N24871*f ISSUE 6 PAGE 2616 CATEGORY 91

RPT#: NASA-CR-194855 NAS 1.26:194855 LPI-TR-93-05 CNT#: NASW-4574

93/00/00 52 PAGES UNCLASSIFIED DOCUMENT

UTTL: Workshop on Atmospheric Transport on Mars

AUTH: A/BARNES, J. R.; B/HABERLE, R. M. PAT: A/ed.; B/ed.

CORP: Lunar and Planetary Inst., Houston, TX.

SAP: Avail: CASI HC A04/MF A01

CIO: UNITED STATES Workshop held in Corvallis, OR, 28-30 Jun. 1993; sponsored by Oregon State Univ. and Oregon Space Grant Consortium

MAJS: /*ATMOSPHERIC CIRCULATION/*ATMOSPHERIC MODELS/*MARS ATMOSPHERE/*PLANETARY METEOROLOGY

MINS: / ATMOSPHERIC CHEMISTRY/ ATMOSPHERIC COMPOSITION/ ATMOSPHERIC PHYSICS/ DUST STORMS/ WIND (METEOROLOGY)

ANN: On June 28-30, 1993, the Workshop on Atmospheric Transport on Mars was held in Corvallis, Oregon. The workshop was organized under the auspices of the MSATT (Mars Surface and Atmosphere Through Time) Program of NASA, and was jointly sponsored by the Lunar and Planetary Institute, Oregon State University, and the Oregon Space Grant Consortium. More than 50 scientists attended the workshop, which was the first such meeting to focus upon circulation processes in the Mars atmosphere. The timing of the workshop placed it almost on the eve of the arrival of Mars Observer at Mars, so that the presented papers gave a picture of the 'state of the

ENTER:

MORE



**WORKSHOP ON
ATMOSPHERIC TRANSPORT ON MARS**

Edited by

J. R. Barnes and R. M. Haberle

Held in
Corvallis, Oregon

June 28-30, 1993

Sponsored by
Lunar and Planetary Institute
Oregon State University and the Oregon Space Grant Consortium
MSATT Study Group

Lunar and Planetary Institute 3600 Bay Area Boulevard Houston TX 77058-1113

LPI Technical Report Number 93-05
LPI/TR--93-05

N94-24871#

Compiled in 1993 by
LUNAR AND PLANETARY INSTITUTE

The Institute is operated by the University Space Research Association under Contract No. NASW-4574 with the National Aeronautics and Space Administration.

Material in this volume may be copied without restraint for library, abstract service, education, or personal research purposes; however, republication of any paper or portion thereof requires the written permission of the authors as well as the appropriate acknowledgment of this publication.

This report may be cited as

Barnes J. R. and Haberle R. M.. eds. (1993) *Workshop on Atmospheric Transport on Mars*. LPI Tech. Rpt. 93-05, Lunar and Planetary Institute, Houston. 46 pp.

This report is distributed by

ORDER DEPARTMENT
Lunar and Planetary Institute
3600 Bay Area Boulevard
Houston TX 77058-1113

Mail order requestors will be invoiced for the cost of shipping and handling.

Preface

On June 28–30, 1993, the Workshop on Atmospheric Transport on Mars was held in Corvallis, Oregon. The workshop was organized under the auspices of the MSATT (Mars Surface and Atmosphere Through Time) Program of NASA, and was jointly sponsored by the Lunar and Planetary Institute, Oregon State University, and the Oregon Space Grant Consortium. More than 50 scientists (including a number from Europe) attended the workshop, which was the first such meeting to focus upon circulation processes in the Mars atmosphere. The timing of the workshop placed it almost on the eve of the arrival of Mars Observer at Mars, so that the presented papers gave a picture of the “state of the art” in Mars atmospheric science just prior to the expected arrival of new data. (Unfortunately, the loss of Mars Observer has now pushed the expected acquisition of such data at least several years into the future.) The workshop highlighted a host of recent advances in atmospheric modeling and analysis—advances that will be relevant to any future observations.



Contents

Summary of Technical Sessions	1
Abstracts	5
<i>The NASA/GISS Mars General Circulation Model: Preliminary Experiments</i> M. Allison, M. A. Chandler, A. D. Del Genio, A. Lacis, D. Rind, W. B. Rossow, L. D. Travis, and W. Zhou	5
<i>Optimal Gains for a Single Polar Orbiting Satellite</i> D. Banfield, A. P. Ingersoll, and C. Keppenne	5
<i>A Diagnostic Model to Estimate Winds and Small-scale Drag from Mars Observer PMIRR Data</i> J. R. Barnes	6
<i>Eddy Mixing Coefficient Values Derived from Simulations with the NASA Ames Mars GCM</i> J. R. Barnes and T. Walsh	6
<i>Mars Dust-driven Tides and Their Impact on the Thermosphere</i> S. W. Bougher and R. W. Zurek	7
<i>Cloud, Dust, and Ozone Vertical Profiles from Solar Occultation Measurements: Implications for Dynamics</i> E. Chassefière and J. E. Blamont	9
<i>Particle Sizes and Composition of Mars Atmospheric Dust Based Upon Viking and Mariner 9 Observations</i> R. T. Clancy, S. W. Lee, and G. R. Gladstone	10
<i>Aspects of the Martian Global Circulation</i> M. Collins and I. N. James	11
<i>Impact of the CO₂ and H₂O Clouds of the Martian Polar Hood on the Polar Energy Balance</i> F. Forget and J. B. Pollack	13
<i>Multiannual Simulations with the Mars Climate Model</i> R. M. Haberle, H. C. Houben, and R. E. Young	14
<i>Regarding Tracer Transport in Mars' Winter Atmosphere in the Presence of Nearly Stationary, Forced Planetary Waves</i> J. L. Hollingsworth, R. M. Haberle, and H. C. Houben	14

<i>Analyzing Martian Winds and Tracer Concentrations Using Mars Observer Data</i> H. Houben	15
<i>The Annual Pressure Cycle on Mars: Results from the LMD Martian Atmospheric General Circulation Model</i> F. Hourdin, F. Forget, and O. Talagrand	16
<i>Northern Hemisphere Dust Storms on Mars</i> P. B. James	17
<i>The Influence of Orography on the Transport of Atmospheric Constituents</i> M. M. Joshi, S. R. Lewis, and P. L. Read	18
<i>Temporal and Spatial Mapping of Surface Albedo and Atmospheric Dust Opacity on Mars</i> S. W. Lee, R. T. Clancy, and G. R. Gladstone	19
<i>Dynamics of the Atmosphere of Mars: Review of Some Outstanding Problems</i> C. B. Leovy	19
<i>Modeling and Data Assimilation for Mars Observer</i> S. R. Lewis and P. L. Read	19
<i>Mars Operational Environmental Satellite (MOES)—A Post-Mars Observer Discovery Mission</i> S. S. Limaye	21
<i>A Study of Cloud Motions on Mars, II: Some Examples of Observations and Analyses Since 1969</i> L. J. Martin	22
<i>Evidence for Dust Transport in Viking IR Thermal Mapper Opacity Data</i> T. Z. Martin	23
<i>Retrieval of Temperature Profiles from Martian Infrared Spectra</i> W. W. McMillan, J. C. Pearl, and B. J. Conrath	24
<i>Dust Transport in the Martian Atmosphere</i> J. R. Murphy	25
<i>Three-Dimensional Numerical Simulation of Near-Surface Flows Over the Martian North Polar Cap</i> T. R. Parish and A. D. Howard	27
<i>The Role of Atmosphere Heat Transport in the Seasonal Carbon Dioxide Cycle</i> J. B. Pollack, R. M. Haberle, J. R. Murphy, J. Schaeffer, and H. Lee	30

<i>Eddy Mixing Coefficient Upper Limit Derived from the Photochemical Balance of O₂</i> J. Rosenqvist and E. Chassefiere	30
<i>Diagnostic Calculations of the Circulation in the Martian Atmosphere</i> M. Santee and D. Crisp	32
<i>Martian Mesoscale Circulations Induced by Variations in Surface Optical and Thermal Characteristics: A Numerical Study</i> T. Siili and H. Savijarvi	33
<i>Two-Dimensional Modeling of Thermal Inversion Layers in the Middle Atmosphere of Mars</i> B. Théodore and E. Chassefière	35
<i>Three-Dimensional Numerical Simulation of Thermal Tides in the Martian Atmosphere</i> R. J. Wilson	37
<i>Vertical Transport of Water in the Martian Boundary Layer</i> A. P. Zent, R. M. Haberle, and H. C. Houben	39
<i>The Mars Aerial Platform (MAP) Mission</i> R. Zubrin, S. Price, T. Gamber, B. Clark, R. Haberle, and J. Cantrell	40
<i>Mars Observer: Applications to Atmospheric Transport</i> R. W. Zurek and D. J. McCleese	42
List of Workshop Participants	43

The first part of the document discusses the importance of maintaining accurate records of all transactions. It emphasizes that every entry should be supported by a valid receipt or invoice. This not only helps in tracking expenses but also ensures compliance with tax regulations. The document further outlines the process of reconciling bank statements with the company's ledger to identify any discrepancies. It suggests that regular reconciliations can help in detecting errors or fraud early on. Additionally, it provides guidelines on how to handle missing receipts, such as using a receipt book or a digital receipt system. The second part of the document focuses on budgeting and financial forecasting. It explains how to create a realistic budget based on historical data and current market conditions. It also discusses the importance of monitoring the budget regularly and making adjustments as needed. The document concludes by highlighting the benefits of good financial management, such as improved cash flow and better decision-making. It encourages the reader to adopt these practices to ensure the long-term success of their business.

Summary of Technical Sessions

SESSION I: ATMOSPHERIC DYNAMICS AND CIRCULATION

It is, of course, winds that act to produce atmospheric transports of various constituents such as dust and water and trace-chemical species. Carbon dioxide makes up most (95%) of the mass of the atmosphere so that, essentially, its transport is the wind (density weighted). As the winds redistribute the total atmospheric mass on the planet, the surface-pressure field reflects these changes. The winds are fundamentally driven by the differential solar heating of the planet, which in turn can be affected dramatically by the distribution of atmospheric dust. There is also, of course, a contribution to the winds associated with the condensation and sublimation of a sizable fraction of the atmosphere in the polar regions. Understanding the winds (that is, the atmospheric circulation and its underlying dynamics) that are responsible for transports was the focus of the opening session of the workshop.

The session opened with an invited paper by C. Leovy on Mars atmospheric circulation. Leovy focused his discussion on three aspects of the circulation: heat transport into the polar regions, thermal tides, and gravity waves. He began by emphasizing the extent to which recent modeling efforts have outstripped the available observations, highlighting the critical importance of Mars Observer-like data. In relation to the heat transports, Leovy focused upon the north-south asymmetry that general circulation modeling experiments have revealed. This is associated with the fact that the atmosphere is dustier near the time of northern winter solstice (as well as the fact that this occurs near perihelion), and with the model result that the transient eddies are considerably weaker during southern winter than northern winter. The latter appears to be at least partly a consequence of topographic differences between the hemispheres. The topography is poorly known at present, however, so the model results must be regarded skeptically; obtaining good topographic data is vital for investigations of the atmospheric circulation. In relation to thermal tides and gravity waves, Leovy emphasized that both may be dominant players in the middle atmospheric region. From a modeling perspective, gravity waves present a difficult challenge since they cannot be resolved without very high resolutions and the current parameterizations of their effects are rather crude.

Following Leovy's review talk, there were four papers that dealt with observations of the atmospheric structure and circulation. M. Santee discussed analyses of the thermal structure and circulation based upon Mariner 9 IRIS data for late northern winter. One of the most interesting aspects of these results was that they indicate that the north polar region was warmer at high levels (above about 40 km) than both low latitudes and the south polar region. This implies a diabatic

mean circulation characterized by sinking motions at high northern latitudes and rising motions in low latitudes. The existence of such a mean meridional circulation implies strong forcing by eddy motions—on the order of 50 m/s/day in the winter polar region. Unfortunately, the Mariner 9 data do not indicate what particular type of eddy motions may be responsible for this forcing. W. McMillan then discussed the retrieval of atmospheric temperature profiles from Mariner 9 IRIS data as part of an effort to develop and test a fast and efficient inversion scheme for use with Mars Observer TES spectra. L. Martin gave a brief review of observations of clouds and cloud motions, obtained telescopically and from spacecraft. To the extent that such motions can be imaged by spacecraft, they can be very valuable as direct wind indicators, but the interpretation of such motions is often ambiguous. Finally, E. Chassefière gave a talk on some of the results from the Phobos 2 solar occultation measurements. These results, for cloud, dust, and ozone abundances in the middle atmosphere, provide constraints on the strength of the vertical mixing in this region.

Following the observational papers, the remainder of the papers discussed recent results from a large variety of modeling studies of the martian atmosphere. Whereas as recently as two years ago the NASA/Ames Mars General Circulation Model (GCM) was the only such model for another planetary atmosphere, several such models are now under development. In particular, there is now a NASA/GISS GCM being developed (reported on by M. Allison), as well as a NOAA/GFDL GCM (reported on by R. J. Wilson). Additionally, there is a French (LMD) GCM effort and a British GCM project (these were reported on by F. Hourdin and S. Lewis in later sessions). There are also several "simplified GCM" studies underway, as reported on by R. Haberle and M. Collins. The study discussed by Haberle was particularly interesting in that continuous multiannual (10 Mars years) simulations had been performed. These appear to show sizable interannual variations—in the absence of topography and interactive dust transport—that peak in the southern summer season. [Haberle also presented some intriguing (but baffling) results on the apparent correlations between global dust storms on Mars and perfect games pitched in major league baseball.] The study discussed by Collins focused upon the transient eddies, and the (sometimes) "regular" nature of their structure. The NASA/GISS GCM is interesting in that it includes parameterized gravity wave effects, and Allison discussed the nature of the zonal wind balances in the model. The NOAA/GFDL GCM has been used primarily for experiments focusing upon thermal tides and the nearly resonant Kelvin wave modes.

The remainder of the modeling papers discussed more specialized and/or nonglobal circulation models. Chassefière

presented results from simulations of the middle atmosphere circulation with a zonally symmetric model incorporating gravity wave drag. J. Hollingsworth then discussed linear modeling of forced stationary waves in the winter hemispheres of Mars. M. Joshi reported on the examination of such waves, having a boundary current character, in simulations performed with the British GCM. A model of the circulation in the very high reaches of the atmosphere, the thermosphere, was discussed by S. Bougher. It is hoped that this model can be noninteractively coupled with the NASA/Ames GCM to yield simulations of the atmosphere from the ground well up into the thermospheric region. Finally, T. Siili and T. Parish reported on results from mesoscale modeling studies. The former study has examined circulation driven by gradients in surface properties, while the latter has focused on katabatic flows in the north polar region.

SESSION II: DUST

Dust can have a tremendous influence upon the heating of the martian atmosphere, which in turn drives the winds that transport and raise the dust. Understanding the raising, transport, and deposition of dust is thus crucial to a full understanding of the atmospheric circulation and climate. J. Murphy began the session on dust with an invited paper discussing dust transport. He began by outlining some of the key questions relating to the dust cycle, and briefly reviewing some of the available observations that bear upon dust transports. Murphy then discussed some of the results from simulations of dust transport and lifting that he has been carrying out with the NASA/Ames GCM coupled to an aerosol transport model. The simulations in which lifting is allowed to take place are especially interesting, despite the uncertainties in the quantitative nature of the lifting process, and appear to show both positive and negative feedback. The simulations evidence considerable lifting in the winter hemisphere in association with midlatitude transient eddies, and appear to show that topography acts to reduce the total amount of dust raising (because of the presence of sizable regions at relatively low pressures).

Following Murphy's review were four papers dealing with various observations of dust. First, P. James discussed Viking imaging observations of dust activity in the northern hemisphere during spring. There was one observation of a quite extensive (regional-scale) storm at high latitudes in the spring season following the 1977 fall and winter global dust storms; the frequency and size of such storms could be important for the global dust cycle. T. Martin presented dust opacity maps derived from Viking IRTM data. S. Lee and R. T. Clancy then reported on dust particle sizes and compositions and studies of dust deposition and removal from the surface. Improving our knowledge of the latter is essential to gaining a better understanding of dust raising and transport.

SESSION III: VOLATILES

The CO₂ and water cycles are intertwined with the dust cycle, and these were the focus of the next session in the workshop. B. Jakosky led off the session with an invited review of these two cycles. He discussed the fact that both the dust and water cycles evidence very large interannual variability, but for the most part the CO₂ cycle does not. The observed changes in the shape and structure of the retreating seasonal polar caps are evidence of interannual variations in the CO₂ cycle. Though the existence of one permanent CO₂ cap seems understandable (as opposed to two), the fundamental reasons why that cap exists in the south at present are not at all clear. Finally, the longer-term behavior of the polar caps is not well understood at all. In the case of the water cycle, Jakosky emphasized the very large interannual variability that is evidenced by Earth-based observations, and the basic question of whether or not a net transport from north to south is currently occurring.

Following the review, there were two papers dealing with recent GCM simulations of the annual pressure variations, given by J. Pollack (the NASA/Ames GCM) and Hourdin (the LMD GCM). Both studies have shown that there is a sizable "dynamic" component of the seasonal variation in surface pressure on Mars. This component is associated with the redistribution of atmospheric mass, in conjunction with seasonal changes in the zonal-mean circulation. Pollack showed that the atmospheric heat transport is very important in producing the observed strong asymmetry in the annual pressure curves, and this is largely due to greater atmospheric dust loading during northern winter. This enhanced dustiness may play a role in the formation of CO₂ ice clouds in the north polar region in winter, evidence (from Viking IRTM temperature data) for which was then discussed by F. Forget. A. Zent followed with a presentation of some recent modeling results for the transport of water in the atmospheric boundary layer. Finally, Chassefière and J. Barnes both touched upon the topic of eddy mixing. Chassefière reported on a photochemical modeling study that suggests a lower limit for the strength of the vertical mixing, and Barnes discussed a project to characterize the nature of tracer transport—both diffusive and advective—that is implied by the Ames GCM-simulated atmospheric circulation.

SESSION IV: MARS OBSERVER AND FUTURE SPACECRAFT MISSIONS

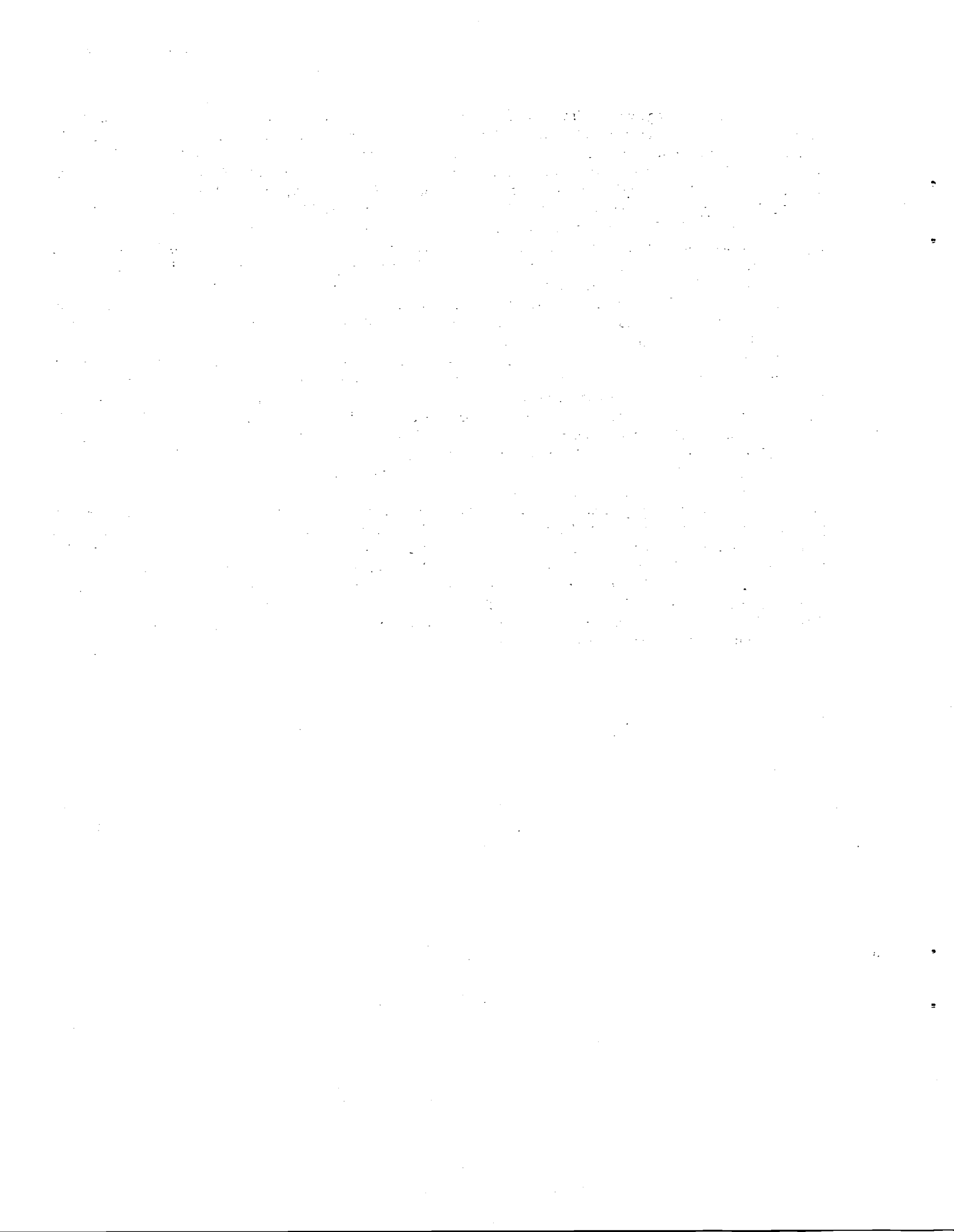
The papers presented during the first two days of the workshop emphasized the fact that the wide range of models that have been developed have outstripped the available data. The final session of the workshop dealt with Mars Observer, as well as with other possible future spacecraft missions. Despite the loss of Mars Observer, the analysis approaches discussed are relevant to future global, remotely sensed data-

sets. R. Zurek began things with an invited review of the various atmospheric measurements planned for Mars Observer. The PMIRR measurements of temperature, dust, and water were perhaps primary, but extremely important observations were also to be made by TES, radio science, MOLA, and MOC. The opportunities for synergistic studies would have been considerable. Four papers that dealt with various aspects of planned analyses of Mars Observer data to infer winds and transports were then presented. Lewis reported on the progress of an effort to develop a GCM to be used for data assimilation with PMIRR temperatures. This project uses the data assimilation code employed by the British Meteorological Office. D. Banfield then presented results from a study of optimal gain functions for data assimilation using a simplified dynamic model. A planned effort to produce synoptic maps from Mars Observer data using a simplified (linear-balance) atmospheric model was then discussed by H. Houben. Finally, a diagnostic scheme designed to infer winds and the small-scale (e.g., gravity wave) zonal drag from the PMIRR temperature data was discussed by Barnes.

The workshop concluded with several papers dealing with possible post-Mars Observer spacecraft missions that could yield advances in our understanding of atmospheric transport. Haberle gave a brief synopsis of recent developments in the MESUR mission planning process (in particular, sharp reductions in the size of the surface network), and then opened the floor to a discussion of the impacts of these developments on atmospheric science as well as ways to try to retain as much of this science as possible in the MESUR

mission. P. Smith followed with a report on the IMP instrument that was recently selected for the MESUR Pathfinder mission that is planned to precede MESUR. This imaging system has the capability of making a number of measurements of atmospheric properties. S. Limaye gave a presentation on two possible orbiter mission concepts, MOES and MOMS. The first could obtain complete local time-of-day coverage of Mars, while the second would be a means of obtaining temperature measurements without any need for sounding instruments (through radio occultations between several satellites). B. Clark then presented the final paper of the workshop, discussing a possible long-lived balloon mission to Mars.

At the conclusion of the workshop, participants generally felt that it had been successful. Because this was the first meeting to focus on circulation processes, it brought together more specialists (including several from outside the U.S.) in Mars atmospheric sciences than had any previous meeting. The workshop showcased the recent developments in modeling of Mars global atmospheric circulation. The number of global models that now exist is remarkable, but it was clear at the workshop that these wonderful tools have gone beyond the available data. It was certainly hoped that the next such gathering of Mars atmospheric scientists will be one at which the data are ahead of the models. While the loss of Mars Observer may have dealt those hopes a strong blow, the meeting certainly did serve to emphasize the vital importance of acquiring global observations of the atmosphere.



Abstracts

THE NASA/GISS MARS GENERAL CIRCULATION MODEL: PRELIMINARY EXPERIMENTS. M. Allison¹, M. A. Chandler², A. D. Del Genio¹, A. Lacis¹, D. Rind¹, W. B. Rossow¹, L. D. Travis¹, and W. Zhou³, ¹NASA Goddard Institute for Space Studies, 2880 Broadway, New York NY 10025, USA, ²University Corporation for Atmospheric Research, NOAA Global Change and Climate Program, Institute for Space Studies, New York NY 10025, USA, ³Hughes STX Corporation, Institute for Space Studies, New York NY 10025, USA.

The NASA/GISS Mars General Circulation Model (GCM) is an adapted version of the GISS Global Climate/Middle Atmosphere Model [1], specifically developed for the diagnostic validation and objective analysis of measured atmospheric temperatures from the Mars Observer Pressure Modulator Infrared Radiometer (PMIRR) experiment. The GISS Mars GCM has 23 vertical layers extending from the surface to approximately 80 km altitude, representing a vertical resolution of about 0.3 scale heights. The primitive (vertically hydrostatic) equations are solved in finite difference form on the Arakawa B grid, with a horizontal resolution of $8^\circ \times 10^\circ$ (latitude-longitude). The model includes a diurnal solar cycle, heat transport within a two-layer ground, and a high-order "slopescheme" for the advection of heat in the upper atmosphere [2]. The radiative transfer scheme is based on the correlated k distribution method for the treatment of nongray gaseous absorption, thermal emission, and multiple scattering [3], including options for suspended dust. A special feature of the model of particular importance for Mars is a parameterization of gravity-wave-induced drag incorporating orographic forcing, wind shear, convection, and radiative damping. The implementation of the GISS Mars model includes global maps of topography, roughness, and albedo.

In a first series of experiments, excluding phase changes and a hydrological cycle, with a pure CO₂ atmosphere, the martian circulation was simulated for the fixed solstice and equinox seasons. The fixed equinox ($L_s = 0^\circ$) simulation includes westerly 40–50 m s⁻¹ jets at midlatitudes and easterly upper-level flow at the equator exceeding 30 m s⁻¹. A hemispheric asymmetry in the zonal wind, temperature, and meridional stream function is apparent, with the rising branch of the Hadley circulation centered at about 15° to the south of the equator and a peak stream function of about 2.5×10^9 kg s⁻¹. The asymmetry is evidently the result of an enhanced surface heating in the southern hemisphere associated with its relatively elevated topography. For the fixed northern summer ($L_s = 90^\circ$) simulation, the zonal velocities, associated temperature, and Hadley circulation (rising in the north and descending in the south) are all somewhat stronger, with largely easterly flow in the northern hemisphere. For the northern winter ($L_s = 270^\circ$) simulation, the zonal velocity and cross-equatorial Hadley circulation pattern is reversed, with westerly 70 m s⁻¹ flow to the north, peaked in the vicinity of the 0.1-mbar level, easterly 90 m s⁻¹ upper level flow to the south, and a mass stream function exceeding 1×10^{10} kg s⁻¹. An isolated 20 m s⁻¹ westerly jet also appears near the surface at this season at southern midlatitudes. A preliminary series of simulations including the radiative effects of fixed airborne dust were also conducted and generally show still stronger zonal winds, sensitively dependent upon the amount and distribution of opacity.

Following the fixed season experiments, an extended running integration of the Mars GCM was initiated, accounting for the variable solar declination and distance, beginning approximately 55 sols before the southern summer and extending for nearly 400 sols of continuous simulated time. The variable season experiments exhibit a temporal lag of several sols with respect to the fixed season simulations, attributed to the thermal inertia of the deep ground layer, but otherwise show a qualitatively similar wind and temperature structure.

References: [1] Rind et al. (1988) *J. Atmos. Sci.*, 45, 329. [2] Russell and Lerner (1981) *J. Appl. Meteor.*, 20, 1483. [3] Lacis and Oinas (1991) *JGR*, 96, 9027.

OPTIMAL GAINS FOR A SINGLE POLAR ORBITING SATELLITE. D. Banfield¹, A. P. Ingersoll¹, C. L. Keppenne², ¹California Institute of Technology, Pasadena CA 91125, USA, ²Jet Propulsion Laboratory, Pasadena CA 91109, USA.

Gains are the spatial weighting of an observation in its neighborhood vs. the local values of a model prediction. They are the key to data assimilation, as they are the direct measure of how the data are used to guide the model. As derived in the broad context of data assimilation by Kalman [1] and in the context of meteorology, for example, by Rutherford [2], the optimal gains are functions of the prediction error covariances between the observation and analysis points. Kalman [1] introduced a very powerful technique that allows one to calculate these optimal gains at the time of each observation. Unfortunately, this technique is both computationally expensive and often numerically unstable for dynamical systems of the magnitude of meteorological models [3], and thus is unsuited for use in PMIRR data assimilation. However, the optimal gains as calculated by a Kalman filter do reach a steady state for regular observing patterns like that of a satellite. In this steady state, the gains are constants in time, and thus could conceivably be computed off-line. These steady-state Kalman gains (i.e., Wiener gains) would yield optimal performance without the computational burden of true Kalman filtering. We propose to use this type of constant-in-time Wiener gain for the assimilation of data from PMIRR and Mars Observer.

We will discuss the ways in which our technique differs from the method of data assimilation commonly used in Earth applications, Optimal Interpolation (OI). These differences include assumptions usually made in the implementation of OI about the shape of the gains, and the way multivariate covariances are handled. Implementations of OI typically make the assumption that the gains are isotropic in space [e.g., 4]. Propagation of atmospheric waves and the westward-marching nature of the observing pattern of Mars Observer cause significant asymmetries (about the observation point) in the shape of the optimal gains. We therefore retain the anisotropic nature of the gains with marked improvement in performance in our models over the isotropic gains of OI. Since PMIRR will only observe one dynamical variable (temperature), analyses must include cross-correlations between temperature and the other variables. A balance (e.g., geostrophic) is often assumed in the cross-correlations of many OI implementations [e.g., 4]; however,

we impose no explicit balance assumptions on our gains. The actual statistical covariances constitute the cross correlations that link the dynamical variables in our technique. Thus, the appropriate balance between the dynamical variables of the system will be maintained.

The optimal gains are, in general, functions of the latitude and longitude of the observation point. Topographic relief is greater on Mars than on Earth, and thus one would expect local topographic (longitudinal) effects to be significant in determining the shape of the optimal gain functions. However, the Wiener gains we will use in assimilation of PMIRR data will be functions of only the spacecraft latitude, ignoring their longitudinal dependence. In our models, performance is only marginally affected by making this simplification as compared to the isotropic assumption discussed above. The benefit is that it greatly reduces the number of unique gain functions that must be maintained.

We have developed a method of determining these optimal Wiener gains through an iterative procedure. As there are very few direct observations of martian weather and none yet that will suffice in providing a dataset for use in assimilation of global phenomena, we use a randomly forced model as a surrogate for Mars. We then assimilate observations of this "Truth" model into a predictive model using a zeroth iterate guess of the gains that are derived from the weather covariances of the model. As the assimilating continues, we compute the prediction error covariances that result, as we know both the prediction state as well as the "Truth" state for this set of systems. These prediction error covariances will then yield a next iterate, which will be a better estimate of the true steady-state optimal (Wiener) gains. This technique is then repeated until the gains converge to the actual optimal Wiener gains. In all our models, we found convergence in about three iterations of this procedure. Furthermore, in comparing with Kalman filters when we could implement them, the Wiener gains derived with this technique converged to the same functions as the steady-state Kalman gains.

To back up these statements, we have used a set of simple (and not so simple) models tuned to behave like the martian atmosphere. The anisotropies in the steady-state Kalman gains (Wiener gains) are well demonstrated through a one-dimensional one-variable Rossby wave model that simulates a latitude circle on Mars. The convergence of the above iterative procedure is also easily seen with this model. A one-dimensional three-variable Rossby gravity wave model was used to test the multivariate nature of the gains when only one dynamical variable is observed. This same model was also used to test the effects of topography on the gains. Mars-like topography was introduced into the model, and the predictive performance was tested with different assumptions about the longitudinal dependencies of the gains. Finally, a spectrally represented shallow-water model on a sphere [5] was used to test this technique with a non-linear model of similar (but less) complexity as a GCM. Experiments with these models suggest to us that this technique should be portable to a GCM with no major conceptual changes.

References: [1] Kalman R. E. (1960) *J. Basic Engineering (ASME)*, 82D, 35–45. [2] Rutherford I. D. (1972) *JAS*, 29, 809–815. [3] Bierman G. J. (1977) *Factorization Methods for Discrete Sequential Estimation*, 244, Academic, New York. [4] Bergman K. H. (1979) *Monthly Weather Review*, 107, 1423–1444. [5] Keppenne C. L. (1992) *Icarus*, 100, 598–607.

A DIAGNOSTIC MODEL TO ESTIMATE WINDS AND SMALL-SCALE DRAG FROM MARS OBSERVER PMIRR DATA. J. R. Barnes, College of Oceanic and Atmospheric Sciences, Oregon State University, Corvallis OR 97331-2209, USA.

Theoretical and modeling studies indicate that small-scale drag due to breaking gravity waves is likely to be of considerable importance for the circulation in the middle atmospheric region (–40–100 km altitude) on Mars [1,2]. Recent Earth-based spectroscopic observations have provided evidence for the existence of circulation features—in particular, a warm winter polar region—associated with gravity wave drag [3]. Since the Mars Observer PMIRR experiment will obtain temperature profiles extending from the surface up to about 80 km altitude, it will be extensively sampling middle atmospheric regions in which gravity wave drag may play a dominant role. Estimating the drag then becomes crucial to the estimation of the atmospheric winds from the PMIRR-observed temperatures.

An iterative diagnostic model based upon one previously developed and tested with Earth satellite temperature data [4] will be applied to the PMIRR measurements to produce estimates of the small-scale zonal drag and three-dimensional wind fields in the Mars middle atmosphere. This model is based on the primitive equations, and can allow for time dependence (the time tendencies used may be based upon those computed in a Fast Fourier Mapping procedure). The small-scale zonal drag is estimated as the residual in the zonal momentum equation; the horizontal winds having first been estimated from the meridional momentum equation and the continuity equation. The scheme estimates the vertical motions from the thermodynamic equation, and thus needs estimates of the diabatic heating based upon the observed temperatures. The latter will be generated using a radiative model. It is hoped that the diagnostic scheme will be able to produce good estimates of the zonal gravity wave drag in the Mars middle atmosphere, estimates that can then be used in other diagnostic or assimilation efforts, as well as in more theoretical studies.

References: [1] Barnes J. R. (1990) *JGR*, 95, 1401–1421. [2] Theodore B. et al. (1993) *JAS*, submitted. [3] Theodore B. et al. (1993) *Icarus*, submitted. [4] Marks C. J. (1989) *JAS*, 46, 2485–2508.

EDDY MIXING COEFFICIENT VALUES DERIVED FROM SIMULATIONS WITH THE NASA AMES MARS GCM. J. R. Barnes and T. Walsh, College of Oceanic and Atmospheric Sciences, Oregon State University, Corvallis OR 97331-2209, USA.

Values of eddy mixing coefficients, especially that for vertical mixing, are of particular importance for various photochemical models of the Mars atmosphere, which are either globally or zonally averaged. These models represent atmospheric transport processes in terms of eddy diffusion. While this is not appropriate for the advective transport by the mean meridional circulation (in general, a part of the eddy diffusion tensor actually does represent advection—a "correction" to the Eulerian-mean circulation), it can be applied to simulate both the small- and larger-scale eddy transports of an atmospheric constituent.

An effort is underway to estimate values of the eddy mixing coefficients for the Mars atmosphere using circulation data generated with the NASA Ames Mars GCM. This model simulates the

three-dimensional winds in the atmosphere, and these are then used as inputs for a tracer transport model. The latter model has previously been used in interactive dust transport experiments with the Ames GCM [1]. Idealized tracer transport experiments, with a conservative or nearly conservative hypothetical tracer, are performed to generate data from which the eddy diffusion coefficients can be estimated. Carrying out matched pairs of tracer experiments, using two very different initial states, permits all four components of the diffusion tensor to be determined [2]. A large number of GCM experiments have been conducted, spanning a range of seasons and atmospheric dust loading, allowing the eddy mixing coefficients to be estimated for a variety of atmospheric conditions.

References: [1] Murphy J. R. (1993) *JGR*, 98, 3197-3220. [2] Plumb R. A. and Mahlman J. D. (1993) *JAS*, 44, 298-327.

MARS DUST-DRIVEN TIDES AND THEIR IMPACT ON THE THERMOSPHERE. S. W. Bougher¹ and R. W. Zurek², ¹Lunar and Planetary Laboratory, University of Arizona, Tucson AZ 85721, USA, ²Jet Propulsion Laboratory, Pasadena CA 91109, USA.

It has been known since the early Mariner 6, 7, and 9 missions that dust loading of the lower atmosphere, and the subsequent aerosol heating during dusty periods, impacts the martian middle and upper atmospheres. A quantitative measure of this lower atmosphere forcing was obtained by the Viking 1 and 2 landers, from which observed amplitudes of semidiurnal surface-pressure oscillations were correlated with normal-incidence dust optical depths [1-3]. It appears that the dominant semidiurnal mode is a good indicator of global dust content or mean dust optical depth, especially during dust storm events. A classical tidal model that reproduces the surface pressure oscillations measured by these Viking landers in 1977 was used to calculate tidal amplitudes and phases up to -43 km [3]. These tidal characteristics were calculated for various dust optical depth conditions ranging from typical dusty periods to global dust storm times. Reasonable extrapolations can be made to higher altitudes if one assumes that the vertically propagating tidal modes continue to grow without dissipation or breaking. It is very likely that gravity waves also play an important role in the structure and dynamics of the middle atmosphere of Mars, since the large topographical relief should produce vigorous gravity wave fluxes [4].

Semidiurnal tidal modes, significantly enhanced by lower atmosphere dust-induced heating, may indeed propagate to the Mars thermosphere (≥ 100 km) before breaking and generating turbulence. The preferential enhancement of the semidiurnal tides during dust storm onset is primarily due to the elevation of the tidal heating source in a very dusty atmosphere. The (2,2) semidiurnal tidal mode was shown to have the largest variation with dust optical depth, as measured by Viking lander instruments [3]. Also, the (2,2) mode has the largest vertical wavelength of all the semidiurnal tidal modes, and thus is most likely to penetrate into the thermosphere before breaking and to modify the largely *in situ* solar-driven behavior otherwise expected. The tides may also be partially responsible for determining the height of the martian homopause (~ 125 km).

Dust-driven tides and their vertical propagation into the lower thermosphere are also important because tidal effects may explain the unexpected behavior of the Mars thermospheric temperatures

and densities observed during the Mariner 9 nominal and extended missions [5,6]. This was a period when Mars experienced a raging global dust storm and its gradual abatement. Solar fluxes were also near a minimum in the 11-year periodic cycle. The Mariner 9-inferred exospheric temperatures of -325 ± 40 K are significantly warmer than the 250 K value given by the solar-driven simulation of a three-dimensional thermospheric general circulation model (MTGCM) using EUV-UV forcing alone [6,7]. This is consistent with an expanded (warmer) lower and middle atmosphere that is reflected in an ionospheric peak altitude nearly 20-30 km higher than expected. A further discrepancy between model and observed fields is evident in the Mariner 9-inferred O-fractional abundances as a function of local time. The calculated O variation is much different than inferred from UVS 130.4-nm airglow intensity scans across the dayside. This discrepancy indicates an additional forcing of the dynamics that is responsible for redistributing O about the planet [5,6]. Evidently, the 1971 dust storm had a significant impact upon the Mariner 9-observed temperatures and densities. These outstanding features imply a significant lower-upper atmosphere coupling that modifies the otherwise diurnal Mars thermospheric structure driven *in situ* by the Sun.

The National Center for Atmospheric Research (NCAR) MTGCM code is the most recent in a hierarchy of thermospheric models developed to examine the thermospheric structure and dynamics of Earth, Venus, and Mars. The MTGCM code is based on the pressure-coordinate primitive equations of lower atmosphere dynamic meteorology. The physical processes incorporated into this model, however, are those appropriate to thermospheric dynamics, i.e., fast molecular vertical diffusion of heat, momentum, and constituents at thermospheric heights. The MTGCM model presently solves primitive equations yielding global solutions for the zonal, meridional, and vertical velocities, total temperatures, geopotential heights, and important neutral (CO_2 , CO, O, N_2 , NOX) and dayside ion (O_2^+ , CO_2^+ , O^+ , NO^+) densities on a 5° latitude and longitude grid. The vertical coordinate is log-pressure, with 24 levels spanning roughly 100-250 km. A vertical spacing of two grid points per scale height is achieved. The boundary conditions are zero fluxes at the top and prescribed winds, densities, temperatures, and the geopotential at the bottom.

A prototype MTGCM tidal model was recently developed to incorporate the effects of the upward propagating semidiurnal tides by modifying the MTGCM lower boundary conditions near 100 km according to classical tidal theory [6,8]. The basic variable used to parameterize the lower boundary is the geopotential. It is formulated as a function of latitude (via Hough functions), longitude, and time in units of days. The other model fields are then derived from the geopotential using the standard classical tidal relations [8]. The lower boundary is thus specified by the complex coefficients, including the amplitude and phase, of the geopotential for each mode. Specific lower boundary tidal amplitudes and phases for the (2,2) semidiurnal mode were estimated from Zurek's classical tidal model [2,3]. Values were calculated for a moderate value of dust optical depth ($\tau = 1.5$) corresponding to average dusty conditions near southern summer solstice. This prescription effectively couples the lower and upper atmospheres in a physically realistic manner.

MTGCM simulations incorporating these semidiurnal tides show a dramatic change in the divergence and convergence of horizontal and vertical winds, thereby modifying the diurnal temperature and density structure throughout the Mars thermosphere. The inclusion

of the (2,2) semidiurnal mode in the model gives rise to enhanced midafternoon temperatures that are closer to the values inferred from the Mariner 9 UVS (see Figs. 1 and 3). The diurnal variation of atomic O is also shown to be strongly dependent on the specified tidal amplitudes and phases, i.e., a greatly improved match of Mariner 9 UVS and modeled O mixing ratios is obtained (see Fig. 2). Increased attenuation of the semidiurnal propagating tides exists at high solar activity (similar to Earth), rendering the upper

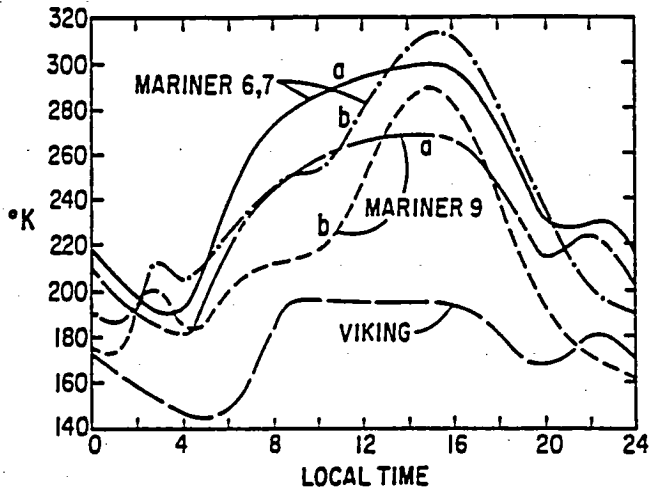


Fig. 1. Solar cycle variation of MTGCM exospheric temperatures as a function of local time about the equator. Mariner 6, 7 and 9 solar only (a) and tidal cases (b) are illustrated. All figures taken from [6].

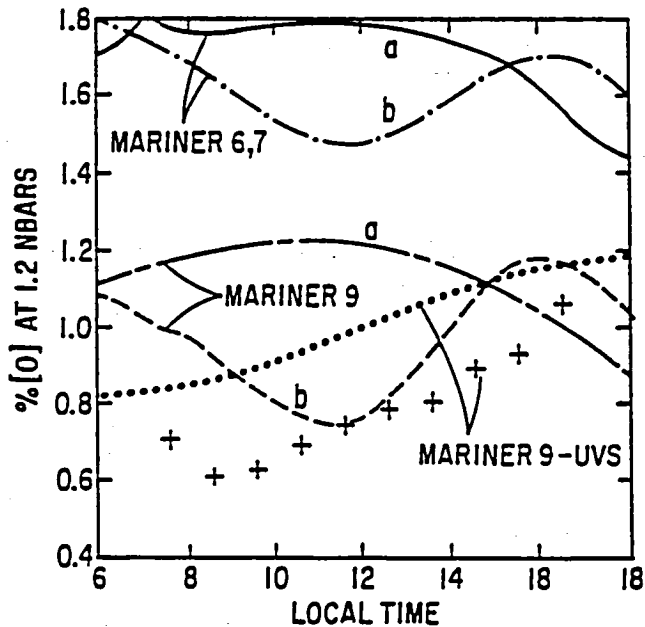


Fig. 2. Diurnal variation of the atomic O mixing ratio at the height of the dayside ionospheric peak. Mariner 6, 7, and 9 solar only (a) and tidal cases (b) are illustrated. The Mariner 9 tidal model distribution more closely matches that observed by the Mariner 9 UVS.

thermospheric response weakened with respect to that at solar minimum. Equivalently, tidal effects are discernable higher in the thermosphere during solar minimum, since the dissipation due to eddy/molecular viscosity and thermal conductivity is diminished (see Fig. 3). This suggests that dust-driven tides, especially during solar minimum time periods, cannot be ignored when addressing the Mars thermospheric structure and dynamics.

Further study of the coupling of the Mars lower and upper atmospheric regions requires the development of a tidal model that explicitly addresses the assumptions of tidal amplitude growth and regular phase shifting throughout the middle atmosphere (50–100 km). The development of a single coupled chemical-energy-dynamical model that realistically addresses the important physics in the entire martian atmosphere is extremely difficult. Various timescales for chemical, radiative, and dynamical processes change radically with altitude. However, it is feasible to run two well-developed general circulation models in tandem: the upper boundary of one would be used to specify the lower boundary of the other. Work is underway to modify the NASA Ames GCM model [e.g., 9,10] to cover 0–80 km; the NCAR MTGCM code will be extended to a 70-km lower boundary. The overlap will permit the Ames GCM to be run for various lower-atmosphere dust conditions and seasons. The GCM pressure surface near 70 km will then be used to progressively extract tidal mode amplitudes and phases for specification of the MTGCM geopotential height field. This procedure will provide an improved way to examine the propagation of dust-storm-driven tides and their effects throughout the entire atmosphere from the ground to the exobase. These two models will provide an improved set of tools for the interpretation of future PMIRR temperature data from the Mars Observer mission.

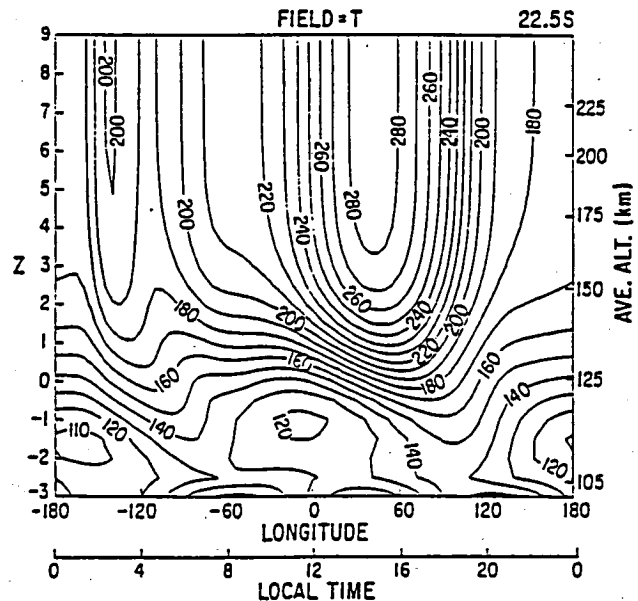


Fig. 3. Mariner 9 MTGCM tidal simulation: a latitude slice of total temperature at 22.5°S, with contours from 110–280 K. Midafternoon exospheric temperatures are 280 K, much warmer than without the (2,2) tidal mode.

References: [1] Pollack J. B. et al. (1979) *JGR*, 84, 2929–2945. [2] Zurek R. W. and Leovy C. B. (1981) *Science*, 213, 437–439. [3] Zurek R. W. (1981) *Icarus*, 45, 202–215. [4] Barnes J. R. (1990) *JGR*, 95, 1401–1421. [5] Stewart A. I. F. et al. (1992) *JGR*, 97, 91–102. [6] Bougher S. W. et al. (1993) *JGR*, 98, 3281–3295. [7] Bougher S. W. et al. (1990) *JGR*, 95, 14811–14827. [8] Fesen C. G. et al. (1986) *JGR*, 91, 4471–4489. [9] Haberle R. M. et al. (1993) *JGR*, 98, 3093–3124. [10] Pollack J. B. et al. (1993) *JGR*, 98, 3149–3182.

CLOUD, DUST, AND OZONE VERTICAL PROFILES FROM SOLAR OCCULTATION MEASUREMENTS: IMPLICATIONS FOR DYNAMICS. E. Chassefière and J. E. Blamont, Service d'Aéronomie du CNRS, BP 3, 91371 Verrières-le-Buisson Cedex, France.

An instrument has been designed for solar occultation measurements of the martian atmosphere from the Phobos spacecraft. It was composed of three different dispersive systems working in the ultraviolet (UV: 0.22–0.32 μm) for the measurement of O_3 and aerosols, in the near infrared (NIR: 0.76 μm , 0.94 μm) for the detection of O_2 and H_2O , and in the infrared (IR: 1.9 μm , 3.7 μm) where CO_2 and H_2O were measured. A detailed description of the instrument may be found in the special issue of *Nature* [1]. Its principle objective is to measure from the Phobos orbit the spectrum of the Sun, modified by atmospheric extinction, during sunset. The UV-NIR spot has an angular diameter of 1 arcmin, or ≈ 3 -km vertical resolution, and is located near the center of the solar disk. The IR field is about twice as large and its line of sight is shifted by 8.5 arcmin, or ≈ 20 km, relative to the previous one. It is therefore located near the edge of the solar disk. Sampling times are generally 0.5, 1, and 2 s for IR, UV, and NIR channels respectively, corresponding to vertical excursions of the line of sight of 1, 2, and 4 km respectively under nominal conditions. The instrument operated from February 8 to March 26 (the martian equinox occurred on February 17). The latitude of the intersection of the Sun-spacecraft axis with the surface of Mars varied from -11° to $+20^\circ$, the seasonal date L_s being in the range 0° – 20° . All measurements were therefore made near northern spring equinox in equatorial regions. Due to an error in the pointing system, only partial results were obtained, the region below ≈ 30 km altitude being never sounded by the UV-NIR spectrometer. On the contrary, nine complete occultations were obtained in the IR channels, whose line of sight was fortunately ≈ 20 km below the UV-NIR axis.

Five clouds were detected above 45 km altitude and their vertical structure recorded at six wavelengths between 0.28 μm and 3.7 μm [2]. They have a small vertical extent (3–6 km) and a vertical optical depth less than 0.03. The thermal structure, as derived from saturated profiles of water vapor observed by the instrument in the infrared [3], does not allow the CO_2 frost point to be reached at cloud altitude, strongly suggesting that cloud particles are formed of H_2O ice. Under the assumption of spherical particles, a precise determination of their effective radius, which varies from cloud to cloud and with altitude, was obtained, ranging from 0.15 to 0.85 μm . An estimate of the effective variance of the particle size distribution is ≈ 0.25 . The number density of cloud particles at the peak extinction level is ≈ 1 cm^{-3} . Assuming that particles are levitated by eddy mixing, the eddy diffusion coefficient, K , was found to be 10^5 –

10^6 cm^2 s^{-1} at 50 km by comparing the results of a simple steady-state model with observations. Indeed, since the clouds are observed at twilight, which coincides with the diurnal maximum of the ambient temperature, they can be assumed to be in a steady state. If their thermodynamic state were to vary quickly during the day, our optical thickness at twilight would correspond to unrealistic values in earlier hours when the temperature is lower. An atmospheric temperature of 165–170 K at ≈ 50 km is inferred. The negative temperature gradient above the cloud is large (1.5 – 2 K km^{-1}).

Dust was also observed and monitored at two wavelengths, 1.9 and 3.7 μm , on nine different occasions [2]. The top of the dust opaque layer, defined as the level above which the atmosphere becomes nearly transparent at the wavelengths of observation, is located near 25 km altitude, with variations smaller than ± 3 km from place to place. The scale height of dust at this altitude is 3–4 km. The effective radius of dust particles near the top of the opaque layer is 0.95 ± 0.25 μm and increases below with a vertical gradient of ≈ 0.05 $\mu\text{m km}^{-1}$. Assuming that particles are levitated by eddy mixing, the eddy diffusion coefficient, K , is found to be $\approx 10^6$ cm^2 s^{-1} at 20–25 km. An effective variance of 0.25 ($\pm 50\%$) for the dust size distribution is obtained on the basis of a simple theoretical model for the observed vertical gradient of the effective radius of dust.

Concerning ozone, only six occultations may be analyzed in the near-UV wing of the Hartley continuum (≈ 0.270 – 0.283 μm). Ozone is detected at one time with a high degree of confidence below ≈ 60 km and above ≈ 37 km altitude [4]. Its number density shows a maximum of $\approx 10^8$ cm^{-3} around 42–45 km. Its scale height above 45 km is 6 ± 2 km. Ozone, present in two other cases with a similar vertical profile, is not detected, that is, not in excess of $\approx 2 \times 10^7$ cm^{-3} , for the three other observations. An analysis based on a one-dimensional steady-state photochemical model indicates that when ozone is present the eddy diffusion coefficient, K , is $\approx 2 \times 10^6$ cm^2 s^{-1} around 40–45 km altitude within a factor of ≈ 2 on either side. Below 50 km, the water vapor mixing ratio is lower than $\approx 2 \times 10^{-5}$. Such a low ratio is consistent with a temperature decreasing with increasing altitude, with a typical temperature of ≈ 150 K at ≈ 50 km altitude. Above 50 km, the H_2O mixing ratio is definitely lower than 10^{-5} , strongly suggesting saturation at high altitude. The agreement between the modeled and observed profiles of ozone is significantly improved by assuming a sharp increase of K over a typical scale of 1 atmospheric scale height around 40–45 km altitude, from $\approx 5 \times 10^5$ cm^2 s^{-1} below 40 km up to $\approx 10^7$ cm^2 s^{-1} above 45 km. The absence of ozone found in at least half the cases may be simply reproduced by using the thermal structure and humidity conditions derived from the analysis of the clouds [2], i.e., a temperature and a H_2O mixing ratio of respectively ≈ 165 K and $\approx 10^{-4}$ at 50 km altitude.

The first implication of these measurements is the good agreement between the different estimates of the eddy diffusion coefficient K . From a simple comparison between observed number density and size profiles of water ice aerosols and dust particles, the value of K is nearly the same at low and high altitude, i.e., $\approx 10^6$ cm^2 s^{-1} around 20–25 km and 10^5 – 10^6 cm^2 s^{-1} around 50 km. From ozone measurements, a most likely value of 2×10^6 cm^2 s^{-1} within a factor of 2 on either side is found around 40–45 km, consistent with values derived from cloud and dust measurements. The suspected sharp increase of K by more than 1 order of magnitude between 40 km and 45 km around the pivot value of 2×10^6 cm^2 s^{-1} could be the signature of breaking gravity waves. From a two-

dimensional modeling of the effect of breaking gravity waves on the general circulation and temperature field in the middle atmosphere of Mars [5] using Lindzen's parameterization, which explains well millimeter wave observations made with the IRAM 30-m telescope [6], such an increase, by about 1 order of magnitude per half atmospheric scale height, may be easily reproduced around 50 km altitude, in the breaking region. Because the ozone profile is extremely sensitive to a sharp increase of K around 30–50 km, the future observation of ozone by stellar and solar occultation from the Mars 94 spacecraft (SPICAM experiment) could bring some interesting information on the breaking level of internal gravity waves.

The second implication concerns the likely presence of an inversion of the temperature profile around 35 km when clouds are observed, in order to allow the rather high temperature (165–170 K) and thermal gradient (-1.5 – 2 K km $^{-1}$) inferred at the cloud level. More precisely, the presence of two condensation levels at ≈ 15 km and ≈ 50 km altitude are inferred from water vapor and cloud measurements respectively. Above ≈ 15 km, a regular decrease of the water vapor mixing ratio up to ≈ 35 km is observed [3] and it is interpreted as the signature of a saturated atmosphere. Around ≈ 50 km, thin clouds, very likely formed of water ice, are detected [2]. This means that above ≈ 35 km exists a region where the atmosphere is not saturated in H_2O , containing enough water vapor to give rise to the formation of clouds. The reason for the temperature inversion might be adiabatic warming due to convective motions induced by breaking gravity waves. It was shown from the two-dimensional modeling that weak temperature inversions are generated above the equatorial region at solstice for certain parameters of the waves [5], and a similar phenomenon could be produced by the model at equinox if the preliminary results of the last millimeter-wave observations made at IRAM are confirmed (Lellouch, personal communication). The second issue is how water molecules are transported from the low atmosphere up to the cloud region. A possible explanation is that upwelling in the ascending branch of the Hadley cell is able to supply water ice in the shape of small particles, across the cold saturated region (≈ 15 – 35 km), to the nonsaturated layer below the clouds, where ice may sublimate and condense again at cloud level (≈ 50 km). A simple heuristic model of water ice vertical transport at equator has been constructed [7]. Different constraints have been introduced relating to the coagulation probability during the upward transport phase, the minimum amount of H_2O that must be deposited at the sublimation level, and the infrared optical thickness of ice particles. It was shown that these constraints are jointly satisfied for reasonable values of parameters, indicating that a quantity (zonally averaged) of $\approx 0.01/\mu\text{m}$ of water ice in the shape of small particles of radius 0.1–0.2 μm might be present in the middle atmosphere (15–35 km) above equatorial regions.

The third implication is that, from a qualitative point of view, thin clouds and an ozone layer seem to be the signatures of two well-defined states of the middle atmosphere, the region around 40–50 km being warm and wet when clouds are observed (15% of cases), cold and dry when ozone is present (≈ 15 –50% of cases). An outstanding fact is that, considering these two typical atmospheric states, the vertical structure of the observed constituent, i.e., water ice particles and ozone molecules respectively, as well as the inferred atmospheric parameters (temperature, water vapor mixing ratio, eddy diffusion coefficient), do not seem to change significantly from place to place, or from time to time. It means that the variability of the middle atmosphere of Mars could not consist in a wide and

continuous range of possible states, with random fluctuations of temperature and water vapor amount, but rather in an organized system of a small number of stable configurations. This general result reinforces our belief that the thermal structure and the degree of humidity of the middle atmosphere of Mars are driven by dynamical processes. The thermal structure could be controlled by meridional winds induced by breaking gravity waves, with associated inversion of the meridional and vertical thermal gradients. Eddy mixing partially reflects the interaction between gravity waves and general circulation, and a sharp change of K at some altitude, as suspected from our analysis of ozone, could be the local signature of this interaction. It must be noted that an intermediate state, for which there is an abundance of water vapor too small to yield the formation of clouds but too large to prevent the ozone density from reaching our detection threshold around 40 km, is also observed (≈ 35 –70% of cases), and the previous schematic picture will certainly have to be refined. The simple typology established from Phobos 2 solar occultation measurements (see Table 1) could be the starting point toward a more extensive study of the dynamical processes controlling the middle atmosphere of Mars with the help of oncoming observations by the Mars Observer mission (PMIRR, Radio Science experiment).

TABLE 1.

Water vapor mixing ratio	$<2 \times 10^{-3}$	$2-6 \times 10^{-3}$	6×10^{-3}
Type of atmosphere	cold/dry		warm/wet
Ozone	yes	no	no
Cloud	no	no	yes
Percentage of occurrences	(15–50%)	(35–70%)	(15%)

References: [1] Blamont J. E. et al. (1989) *Nature*, 341, 600–603. [2] Chassefière E. et al. (1992) *Icarus*, 97, 46–69. [3] Krasnopolsky V. A. et al. (1991) *Icarus*, 94, 32–44. [4] Blamont J. E. and Chassefière E. (1993) *Icarus*, revised March 1993. [5] Théodore B. et al. (1993) *J. Atmos. Sci.*, submitted. [6] Théodore B. et al. (1993) *Icarus*, submitted. [7] Chassefière E. and Blamont J. E. (1992) *GRL*, 19, 945–948.

PARTICLE SIZES AND COMPOSITION OF MARS ATMOSPHERIC DUST BASED UPON VIKING AND MARI-NER 9 OBSERVATIONS. R. T. Clancy¹, S. W. Lee¹, and G. R. Gladstone², ¹Laboratory for Atmospheric and Space Physics, University of Colorado, Boulder CO 80309, USA, ²Southwest Research Institute, P.O. Drawer 28510, 6220 Culebra, San Antonio TX 78228, USA.

Mars atmospheric dust can play an important role in the thermal structure of the Mars atmosphere during periods of high dust loading [1]. However, the radiative properties of Mars atmospheric dust remain uncertain due to uncertain definitions of the dust composition and size distribution. The analysis by Toon et al. [2] of Mariner 9 IRIS spectra during the 1971–1972 global dust storm indicated a reasonable match between the modeled 9- μm absorption of montmorillonite and the observed 9- μm absorption. Toon et al. also determined that an effective (cross-section weighted) mean radius of 2.5 μm ($R_{\text{mode}} = 0.4 \mu\text{m}$) provided a consistent fit of montmorillonite to the IRIS dust spectra at 9 μm . Pollack et al. [1] analyzed Viking lander observations of atmospheric extinction and scattering at

visible-near IR wavelengths (0.5–1.0 μm), and obtained consistency with the Toon et al. dust size distribution when the effects of nonspherical particle shapes were included. An additional, minor (1%) component of visible-ultraviolet absorbing material was required to model the derived visible (0.86) and ultraviolet (0.4–0.6) [3] single-scattering albedos of the dust, since montmorillinite does not absorb sufficiently in this wavelength region [4].

There are, however, several deficiencies with the Toon et al. model of Mars atmospheric dust. As Toon et al. and subsequent analyses of Viking IRTM observations [5] point out, montmorillinite exhibits strong, structured absorption near 20 μm that is not exhibited by the IR observations. Furthermore, the observed ratio of visible-to-infrared extinction opacities for Mars atmospheric dust is approximately 2 [6], which is twice the calculated ratio for montmorillinite with a cross-section weighted mean radius of 2.5 μm [7,8]. In addition, higher values for the visible single-scattering albedo of the dust (0.92 vs. 0.86) have been derived from the Viking IRTM albedo channel, as well as a corrected value of 0.55 for the single-scattering asymmetry parameter [8].

We have conducted a combined analysis of the Viking IRTM and Mariner 9 observations to reassess the model of Mars atmospheric dust in terms of a single optical component, which might satisfy the ultraviolet-to-infrared measurements of dust absorption and scattering. The optical constants for palagonite [9,10] are incorporated in a doubling-adding radiative transfer model of the Mars atmosphere to simulate Mariner 9 IRIS spectra as well as the Viking IRTM IR band observations. We also derive visible and ultraviolet single-scattering albedos based on the Hansen and Travis Mie scattering code [11]. A tentative conclusion is that smaller dust particles ($R_{\text{mode}} = 0.15 \mu\text{m}$, cross-section weighted mean $R = 1.2 \mu\text{m}$) composed of palagonite provide a much improved fit to the Mariner 9 IRIS spectra; agreement with the observed ratio of visible-to-infrared extinction opacities; and ultraviolet and visible single-scattering albedos comparable to their observed values.

References: [1] Pollack J. B. et al. (1979) *JGR*, 84, 2929–2945. [2] Toon O. B. et al. (1977) *Icarus*, 30, 663–696. [3] Pang K. et al. (1976) *Icarus*, 27, 55–67. [4] Pollack J. B. et al. (1977) *JGR*, 82, 4479–4496. [5] Hunt G. E. (1979) *JGR*, 84, 8301–8310. [6] Martin T. Z. (1986) *Icarus*, 66, 2–21. [7] Zurek R. W. (1982) *Icarus*, 50, 288–310. [8] Clancy R. T. and Lee S. W. (1991) *Icarus*, 93, 135–158. [9] Roush T. (1993), personal communication. [10] Clark R. N. et al. (1990) *JGR*, 95, 14463–14480. [11] Hansen J. E. and Travis L. D. (1974) *Space Sci. Rev.*, 16, 527–610.

ASPECTS OF THE MARTIAN GLOBAL CIRCULATION.

M. Collins and I. N. James, Department of Meteorology, University of Reading, Reading RG2 6AU, UK.

Introduction: Recent advances in high-speed computers have given atmospheric scientists a new laboratory in which to work. Numerical models of the Earth's atmosphere and its dynamics have provided great insight. Given the lack of observations of the martian atmosphere it is natural to apply such models to help us understand aspects of, for instance, large-scale circulation patterns. Here we have modified a global circulation model of the Earth's atmosphere for use with martian parameters and have studied the relevant regimes of planetary flow.

Method: The model solves the primitive equations on the sphere using a spectral method in the horizontal and finite differences in the vertical. The coarse resolution ($\sim 5^\circ$ longitude \times 5° latitude and 10 vertical levels) requires some parameterization of subgridscale friction and heating. It is tempting to embark on a series of complicated representations of radiation, turbulence, etc. This soon becomes a burden with the specification of a large number of arbitrary parameters. Also the computational cost increases, which precludes long integrations and regime studies. We have developed two distinct models: (1) The Simplified Global Circulation Model (SGCM) has for its thermodynamic forcing a linear relaxation to a prescribed radiative equilibrium temperature profile on a certain timescale. Frictional forces are similarly linear and are applied at the lower boundary of the model. (2) The Intermediate Global Circulation Model (IGCM) has a prescribed surface temperature distribution and a boundary layer scheme that mixes heat and momentum into the atmosphere. Radiative cooling is assumed constant throughout the atmosphere and a dry convective adjustment scheme is in place.

Both models provide a computationally cheap and conceptually simple framework in which to study regimes of planetary scale flow.

No Mountain Flows: The Viking landers relayed data that suggested the existence of baroclinic waves in the northern winter midlatitudes. Among the seemingly random fluctuations there appeared highly periodic phases when synoptic systems passed over the landers with monotonous regularity [1]. This would be in stark contrast to the Earth's rather chaotic weather patterns. Martian baroclinic waves may be closer to the regular waves found in the rotating annulus experiment [3].

In order to study such baroclinic waves the SGCM was set up to run with no mountains and hence remove the possibility of stationary waves. Radiative equilibrium temperatures, representing southern hemisphere winter, were taken from [5]. The sensitivity of the modeled climatology was then investigated by varying (principally) the frictional and thermal relaxation timescales.

In general the modeled baroclinic waves appear as small undulations propagating on a zonally orientated jet stream (Fig. 1a). The fast radiative relaxation timescale of the atmosphere limits the amplitude of the waves. Compare this with the Earth's midlatitudes where cyclones grow to finite amplitude in turbulent storm tracks. In many of the integrations, however, a zonal wavenumber 3 pattern (Fig. 1b) emerges and grows to large amplitude, dominating the flow. This wave 3 propagates eastward around the midlatitudes at a constant phase speed for at least 1000 days (the longest run). The resulting flow is very reminiscent of the single wavenumber steady waves found in the rotating annulus laboratory experiments [3].

Read [6] and White [7] have suggested that the steady annulus waves may be "free modes" of the full nonlinear governing equations. It is assumed that, in the interior of the fluid, heating and friction are small and the nonlinear terms are zero, i.e., if $u \cdot \nabla \zeta$ is a nonlinear term $u \cdot \nabla \zeta = 0$ while neither u nor $\nabla \zeta$ is zero. A similar approach is used in modon studies of, e.g., atmospheric blocks and jovian vortices. The assumption of zero heating is clearly not valid here. Also the existence of the wave 3 is sensitive to both heating and frictional timescales. A close examination of the potential vorticity budget reveals that (away from the ground) a stable balance is struck between the nonlinear and heating terms, the rapid radiative timescale allowing the wave to be maintained at finite amplitude.

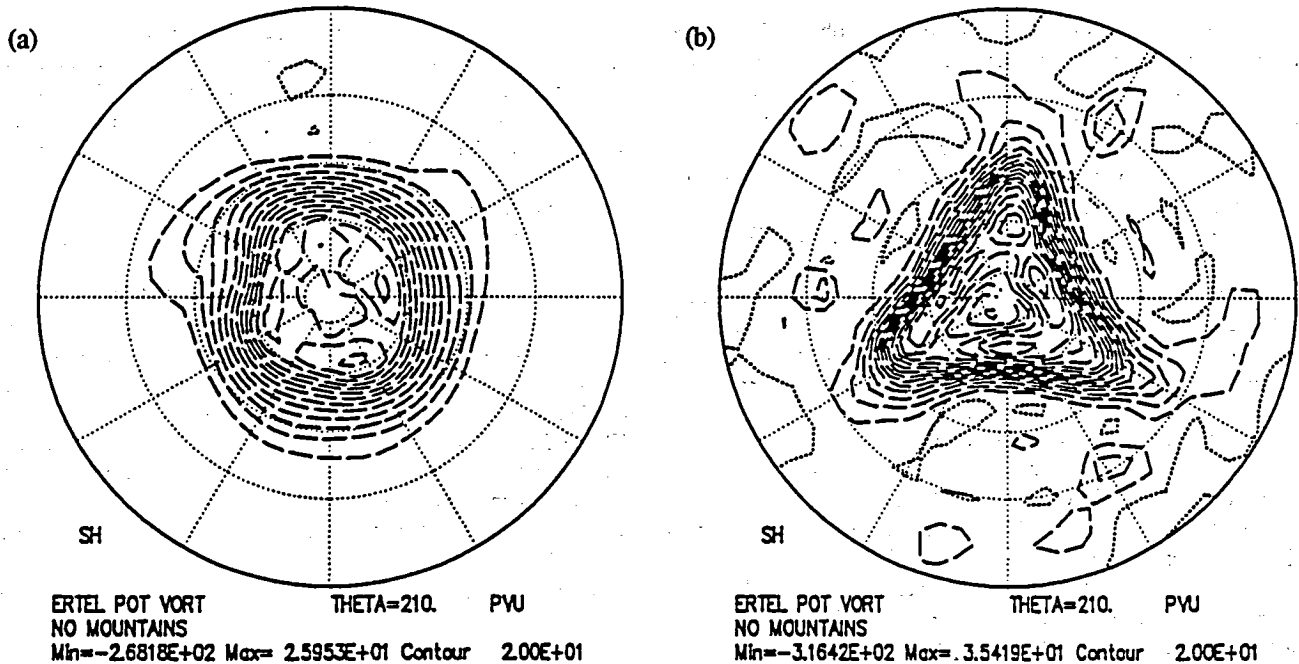


Fig.1.

Integrations with other radiative equilibrium temperature profiles have large amplitude zonal wavenumber-4 patterns (Fig. 2) with similar properties, so we believe these results to be robust. The connection between these waves and the regular oscillations found in the Viking data is unclear, especially considering the relative simplicity of the SGCM. It is desirable then to add an extra degree of realism to the model.

Flows with Mountains: The SGCM uses a terrain-following σ coordinate system in the vertical. In these simulations the more recent DTM orography is used. Again the southern hemisphere winter radiative equilibrium temperatures from Pollack et al. [5] were interpolated onto the model grid and the flow was spun up from a resting isothermal state.

Orography generates stationary waves that can either propagate vertically through the atmosphere or exponentially decay away from the surface. Vertically propagating waves can mix heat and momentum meridionally and thus contribute to the maintenance of the global circulation. Partitioning eddy statistics into stationary and transient components showed that the stationary waves were dominating with the transients virtually absent. A similar result has been found by [2]. This would constitute a considerable asymmetry between the hemispheres, the northern winter midlatitudes being the only place where traveling synoptic systems are present.

The eddy kinetic energy maximum for these integrations is near the model top (Fig. 3), which is a rigid lid. This implies that stationary waves are being spuriously reflected when really they should propagate out of the model domain. To partially resolve this problem linear friction (sponge layer) is added to "soak up" the energy. Examination of the eddy statistics then showed the existence of some transient behavior. It appeared that the stationary waves were saturating and choking off the transients. In other integrations, however, the sponge layer reduced the transient amplitude. This shows that a careful treatment of the top boundary of any model of the martian atmosphere is necessary.

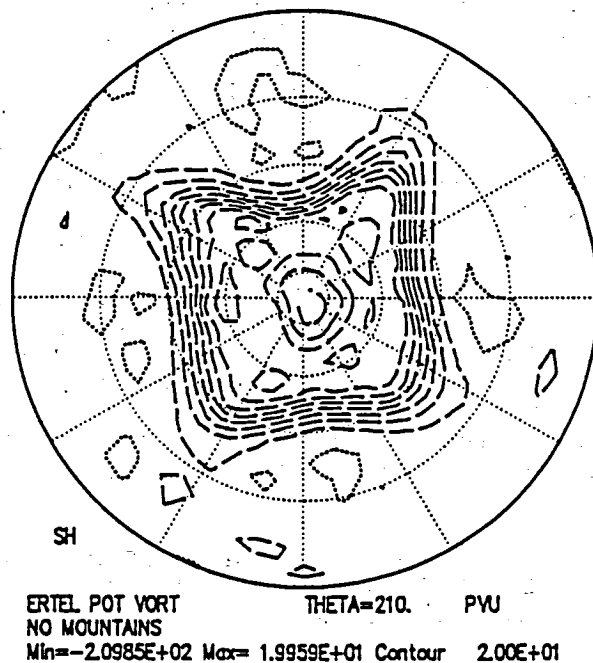


Fig. 2.

The IGCM: Although the SGCM provides adequate simulations of the martian circulation, some aspects of the flow are not well represented. The introduction of more complicated physical parameterizations requires the specification of more arbitrary constants. These are not certain even for the Earth and are difficult to determine for Mars. Here, we have kept the level of parameteriza-

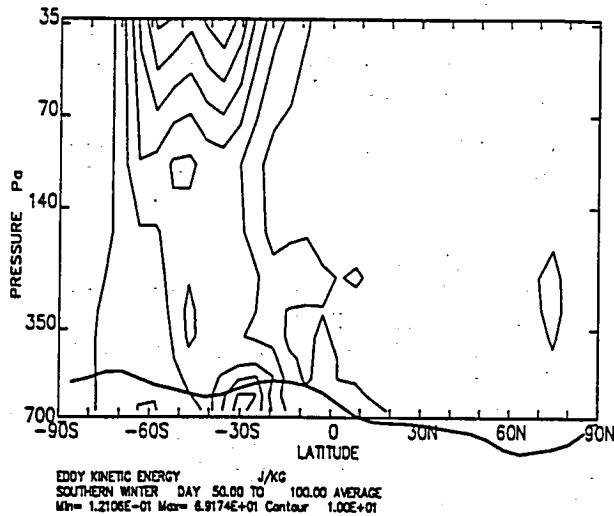


Fig. 3.

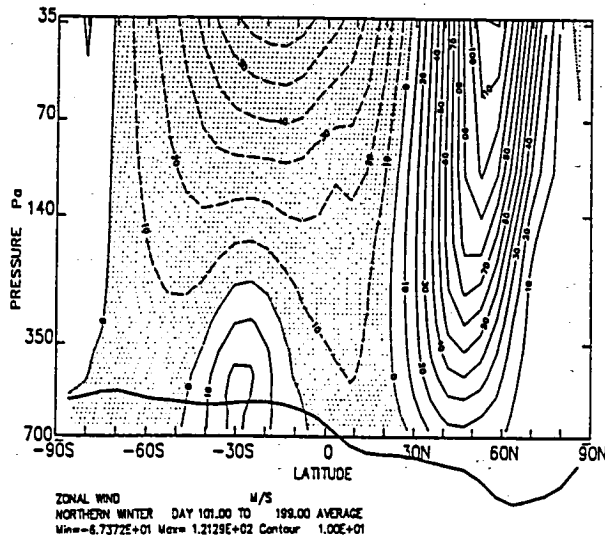


Fig. 4.

tion to a minimum. A boundary layer scheme with prescribed surface temperatures heats the atmosphere, which is in turn cooled at a constant rate. Convective instability is possible and a simple adjustment scheme is applied. The model reproduces fairly well the zonally averaged climatology of [2] (Fig. 4).

Examining the flow at the Viking lander sites in the model shows the existence of mobile baroclinic systems. A spectral analysis of pressure has strong spectral peaks at similar frequencies to those found by [1]. The flow shows high temporal coherence compared to that of the Earth.

An interesting aspect that was first pointed out to us by [4] concerns the annual pressure cycle. The large annual signal in the Viking data has been attributed to the melting and freezing of the polar CO_2 frost caps and would constitute a significant change in the mass of the atmosphere. This model has no evaporation/condensation and the atmospheric mass is conserved. A sizable annual pressure cycle is, however, still evident. The redistribution of mass,

required by geostrophic balance of the midlatitude jets, gives a large pressure gradient term that fluctuates throughout the year as the flow switches from easterly to westerly.

Conclusions: The two models described have succeeded in modeling some observed aspects of the martian atmospheric circulation and some aspects that have been generated by other, more complicated GCMs. The regularity of synoptic systems on Mars sets it aside from the Earth where weather systems are highly unpredictable. Martian baroclinic waves may be more akin to the regular waves found in rotating annuli. The large amplitude orography also gives a different regime with stationary waves swamping the flow. This is in contrast to the Earth's northern hemisphere where stationary and transient waves are of equal importance.

References: [1] Barnes J. R. (1981) *J. Atmos. Sci.*, 38, 225-234. [2] Barnes J. R. et al. (1993) *JGR*, in press. [3] Hide R. and Mason P. J. (1975) *Adv. Phys.*, 24, 47-100. [4] Hourdin F. (1992) Ph.D. thesis, l'Université Paris 7. [5] Pollack J. B. et al. (1981) *J. Atmos. Sci.*, 38, 3-29. [6] Read P. L. (1985) *Dyn. Atmos. Oceans*, 9, 135-270. [7] White A. A. (1986) *Q. J. R. Met. Soc.*, 112, 749-774.

IMPACT OF THE CO_2 AND H_2O CLOUDS OF THE MARTIAN POLAR HOOD ON THE POLAR ENERGY BALANCE. F. Forget and J. B. Pollack, NASA Ames Research Center, Moffett Field CA 94035-1000, USA.

Clouds covering extensive areas above the martian polar caps have regularly been observed during the fall and winter seasons of each hemisphere. These "polar hoods" are thought to be made of H_2O and CO_2 . In particular, the very cold temperatures observed during the polar night by Viking and Mariner 9 around both poles have been identified as CO_2 clouds [1,2] and several models, including GCM [3], have indicated that the CO_2 can condense in the atmosphere at all polar latitudes.

Estimating the impact of the polar hood clouds on the energy balance of the polar regions is necessary to model the CO_2 cycle and address puzzling problems like the polar caps asymmetry. For example, by altering the thermal radiation emitted to space, CO_2 clouds alter the amount of CO_2 that condenses during the fall and winter season.

We have analyzed the complete set of Viking IRTM data to define the spatial and temporal properties of the polar hoods, and estimated how their presences affect the energy radiated by the atmosphere/caps system to space.

The IRTM observations provide good spatial and temporal coverage of both polar regions during fall, winter, and spring, when a combination of the first and the second Viking year is used. Only the IRTM brightness temperatures at 11, 15, and 20 μm are reliable at martian polar temperatures. To recover the integrated thermal fluxes from the IRTM data, we have developed a simple model of the polar hood, thought to consist of "warm" H_2O clouds lying above colder and opaque CO_2 clouds. Such a model is based on the analysis of the IRTM spectra [4], and is consistent with the IRTM data used here.

The high thermal emissivity of the CO_2 ice particles is possible because of contamination by dust and water [5]. Besides, we have found new evidence for such opaque CO_2 clouds in the IRTM data.

The model has been calibrated and validated by testing its ability to reproduce polar hood IRIS spectra from simulated IRTM temperatures.

A specific treatment of the IRTM data has also allowed us to recover the "true" ground-ice temperatures, which only depend on the atmospheric pressure (solid-gas equilibrium), but which were difficult to measure directly because of the presence of the CO₂ and H₂O clouds.

We have also obtained estimations of the amount of water ice in the polar clouds during winter, and a climatology of the frequency and temperature of the CO₂ clouds.

Thus, we have been able to estimate the wavelength-integrated thermal emission by the surface/atmosphere system at the top of the atmosphere and to compare this with what would have been emitted by the bare polar caps. In the future, this information will allow us to address polar process questions with a realistic parametrization of the polar hood.

References: [1] Hunt G. E. (1980) *GRL*, 7, 481–484. [2] Paige D. A. (1985) Ph.D. thesis, Caltech. [3] Pollack J. B. et al. (1990) *JGR*, 95, 1447–1473. [4] Paige D. A. (1992) personal communication. [5] Warren S. G. et al. (1990) *JGR*, 95, 717–741.

MULTIANNUAL SIMULATIONS WITH THE MARS CLIMATE MODEL. R. M. Haberle¹, H. C. Houben², and R. E. Young¹, ¹NASA Ames Research Center, Moffett Field CA 94035-1000, USA, ²Space Physics Research Institute, Sunnyvale CA 94087-1315, USA.

We have simulated the martian atmospheric circulation for 10 Mars years using a simplified three-dimensional climate model that is briefly described below. Analysis of these simulations reveals several interesting behaviors not previously recognized in other three-dimensional models. The first concerns the potential for interannual variability in the martian climate system. We now know from the aperiodic frequency of planet-encircling storms, as well as differences in atmospheric water vapor from one year to the next, that the real planet exhibits interannual variations. The results of our simulations also show significant interannual variability and, interestingly, that variability maximizes during southern spring, the dust storm season. A second and related finding is that transient eddies in the southern hemisphere during winter are indeed weaker than their northern hemisphere counterparts as was found in more sophisticated models. However, southern hemisphere eddy activity rises dramatically during spring and is greater than that in the northern hemisphere at any season.

The model we use is based on the primitive equations in log-pressure coordinates. The model is spectral (spherical harmonics) in the horizontal, and finite-differenced in the vertical. For the multiannual simulations, we run with trapezoidal truncation using 6 zonal waves, and a maximum total wavenumber of 16. There are 14 vertical levels that gradually increase in thickness from ~500 m in the lowest layer to about one-half scale height in the upper layer. The model runs on a dedicated Silicon Graphics Workstation; with half-hour time steps, it takes about 8 hours to simulate 1 Mars year.

However, the difference between this model and a GCM is its greatly simplified physics. We use Newtonian cooling with a 2-day damping time for thermal forcing, with a Rayleigh friction "sponge" layer at the top and a quadratic drag force at the bottom. The rest of the atmosphere is inviscid. The relaxation temperature field is zonally symmetric and is computed off line from a separate model.

In spite of these simplifications the model zonal mean and eddy statistics are very similar to those of more sophisticated models.

To assess the nature of the model's interannual variability we have looked at the hemispherically integrated zonal (ZKE) and eddy (EKE) kinetic energies per unit mass. In the southern hemisphere EKE is lowest during summer (~10 mks units) and then steadily rises during fall. However, just before winter it peaks (~35) and then declines to a local minimum (~25) at solstice. It remains near this minimum until mid winter, when it rises, dramatically reaching ~100 by spring. Following this there is an abrupt decline in EKE, which appears to be related to a weakening in the wave-3 disturbances. The decline is short-lived, however, as EKE rises dramatically once more but this time to even higher values (~125) by mid spring. This is the largest value of EKE in either hemisphere at any time of year. The resurgence in EKE at this time is not well understood, but it occurs at a time when ZKE is rapidly declining and wave-1 disturbances are rapidly growing. This suggests that barotropic processes are playing a role, but more analysis is needed to confirm this.

Interestingly, the EKE in the northern hemisphere shows a similar seasonal pattern, although the amplitude of the fluctuations is much less pronounced. Furthermore, the springtime peak in northern hemisphere EKE (~50) is comparable to that during late fall and mid winter, which is considerably different from that in the southern hemisphere.

We have also looked at the maximum and minimum EKE for any given seasonal date for the 10-year simulation. This we take to be a measure of the magnitude of interannual variability. The greatest variability occurs in the southern hemisphere during the late winter and spring seasons. At this time, EKE can be as high as 150 and as low as 50. Thus, southern-hemisphere EKE can vary from year to year by as much as a factor of 3. Evidently, this variability is also manifest in the model's "surface stress," which also shows similar variations.

We find these results to be very intriguing, particularly since they occur in a model with simple but repeatable forcing. They suggest that the martian climate system has enough nonlinearity to produce substantial interannual variability.

REGARDING TRACER TRANSPORT IN MARS' WINTER ATMOSPHERE IN THE PRESENCE OF NEARLY STATIONARY, FORCED PLANETARY WAVES. J. L. Hollingsworth¹, R. M. Haberle¹, and H. C. Houben², ¹NASA Ames Research Center, Moffett Field CA 94035, USA, ²Space Physics Research Institute, Sunnyvale CA 94087, USA.

Large-scale transport of volatiles and condensates on Mars, as well as atmospheric dust, is ultimately driven by the planet's global-scale atmospheric circulation. This circulation arises in part from the so-called mean meridional (Hadley) circulation that is associated with rising/poleward motion in low latitudes and sinking/equatorward motion in middle and high latitudes [1]. Intimately connected to the mean circulation is an eddy-driven component due to large-scale wave activity in the planet's atmosphere. During winter this wave activity arises both from traveling weather systems (i.e., barotropic and baroclinic disturbances) [2] and from "forced" disturbances (e.g., the thermal tides and surface-forced planetary

waves) [3,4]. In this paper we investigate possible contributions to the effective (net) transport circulation from forced planetary waves.

A three-dimensional global spectral primitive equations model is applied in this investigation to simulate "perpetual" northern and southern winter solstice conditions. Previously this model has been applied to investigate the sensitivity of winter transient-eddy activity to changes in thermal dissipation and to examine the transport circulation associated with traveling baroclinic eddies [5,6]. Recently the model has been modified to include kinematic effects of topography using a terrain-following vertical coordinate (i.e., effectively $\log-\sigma$, where $\sigma = p/p_s$). In the calculations to be presented, a trapezoidal truncation of total wavenumber 16 and zonal wavenumber 6 is used and simplified physics are applied: Thermal radiative forcing is prescribed in the form of constant Newtonian cooling, and momentum drag is specified in the form of a height-dependent Rayleigh friction. Planetary-scale surface zonal asymmetries in Mars' topography excite planetary waves having deep vertical structure. Because of the nature of the mean circulation and the planet's size, forced responses can be "global" (occurring in both eastern and western hemispheres) and can become "focused" into a finite latitude band in the winter extratropics, similar in respects to results of a linear analysis of forced stationary waves on Mars [4]. In the presence of a nonzero mean meridional circulation, we evaluate the effective steady transport circulation associated with the planetary-wave activity and compare it with the so-called "residual" mean meridional circulation, which is frequently used as an approximation to the former. In particular, we examine potential hemispheric asymmetries in the net transport circulation due to differences in the wave forcing in northern and southern hemispheres. We also investigate changes to the effective transport under highly dusty, northern winter conditions. Potential impacts steady planetary waves can have on the poleward transport of tracers during northern and southern winter will be discussed.

References: [1] Haberle R. M. et al. (1993) *JGR*, 98, 3093-3124. [2] Barnes J. R. et al. (1993) *JGR*, 98, 3125-3148. [3] Zurek R. W. and Haberle R. M. (1988) *J. Atmos. Sci.*, 45, 2469-2485. [4] Hollingsworth J. L. and Barnes J. R. (1993) *J. Atmos. Sci.*, submitted. [5] Haberle R. M. et al. (1993) in preparation. [6] Houben H. et al. (1989) *Eos*, 70, 1179-1180.

ANALYZING MARTIAN WINDS AND TRACER CONCENTRATIONS USING MARS OBSERVER DATA.
H. Houben, Space Physics Research Institute, Sunnyvale CA 94087-1315, USA.

During the course of a day, the Mars Observer spacecraft will acquire globally distributed profiles of the martian atmosphere. It is highly desirable that this data be assembled into synoptic weather maps (complete specifications of the atmospheric pressure, temperature, and winds at a given time), which can in turn be used as starting points in the study of many meteorological phenomena. Unfortunately, the special nature of the Mars Observer data presents several challenges above and beyond the usual difficult problem of data initialization.

Mars Observer atmospheric data will consist almost exclusively of asymptotic vertical profiles of temperatures (or radiances) and pressures, whereas winds are generally in balance with horizontal

gradients of these quantities (which will not be observed). It will therefore be necessary to resort to dynamical models to analyze the wind fields. As a rule, data assimilation into atmospheric models can result in the generation of spurious gravity waves, so special steps must be taken to suppress these. In addition, the asymptotic nature of the data will require a four-dimensional (space and time) data assimilation scheme. The problem is to find a full set of meteorological fields (winds and temperatures) such that, when marched forward in time in the model, they achieve a best fit (in the weighted least-squares sense) to the data.

The proposed solution is to develop a model especially for the Mars Observer data assimilation problem. Gravity waves are filtered from the model by eliminating all divergence terms from the prognostic divergence equation. This leaves a diagnostic gradient wind relation between the rotational wind and the temperature field. The divergent wind is diagnosed as the wind required to maintain the gradient wind balance in the presence of the diabatic heating. The primitive equations of atmospheric dynamics (with three principal dependent variables) are thus reduced to a simpler system with a single prognostic equation for temperature—the variable that will be best observed. (This balance system was apparently first derived by Charney as a first-order Rossby number expansion of the equations of motion.) Experience with a full primitive equation model of the martian atmosphere indicates that a further simplification is possible: at least for short-term integrations, the model can be linearized about the zonally symmetric basic state.

The above linearized spectral model has the property that the solution at any point (in space and time) is a known linear function (represented by a matrix operator) of the initial state. Finding the initial state that best fits the observed data requires an inversion of this matrix. If the problem is overdetermined (more data points than unknowns), the best fit in the least-squares sense is obtained by a generalized inverse (singular value decomposition) of the matrix. The proposed model has 14 vertical levels, 7 zonal waves, and 16 meridional modes, for about 1500 complex variables. The PMIRR instrument alone, with approximately 1000 vertical profiles per day, should easily provide enough data in a day to overdetermine the model. Thus, a daily weather map appears to be quite feasible. (Of course, it is probable that there are errors in this model. There is, however, a generalization of the singular value decomposition—the total least-squares solution—that allows for errors in the model as well as in the observations.) There are two classes of motion in the martian atmosphere that are not well represented by the gradient wind relation—atmospheric tides and equatorial Kelvin waves. These modes must be independently modeled and removed from the observations before the assimilation procedure is performed. (The fact that Mars Observer will orbit at a nearly constant time of day will inhibit the direct observation of atmospheric tides in any case.)

Atmospheric tracers, such as water vapor and dust, are easily incorporated into the balance system model with continuity equations. The sole difficulty arises from the possibility that a spectral tracer model will show negative tracer amounts at various points. It is therefore necessary to constrain the solution of the least-squares problem so that the tracer concentrations at all of the model's (~620) transform grid points are positive. This is facilitated by the introduction of surface source/sink terms into the model. Again, there are mathematical algorithms available for the solution of this problem. The above program indicates that the assimilation of Mars Observer

profiles into daily synoptic maps of temperature, winds, and tracers is quite feasible, if computationally demanding.

THE ANNUAL PRESSURE CYCLE ON MARS: RESULTS FROM THE LMD MARTIAN ATMOSPHERIC GENERAL CIRCULATION MODEL. F. Hourdin, F. Forget, and O. Talagrand, Laboratoire de Météorologie Dynamique du CNRS, Ecole Normale Supérieure, Paris, France.

At Laboratoire de Météorologie Dynamique (LMD) in France we have been developing a General Circulation Model (GCM) of the martian atmosphere since 1989. The model has been described rather extensively elsewhere [1] and only the main characteristics are given here.

The dynamical part of the model, adapted from the LMD terrestrial climate model, is based on a finite-difference formulation of the classical "primitive equations of meteorology." The radiative transfer code includes absorption and emission by CO_2 (carefully validated by comparison to line-by-line calculations [2]) and dust in the thermal range, and absorption and scattering by dust in the visible range. Other physical parameterizations are included: modeling of vertical turbulent mixing, dry convective adjustment (in order to prevent vertical unstable temperature profiles), and a multilayer model of the thermal conduction in the soil. Finally, the condensation-sublimation of CO_2 is introduced through specification of a pressure-dependent condensation temperature. The atmospheric and surface temperatures are prevented from falling below this critical temperature by condensation and direct precipitation onto the surface of atmospheric CO_2 . The only prespecified spatial fields are the surface thermal inertia, albedo, and topography.

The first simulations were performed for a visible dust optical depth constant in both space and time, $\tau_{\text{vis}} = 0.2$, a value typical of clear-sky conditions [3]. Starting from an isothermal state at rest, without polar caps, the model quickly adjusts (in less than one martian year) to a regime in which the annual atmospheric mass cycle, due to condensation of the atmospheric CO_2 into the polar caps, is essentially repeatable from one year to the next. This mass cycle is in great part responsible for the large-amplitude seasonal oscillations of the surface pressure recorded by the Viking landers. Those oscillations were rather well reproduced in those first simulations, as well as the synoptic pressure oscillations observed during winter that are due to traveling planetary waves [1]. The agreement with temperatures retrieved from the Mariner 9 infrared measurements is also very good.

However, the surface pressure cycle was found to vary strongly, with latitude. This meteorological contribution, due to internal mass redistribution, can be divided into two parts: the first one results from the modulation by temperature of the latitudinal pressure variations due to orography; the second one is a purely dynamical contribution due to geostrophic balance between the strong zonal winds and latitudinal pressure gradients [1]. These dynamical and orographic contributions appear to have comparable magnitudes and are stronger in high latitudes where the dynamical effect becomes predominant. At 75°S , for instance, the dynamical component contributes to a 25% temporal variation of the surface pressure over the course of the year, about the same magnitude as the variations due to the condensation-sublimation cycle. The two effects tend to reinforce each other in midlatitude and counteract

each other in polar regions. Longitudinal variations also strongly amplify the orographic effect.

More recent simulations were performed in order to test the sensitivity of the model to the most uncertain parameters and especially to the visible albedo of the ice, A_{ice} , and its thermal emissivity, ϵ_{ice} . Model results have shown that they strongly influence the energy and mass atmospheric budget [3,4]. In our simulations, the best agreement to Viking pressure data is obtained for very different values of these parameters for the two caps. Using $A_{\text{ice}} = 0.62$ and $\epsilon_{\text{ice}} = 0.6$ for the northern cap and $A_{\text{ice}} = 0.45$ and $\epsilon_{\text{ice}} = 0.76$ for the southern cap, very good agreement is achieved as shown in Fig. 1. The latitudinal time evolution of the edge of both caps is also very close to Viking orbiter data as shown in Fig. 2 (except at the very end of the recession phase). As already mentioned by other authors [4] these "best fit" values of the ice parameters must not be interpreted as real physical properties of ice materials since they also account for some model deficiencies and, in particular, for the nonrepresentation of CO_2 ice clouds, resulting from atmospheric

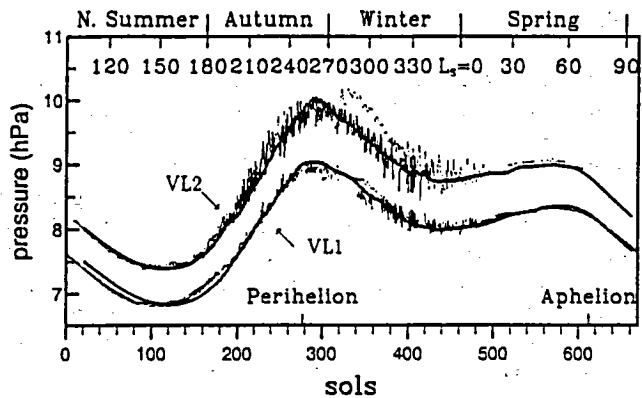


Fig. 1. A comparison of the time evolution of the pressure simulated at both Viking landing sites to that observed ("best-fit" simulation). The thin curves are the observed pressure for year 1 (dotted), 2 (solid) and 3 (dashed) of the mission. The black heavy curve is the simulated pressure, which has been smoothed by applying a 15-sols average. Sols are martian solar days; sol 0 corresponds to the landing of Viking 1.

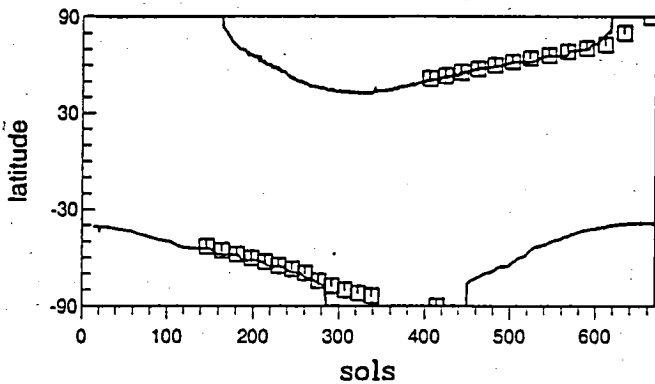


Fig. 2. The time evolution of the mean latitude of the polar cap boundaries as simulated by the LMD GCM and deduced, during cap recession, from Viking orbital imaging.

condensation during the cap formation. This may explain the very low value of the "best fit" emissivity of the northern cap, which has been observed to be preferentially covered by polar haze. The low emissivity will account for the trapping of thermal radiation by clouds during the formation phase. However, this value of emissivity is too low for the recession phase during which no atmospheric condensation occurs and would produce too fast a recession of the cap. This is compensated by a high value of the "best fit" albedo (which has a larger impact during the recession than during the formation phase since condensation essentially occurs in the polar night), which decreases the recession rate by reducing the part of the incoming solar radiation absorbed by the ice.

It must be noted that the dust amount has been kept at its clear-sky value $\tau_{vis} = 0.2$, whereas atmospheric dust content was observed to strongly increase during northern winter, even during the clear years of the Viking mission. This strong simplification could be relaxed in the future, either by specifying the dust atmospheric content as a function of time and space (for instance by using the results of the IRTM experiment aboard Viking [5] or results from future martian missions), or by modeling the atmospheric transport, which has not been done in the LMD GCM until now.

As far as the atmosphere is concerned, an important scientific by-product of future missions would be an accurate estimation of the atmospheric mass budget. The evaluation of the meteorological contribution to the temporal and spatial pressure variations will also be very useful since it contains indirect but accurate information on the near-surface winds and may help to validate the circulation models. Finally, the spatial results of future martian missions will be fully exploited only if they are used in conjunction with an adequate description of the physical laws of the atmosphere, as provided by an atmospheric general circulation model. This is currently done for weather forecasting using data assimilation methods. For Mars, since we are concerned with *a posteriori* analysis, the problem of the computational cost of the assimilation techniques is much less crucial than for operational forecasting and some powerful methods such as variational assimilation [6] may easily be used. The development of those methods for Mars is presently under study at LMD [7].

References: [1] Hourdin F. et al. (1993) *J. Atmos. Sci.*, in press. [2] Hourdin F. (1992) *JGR*, 97, 18319–18335. [3] Wood S. E. and Paige D. A. (1992) *Icarus*, 99, 1–14. [4] Pollack J. B. et al. (1993) *JGR*, 98, 3149–3141. [5] Martin T. Z. (1986) *Icarus*, 66, 2–21. [6] Talagrand O. (1992) In *Energy and Weather Cycles in the Climate System* (A. Raschke and D. Jacob, eds.), 187–213, NATO Advanced Study Institute. [7] Talagrand O. and Hourdin F. (1990) *International Symposium on Assimilation of Observations in Meteorology and Oceanography*, 578–580, World Meteorological Organization.

NORTHERN HEMISPHERE DUST STORMS ON MARS. P. B. James, University of Toledo, Toledo OH 43606, USA.

Dust storms in the northern hemisphere of Mars appear to be less common than the more familiar southern hemisphere storms, and essentially no activity north of about 30° latitude has been documented [1]. The data are, however, subject to an observational bias because Mars is near aphelion during oppositions, which occur during the most likely seasons for dust activity in the north.

The amount of dust activity in the northern hemisphere is clearly very relevant to the role of atmospheric transport in the dust cycle. The classic global storms that occur during spring in the southern hemisphere are observed to transport dust from sources in the southern hemisphere to sinks or temporary depositories in the north. The question of whether atmospheric transport can close the dust cycle, i.e., return the dust to the southern hemisphere sources on some timescale, is clearly relevant to the solution of the puzzle of how the dust storm cycle is modulated, i.e., why storms occur in some years but not in others.

There are data that suggest that the spring/early summer season in the northern hemisphere of Mars during the year following the major 1977 storms observed by Viking was very dusty. A number of observations of the vicinity of the receding north polar cap showed clear evidence of substantial dust activity in the sub-Arctic region.

Although some of the activity was less well organized and less extensive than what was observed near the south cap during spring, at least one set of observations define a regional dust storm event that, if merely an example of dust storms in the northern hemisphere, could play a crucial role in closing the dust cycle. Though the observations have been previously reported [2], their possible significance relative to the question of atmospheric dust transport justifies a review in this workshop. Observations on three consecutive orbits of Viking Orbiter 2 at $L_s = 65$ are consistent with a single storm moving to the south-southeast (prograde and equatorward) at an average speed of 6 m s⁻¹. The storm is observed in the region to the north of Olympus Mons and Alba Patera between 60° and 75° latitude and between 150° and 110° longitude.

Unfortunately there was no color coverage of this event, so no definitive conclusions on composition can be reached. The designation of this storm as a dust storm is based on its very low contrast with the surface and with the morphology, which is similar to other dust storms observed on the planet. The dust storm is not monolithic; rather, the storm is composed of many discrete billows similar in structure to those observed within the 1977a global storm observed by Viking.

The leading edge of the storm is defined by a very sharp front, and the trailing edge was also well defined. Since the coverage on any single orbit of the spacecraft was insufficient to image the entire leading or trailing edges of the storm, only a lower limit on the dimension transverse to the motion can be made; the largest observed dimension is roughly 500 km, but the geographical distribution of the three images suggests a considerably larger extent. The dust is more narrowly confined to a strip 350 km wide parallel to the direction of motion with a strong suggestion of expansion between the earliest and latest views.

With only one example in the class, the frequency of this sort of northern regional dust storm is clearly undetermined. Similarly, the question of whether these are annual events or whether they take place only in years following global storms is completely open. It is hoped that the synoptic monitoring provided by the MOC experiment will be able to answer the first question, though the answer will still be confined to only a single year with its own unique dust history.

References: [1] Martin L. J. and Zurek R. W. (1993) *JGR*, 98, 3221–3247. [2] James P. B. (1985) *Recent Advances in Planetary Meteorology*, Cambridge, 85–100.

THE INFLUENCE OF OROGRAPHY ON THE TRANSPORT OF ATMOSPHERIC CONSTITUENTS. M.M. Joshi, S. R. Lewis, and P. L. Read, Atmospheric, Oceanic and Planetary Physics, Clarendon Laboratory, Parks Road, Oxford OX1 3PU, UK.

Given the fact that martian orography varies over a range of two scale heights (cf., about one scale height on Earth), it is thought that on Mars some aspects of the circulation should be affected to a large degree by the presence of orography. Initial results from two numerical models are presented that illustrate the effect of orography on cross-equatorial transport on Mars.

On Earth, western boundary currents are found not only in the oceans as one would expect, but also in the troposphere, the most notable example being the East African Jet, which has an important effect on the monsoon circulation of the Eastern Indian Ocean [1].

Two models were used for this investigation: a simple GCM (hereafter referred to as the SGCM) and a simple one-level barotropic model (BM). The SGCM, originally developed by Hoskins and Simmons [2], solves the hydrostatic primitive equations on a sphere by representing model variables by spherical harmonics in the horizontal, with nonlinear terms being calculated in grid-point space. In the vertical, the model uses the σ coordinate system in finite-difference form. The model represents the radiative processes in the atmosphere by a Newtonian relaxation to a specified zonal mean temperature state, and surface drag by Rayleigh friction in the lowest model level.

BM is a nonlinear spectral barotropic model [3], which solves the barotropic vorticity equation on the sphere

$$D\zeta/Dt = -f \mathbf{V} \cdot \nabla (h/H) + (\zeta_0 - \zeta)/\tau \quad (1)$$

ζ_0 represents a specified zonal mean absolute vorticity state to which the model is relaxed over a timescale τ . h is the height of the orography and H is a scale height. The main advantage of this model is that many runs can be carried out relatively quickly and runs can also be carried out at spatial resolutions, which would be impractical with the SGCM.

Nonlinear barotropic boundary current theory states that, in the steady state, the width of an inertial (i.e., where friction is negligible) boundary current will be given by $(U/\beta)^{1/2}$. It is to be noted, however, that while the width of the jet is given by $(U/\beta)^{1/2}$, the width of the core of the jet, where most of the mass is transported, is much less than this [1] and so higher model resolution, as well as significantly changing the character of the orography that controls the jet, may actually be needed to resolve the core of the jet.

As an initial experiment, BM is initialized with a restoration ζ_0 corresponding to a constant small zonal velocity representative of that near the surface. The steady-state velocity vectors, overlaid on an orography contour plot, are shown in Fig. 1. The run is carried out at resolution T21, equivalent to a grid-point spacing of about 6° . It can be seen that there is a tendency for the cross-equatorial flow to form into a western boundary current, especially at about 90°W , i.e., at the eastern edge of the Tharsis plateau. The width of this current is approximately $(U/\beta)^{1/2}$. The effect of model resolution on this result can be tested by repeating this experiment at T42 or even T63.

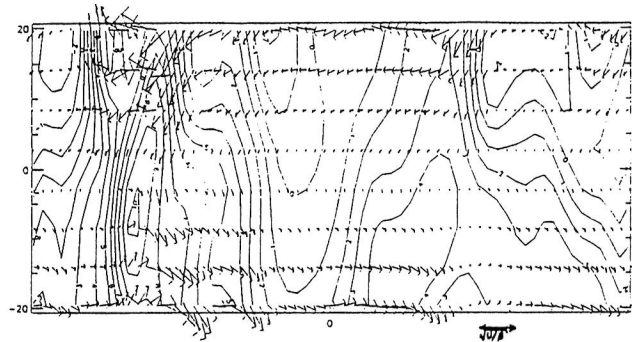


Fig. 1. Longitude/latitude plot of velocity vectors superimposed on orography contours (interval 1km): $(U/b)^{1/2}$ scale is shown at bottom, right.

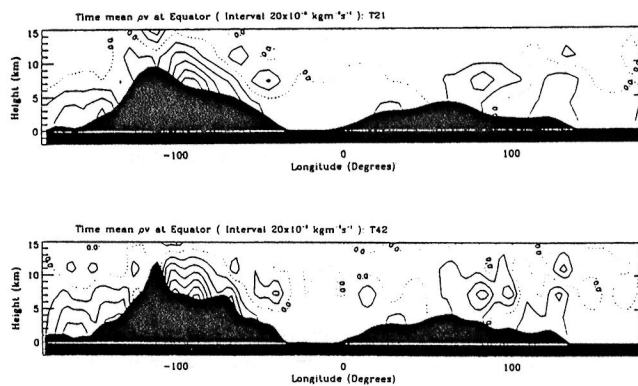


Fig. 2. Comparisons of cross-equatorial mass transport for SGCM model runs at T21 and T42.

While BM can show regions where the effect of orography is likely to be important, the SGCM is needed to show directly how orography affects mass transport as it is only in the SGCM that the mountains act explicitly as boundaries and not just as large vorticity forcing regions. Initial results compare favorably with the BM and do tend to show the presence of western boundary currents.

Initial SGCM results also suggest that runs at model resolution T21 give slightly less intense western boundary jets when compared to runs done at T42, as shown in Fig. 2. T21 runs, therefore, may not sufficiently resolve these boundary currents and hence not adequately model cross-equatorial mass transport.

The presence of these boundary currents in the tropics will have important implications for mass transport in the lower branch of the Hadley Cell on Mars, and, as this cell plays such an important role in the martian circulation, on the cross-equatorial transport of atmospheric constituents such as dust and water vapor, it is important to model them as accurately as possible.

References: [1] Anderson D. L. T. (1980) Orographically Controlled Cross-Equatorial Flow, *G.A.R.P. Publications Series*, 23, 317-355. [2] Hoskins B. J. and Simmons A. J. (1975) *Q. J. R. Met. Soc.*, 101, 637-655. [3] James I. N. (1988) *Q. J. R. Met. Soc.*, 114, 619-637.

TEMPORAL AND SPATIAL MAPPING OF SURFACE ALBEDO AND ATMOSPHERIC DUST OPACITY ON MARS. S. W. Lee¹, R. T. Clancy¹, and G. R. Gladstone², ¹Laboratory for Atmospheric and Space Physics, University of Colorado, Boulder CO 80309, USA, ²Southwest Research Institute, P.O. Drawer 28510, 6220 Culebra, San Antonio TX 78228, USA.

The Mariner 9 and Viking missions provided abundant evidence that eolian processes are active over much of the surface of Mars [1,2]. Past studies have demonstrated that variations in regional albedo and wind-streak patterns are indicative of sediment transport through a region [3,4], while thermal inertia data [derived from the Viking Infrared Thermal Mapper (IRTM) dataset] are indicative of the degree of surface mantling by dust deposits [5-9]. The visual and thermal data are therefore diagnostic of whether net erosion or deposition of dust-storm fallout is taking place currently and whether such processes have been active in a region over the long term. These previous investigations, however, have not attempted to correct for the effects of atmospheric dust loading on observations of the martian surface, so quantitative studies of current sediment transport rates have included large errors due to uncertainty in the magnitude of this "atmospheric component" of the observations.

We have developed a radiative transfer model that allows the atmospheric dust opacity to be determined from IRTM thermal observations. Corrections for the effects of atmospheric dust loading on observations of surface albedo can also be modeled. This approach to determining "dust-corrected surface albedo" incorporates the atmospheric dust opacity, the single-scattering albedo and particle phase function of atmospheric dust, and the bidirectional reflectance of the surface, and accounts for variable lighting and viewing geometry. The most recent dust particle properties [10,11] are used. The spatial and temporal variability of atmospheric opacity (τ) strongly influences the radiative transfer modeling results. This approach allows τ to be determined at the highest spatial and temporal resolution supported by the IRTM mapping data; maps of "dust-corrected surface albedo" and atmospheric opacity can be constructed at a variety of times for selected regions. Information on the spatial and temporal variability of surface albedo and atmospheric opacity, and inferences of the amount of dust deposition/erosion related to such variability, result.

Analyses of IRTM mapping observations of the Syrtis Major region, covering a time span of more than a martian year, will be presented.

References: [1] Veverka J. et al. (1977) *JGR*, 82, 4167-4187. [2] Thomas P. et al. (1981) *Icarus*, 45, 124-153. [3] Lee S. W. et al. (1982) *JGR*, 87, 10025-10042. [4] Lee S. W. (1986) *Symposium on Mars: Evolution of its Climate and Atmosphere* (V. Baker et al., eds.), LPI Tech. Rpt. 87-01, 71-72. [5] Kieffer H. H. et al. (1977) *JGR*, 82, 4249-4295. [6] Christensen P. R. (1982) *JGR*, 87, 9985-9998. [7] Christensen P. R. (1986) *JGR*, 91, 3533-3545. [8] Christensen P. R. (1986) *Icarus*, 68, 217-238. [9] Jakosky B. M. (1986) *Icarus*, 66, 117-124. [10] Clancy R. T. and Lee S. W. (1991) *Icarus*, 93, 135-158. [11] Clancy R. T. et al., this volume.

DYNAMICS OF THE ATMOSPHERE OF MARS: REVIEW OF SOME OUTSTANDING PROBLEMS. C. B. Leovy, Department of Atmospheric Sciences, University of Washington, Seattle WA 98195, USA.

Theoretical and modeling studies based on fragmentary data are responsible for our current level of understanding of the dynamics of Mars' atmosphere at the planetary scale. Largely because the boundary conditions and governing parameters are such that the large-scale circulation regime is similar to that of Earth, it has been possible to derive a remarkable amount of information from a relatively small number of observations [1]. Nevertheless, the level of detail available from theoretical and modeling studies far exceeds the validation capability of existing data. Global observations from Mars Observer instruments are expected to go far to remedy this mismatch. This review will present and examine several outstanding dynamical questions, which Mars Observer measurements should help to answer. These include: What are the temporal and three-dimensional spatial distributions of thermal tides? What is the distribution of momentum flux divergence due to internal gravity waves? Are normal modes an important component of the general circulation? If so, how do they vary with season? Do normal modes contribute to the initiation of planetary-scale dust storms? What are the details of the global circulation response to large and rapid injections of dust? Current understanding of these problems, the potential role of Mars Observer observations for addressing them, and the implications of answers for our understanding of the present climate and past climate regimes will be discussed.

References: [1] Zurek et al. (1992) in *Mars* (H. Kieffer et al., eds.), 835-933, Univ. of Arizona.

MODELING AND DATA ASSIMILATION FOR MARS OBSERVER. S. R. Lewis and P. L. Read, Atmospheric, Oceanic and Planetary Physics, Department of Physics, University of Oxford, Parks Road, Oxford OX1 3PU, UK.

The Mars Observer mission will return a substantial set of meteorological data for the atmosphere of Mars, principally in the form of thermal infrared soundings from the Pressure Modulator Infrared Radiometer (PMIRR). The dataset will enable global studies of a range of dynamical and physical phenomena in the martian atmosphere. The polar orbital configuration of Mars Observer, however, means that the coverage of the martian atmosphere and surface by remote sounding instruments will be asynchronous. This leads to difficulties of interpretation when studying synoptic-scale phenomena with timescales of a few days. In an attempt to overcome such problems we propose to use data assimilation techniques, as currently employed for operational weather forecasting on the Earth, in conjunction with a Martian General Circulation Model (MGCM) that is under development at Oxford and Reading Universities. An overview of the model and assimilation scheme will be given, with reference to problems encountered so far in applying such methods to remote-sensing observations of the martian atmosphere.

The MGCM is based on a semispectral primitive equations model [1], which covers the surface to 80 km altitude, using about 20 σ levels in the vertical, and with a triangular spectral truncation

at wavenumber 42 in the horizontal, equivalent to a grid spacing of 2.8° in latitude and longitude. The resolution is chosen to be somewhat greater than that necessary to resolve the smallest features potentially visible in the PMIRR data in order to model realistically the effects of topography, etc. The martian surface is represented using the U.S. Geological Survey Digital Topographic Map (DTM). Some experiments with a simple form of the model are described in a companion submission (Joshi et al.). Parameterization schemes for poorly understood processes are kept simple wherever possible. New schemes for the MGCM are under development in collaboration with a small group at Reading University. These include a boundary layer scheme, a dry convection scheme, a diffusive soil model, and a scheme for orographic gravity wave drag. The radiation scheme will initially be based on that developed at Laboratoire de Météorologie Dynamique, Paris [2], with the possibility of further refinement to include the effects of nonlocal thermodynamic equilibrium in the upper atmosphere in collaboration with colleagues at Granada University.

Data assimilation will be conducted using a modified form of the Analysis Correction Scheme that is in current operational use at the U.K. Meteorological Office [3]. This scheme is an approximation to the optimum analysis, which involves a form of successive-correction iterated between each time step of the model. Continuous (asynoptic) repeated insertion is conducted sequentially, assimilating each measurement at the time and place it is valid without prior interpolation. Observational increments to the model are spread in time and space by empirically determined functions with scales that depend on the difference between the current model time and the time at which the data are valid. Observations typically enter the model five hours before they become valid with a low weight and with their influence spread over large horizontal scales. As an observation's valid time approaches, its weight increases and the scale it affects becomes smaller. Finally, an observation is discarded about one hour after the model has passed its valid time. The weight of each observation is scaled by the relative magnitudes of observational and forecast model error. Within each cycle of the assimilation scheme each model variable is analyzed sequentially followed by the derivation of multivariate increment fields for dynamical balance in order to avoid losing much of the newly introduced information. For example, following the analysis of the temperature field from PMIRR soundings, the thermal wind equation will be used to derive velocity increments in balance with the temperature increments (Fig. 1).

The Analysis Correction Scheme has been found to produce improved analyses in the Southern Hemisphere on Earth compared to the previous Optimum Interpolation scheme in use at the U.K. Meteorological Office, primarily because observational increments are spread over larger areas. In the case of Mars, however, there will be no surface observations and the use of satellite temperature soundings alone may introduce particular problems. Surface pressure measurements are strictly required for direct information about the barotropic component of the circulation, and for verification of the mass of the model atmosphere, which otherwise will depend on the highly uncertain parameterizations of atmospheric CO_2 condensation and sublimation in polar regions. Estimates of surface pressure may be retrieved from PMIRR nadir observations and will be used by the assimilation scheme whenever possible. Radio occultation

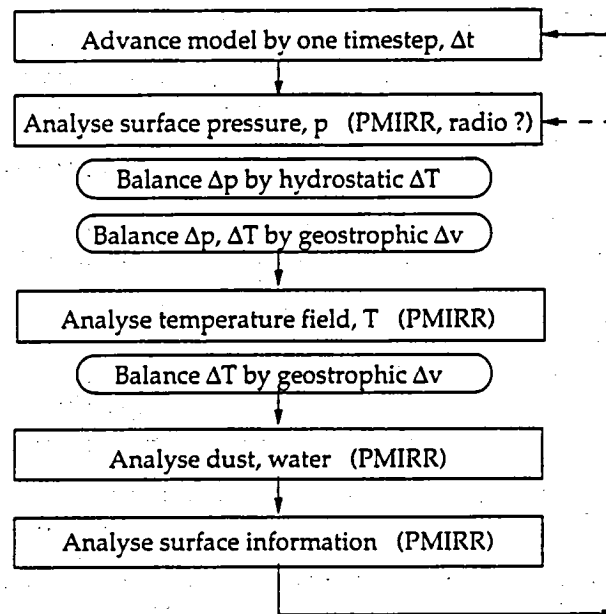


Fig. 1. Assimilation scheme cycle with multivariate balancing increments.

measurements may also be used to derive more accurate surface pressures at a few locations per sol at high latitudes; these measurements will also be assimilated if available.

Trials of the scheme are currently being conducted using synthetic data generated from parallel model runs. In future it will be important to test the assimilation scheme with artificial data generated by a different model in order to avoid the "identical twin" problem. Once the Mars Observer spacecraft is in its mapping orbit and verified retrievals of PMIRR data are routinely available (around early 1994) the assimilation scheme and model may be run in batch mode, processing about one week's data in a day on a dedicated workstation. Typical output from the assimilation will consist of fields as represented in the model (velocity, temperature, and surface pressure) stored at regular intervals from which derived quantities and diagnostics (potential vorticity, energy budgets, transport of heat, momentum and material tracers, Eliassen-Palm fluxes, etc.) may be calculated and which may be used, for example, as initial states for further independent model studies.

Major scientific objectives to be addressed during the course of the mission will include (1) determination of the role of transient baroclinic waves in heat and momentum transport on Mars, (2) the factors influencing their spatial and temporal regularity, and (3) the influence of surface orography on mass transport and of other major meteorological variables and tracers (see also the companion contribution by Joshi et al.). It is also hoped to make use of the zonally averaged assimilated transport fields in conjunction with retrieved fields of water vapor from PMIRR in studies of the synoptic and seasonal transport of water during the Mars Observer period.

References: [1] Hoskins B. J. and Simmons A. J. (1975) *Q. J. R. Met. Soc.*, 101, 637-655. [2] Hourdin F. (1992) *JGR*, 97, 18319-18335. [3] Lorenc A. C. et al. (1991) *Q. J. R. Met. Soc.*, 117, 59-89.

MARS OPERATIONAL ENVIRONMENTAL SATELLITE (MOES)—A POST-MARS OBSERVER DISCOVERY MISSION. S. S. Limaye, University of Wisconsin-Madison, Madison WI 53706, USA, and the MOES Team.

The study of the general circulation of planetary atmospheres in terms of the constituent atmospheric transport processes has been a subject just beyond our reach for most planets, despite the numerous spacecraft missions. The primary reason has been the lack of adequate systematic spatial and temporal observations. We do not yet have any systematic observations of important martian atmospheric phenomena such as regional and global dust storm evolution and decay stages, planetary-scale waves, and cloud systems. Yet such systems are key components of the processes invoked to explain major features in the evolution of the martian environment such as the polar layered terrain and regional albedo changes. Mars Observer (MO) presents the first real opportunity of making global atmospheric and surface observations, but its Sun-synchronous polar orbit limits the temporal and global coverage and resolution. Observations $\pm 60^\circ$ latitudes are limited to within about an hour of 2:00 a.m. and 2:00 p.m. local time throughout the mission life. Thus while the diurnal tidal amplitudes will be well determined (supplemented by modeling), the precise phase relationships of the diurnal components and the amplitudes and phases of the semidiurnal tides and other higher-frequency waves and the associated atmospheric transports will not be sampled. At polar latitudes the high-inclination orbit provides substantial overlap so that the polar processes will indeed be well observed in local time over the mission duration, but their connection to the lower latitudes will remain largely unknown.

Lacking an infrared imaging system, MO can sample only a fraction of the martian globe with nighttime observations of the atmospheric phenomena from the infrared channels of the Pressure Modulated Infrared Radiometer (PMIRR) and the Thermal Emission Spectrometer (TES). These will supplement the daytime global synoptic and high-resolution local visible images from the Mars Observer Camera (MOC). Similarly, the investigation of the global water vapor transport is also limited due to observational and orbital constraints. Mars Observer is more capable of yielding seasonal cycles of the martian atmosphere than the shorter-term atmospheric and surface phenomena that occur on a timescale of minutes and hours to days. These deficiencies are addressed by a new Discovery-class mission that is currently being investigated.

Mars Operational Environmental Satellite (MOES) is a Discovery concept mission that is designed to observe the global short-term weather phenomena on Mars in a systematic fashion. Even after the Mariner, Viking, and, soon, Mars Observer missions, crucial aspects of the martian atmosphere will remain unobserved systematically. Achieving a better understanding of the cycles of dust, water vapor, and ices on Mars requires detailed information about atmospheric transports of those quantities associated with the weather systems, particularly those arising in mid latitudes during fall and winter. It also requires a quantitative understanding of the processes responsible for the onset and evolution of dust storms on all scales. Whereas on Earth the system of geosynchronous and polar orbiting satellites provides continuous coverage of the weather systems, on Mars the time history of important events such as regional and global dust storms remains unobserved.

To understand the transport of tracers in the martian atmosphere, and particularly to identify their sources and sinks, it is necessary to have systematic global, synoptic observations that have yet to be attained. Clearly these requirements are not easy to achieve from a single spacecraft in orbit, but if we focus on specific regions of the planet, e.g., polar vs. low and mid latitudes, then it is possible to attain a nearly ideal coverage at a reasonable spatial and temporal resolution with a system of just two satellites. Mars Observer is about to yield good coverage of the polar latitudes, so we focus initially on the region not covered well in terms of diurnal coverage, and in terms of desired observations. These observations will provide the initial data for the numerical models of the martian weather and climate that can be verified only with better temporal and spatial data.

To begin with, we desire observations of Mars and its atmosphere at a spatial resolution of about 3–5 km for visible and infrared imaging (for nighttime coverage) so that the evolution cycles of the dust storms and cloud systems on different scales can be observed both during the day and night. In addition, we desire vertical profiles of temperature, water vapor, and dust globally, but at a lower horizontal resolution, somewhere between 30 and 75 km, corresponding to a grid point resolution between 1° and 2.5° , comparable to the resolution of the numerical models. For the Earth atmospheric weather models the initial state is determined from the global network of surface and upper stations and augmented with the satellite observations of winds (cloud drift) and vertical temperature profiles at synoptic times. On Mars, lacking a synoptic observation network of stations, all the data need to be determined from the satellite observations, which are difficult to attain at the same observation time at all locations, which necessitates the use of assimilation of these observations in the numerical model. The minimum temporal resolution of these observations necessary to resolve the diurnal and the semidiurnal components adequately is about three hours (one eighth of the martian day, sol). If these are to be obtained from a satellite in a low-altitude orbit as opposed to an aerosynchronous satellite, the temporal resolution in essence defines a maximum allowable altitude on the orbit of the single satellite. The altitude of the orbit also determines how much of the planet one is able to observe for different orbit inclinations.

The MOES mission concept design is based upon these considerations and the payload is chosen to meet the observational requirements. With its emphasis on short-term weather and time-of-day variations, MOES complements Mars Observer and Mars '94 missions, which are optimal for seasonal-scale variations. A single MOES spacecraft deployed in a retrograde low-inclination (155°), 216-minute orbit will yield observations of Mars surface and atmosphere within $\pm 75^\circ$ latitudes up to 8 times per martian day. To observe the polar latitudes at the same time will require an additional spacecraft in a polar orbit that can be Sun-synchronous. Launch is on a Delta II 7925 and can take place in any of the Mars windows that recur. Orbit insertion at Mars is relatively easy due to the low inclination of the orbit, and no plane changes are required such as for MO. The candidate spacecraft is three-axis stabilized and is nadir oriented to provide the instrument coverage.

The MOES primary science payload consists of two instruments, Mars Imaging Radiometer (MIR), a multispectral imaging system (five channels), and Microwave Atmospheric Sounder (MAS), a multispectral microwave sounder to determine the vertical profiles

of temperature and water vapor by passive sounding. Both are identical twins of current Earth satellite counterparts with the exception of the filter set. There are two instruments that currently provide the capability that MIR is required to have: the AVHRR being flown on the NOAA polar orbiting satellites and the VIRS on TRMM (to be launched in 1996). For Mars imaging applications we desire two visible (0.45 and 0.59 μm) and three infrared wavelengths (6.9, 7.7, and 9.3 μm). The infrared channels are chosen for optimal coverage of the surface, water vapor, and atmospheric dust.

The Microwave Atmospheric Sounder is similar to the 183-GHz water vapor sounding instrument SSM/T2 currently in operation on the DMSP satellites and also has a separate receiver (230.5 GHz CO line) for deducing the martian atmospheric temperature profiles. Use of the CO channel for determining thermal structure is superior to the use of passive infrared techniques as it is unaffected by atmospheric dust and water vapor. The usefulness of the 183-GHz water vapor line to determine the atmospheric water vapor content on Mars has already been demonstrated by [1] from Earth-based observations using the VLA. A combined analysis of the infrared radiances and the temperature and moisture profiles will yield estimates of the dust content. The primary payload is thus capable of satisfying the observational requirements.

The visible and infrared imaging provides coverage of all martian latitudes within $\pm 75^\circ$ up to eight times per sol by cross-track scanning with a nadir resolution of 4×4 km. Spatial coverage of temperature and moisture profiles is also obtained by cross-track scanning, but at a lower resolution of about 40×40 km at nadir. Additionally, MOES is occulted as seen from Earth on every orbit due to its low inclination, and provides independent estimates of high-vertical-resolution temperature profiles of the martian atmosphere that will be used for calibrating the microwave temperature profiles and dust abundance.

Finally, the nominal orbit chosen for this mission will place MOES in sight of all the surface stations (within $\pm 75^\circ$) planned to be deployed by MESUR and MARSNET for as much as 40 min per orbit, or more than 5 hr per martian day, allowing ample opportunity to collect the data using its omnidirectional antennas for relay to the DSN using the High Gain Antenna. For coverage of the polar latitudes and also to receive the data from the polar surface stations, a second MOES spacecraft in a polar orbit is required and the two together would provide complete coverage of the planet. Thus MOES mission(s) complement(s) not only the presently planned Mars orbiting missions in terms of science, but will also provide a global context for the MESUR observations, as well as be capable of providing a relay service for the surface network data.

The mission operations plan is simple and essentially fixed: The two nadir-looking instruments observe continuously and the data are stored in onboard memory for transmission to the Deep Space Network (DSN) utilizing a single 34-m station pass per day. The HGA can support data rates from 587–17.3 kbps using the 34-m DSN stations for Earth-Mars range between 0.45–2.62 AU. We envision routine spacecraft operations to be handled by the Jet Propulsion Laboratory (JPL) and the science data to be processed at the University of Wisconsin-Madison and made available in real time to the scientific community as resources.

To summarize, MOES will yield spatially and temporally resolved observations of atmospheric and surface temperatures, and vertical profiles of temperature and water vapor, as well as estimates of dust abundance at all longitudes. These observations will

enable determination of the atmospheric transports by the martian general circulation, enable better characterization of the martian surface properties through infrared and visible observations, and provide crucial data for the initialization and verification of martian weather and climate models. This the scientific return is complementary to the other missions to Mars of the past and those currently underway. By utilizing existing Earth applications instruments for martian application, substantial cost savings are expected to be realized.

Acknowledgments: The MOES team currently consists of D. O. Muhleman (PI, MAS), A. Ingersoll (California Institute of Technology), D. McCleese, R. Kahn, and R. W. Zurek (JPL), M. Allison (NASA Goddard Institute for Space Studies), D. Paige (U. of California, Los Angeles), R. Haberle (NASA Ames Research Center), R. T. Clancy (U. of Colorado, Boulder), H. Revercomb, L. Sromovsky, S. Ackerman, and C. Hayden (U. of Wisconsin-Madison). VIRS, one of the candidates for MIR is being built by Santa Barbara Research Center (S. Silverman) for NASA's TRMM mission to be launched in 1996, while the AVHRR on NOAA polar satellites are built by ITT (Ft. Wayne, Indiana). Millitech (South Deerfield, MA) will build the MAS. Spacecraft design support has been provided by TRW (C. Lillie) while mission design support has been provided by S. Weinstein (JPL).

References: [1] Clancy et al. (1993) *Icarus*, 100, 48–59.

A STUDY OF CLOUD MOTIONS ON MARS, II: SOME EXAMPLES OF OBSERVATIONS AND ANALYSES SINCE 1969. L. J. Martin, Lowell Observatory, Flagstaff AZ 86001, USA.

The purpose of this paper is to remind everyone of the varied database on cloud motions that does exist but has often been underused in dynamical studies. Some striking examples of these cloud motions will be described. As the title implies, an earlier study was made by the author, with W. A. Baum, to analyze observations of martian cloud motions [1]. That research was supported by the Mariner missions in the late 1960s under a contract with the Jet Propulsion Laboratory. Compared to data acquired since that study, the data used were weak and the conclusions were limited. This was primarily because the only observations available were sparse and noncontiguous. That project was completed in 1969; during that same year, Lowell Observatory, with NASA support, initiated a more comprehensive observing program under the direction of W. A. Baum [2]. This International Planetary Patrol Program established a network of observing stations around the world that could provide nearly continuous observations of Mars throughout its apparitions. The primary objective of this network was to overcome the difficulties in attempting to document the motions of atmospheric activity using intermittent data. The network aspect of the Planetary Patrol tapered off after only three Mars oppositions, but observations from that period still provide the best data available, from any source, on martian cloud motions.

Using the Planetary Patrol data from 1969, the hourly motions of the north polar hood clouds were mapped for each day for a period of several months [3]. During the same period, movements of the nonpolar clouds were also mapped hourly. Of greater interest, however, were the hourly cloud positions seen in the developing stages of the great planet-encircling dust storms of 1971 [4] and

1973 [5]. Maps of these motions were compiled for the first 20 days of each of these storms. After 20 days, these storm clouds began to merge into continuous dense hazes on these Earth-based images. This made it impractical to continue delineating individual clouds, but because of those early studies, the motions of the 1971 and 1973 planet-encircling storms are better documented than the motions of any other martian dust storms. Daily diurnal expansions of these storms showed them moving farther west each day, although apparently retreating to the east before rotating into view each morning. During these early stages of storm development, condensate clouds (blue-filter images) were often seen in association with, but usually separate from, the dust clouds (on red-filter images).

The extent of transport of dust and condensates within these cloud motions is not straightforward. Since it is unlikely that dust particles moved at rotation speeds, we assume that the dust clouds brightened diurnally by a mechanism that was triggered by solar heating or some type of thermal tides. Therefore, observed cloud motions are probably not a measure of motions of materials that make up the clouds. Likewise, vertical motions of cloud particles cannot be measured, although they are readily apparent on the more detailed Viking images. Because initial clouds of the 1973 encircling storm sprang up at different locations within a few hours or days of each other [5], and because there is evidence from several datasets that the martian atmosphere became dustier prior to the first planet-encircling 1977 storm [6,7], it seems possible that the expansion of these storms feeds upon dust that is already in the atmosphere rather than either horizontal transport or the continuous uplifting of dust from the surface as the storm advances. Horizontal transport in itself probably requires too much speed and too much dust. Continuous uplifting requires a path of continuous surface locations that are both sources of dust and conducive to its uplift. Furthermore, given the special circumstances that are required to initiate a storm (based upon their infrequency [8]), it seems unlikely that they could form initial clouds at widely separated locations (as in 1973) without some common conditions. Since surface conditions do not appear to be similar, it seems possible that the atmosphere's increasing dust load might be. The similarity of the 1973 storm, observed from Earth, and the early 1977 storm, observed by Viking [9], allowed us to merge the data from sources with vastly different scales to provide a more comprehensive analysis of these events.

The Viking data include several other examples of cloud motion, including a few cases where imaging of the same cloud was repeated during the same orbit providing hourly measures of motion. Most of these cloud events have been analyzed individually, but a comprehensive catalog of all the cloud motions recorded by Viking has not yet been compiled. This is also true for recent Mars apparitions observed from Earth, although in the absence of a well-funded observing network, the number of documented cloud motion events is limited.

A unique Viking observation of a motion event was recorded during a single orbit at half-hour intervals. Several clouds, identifiable by their shadows, were seen over the south flank of Arsia Mons on the earliest of the three sequences of images. Half an hour later, on the second sequence, a small, bright cloud appeared directly over a rille and near the larger, earlier clouds (which showed movement since the earlier sequence). Because of the sudden appearance and special location of this new cloud, I had suggested that it might have been some type of eruption [10], although the possibility of something else like a dust devil cannot be ruled out. Within

the half-hour that followed, this cloud dissipated, but motions of the surrounding clouds had continued. Their apparent motions were radially outward from the location of the more discrete (but then gone) rille cloud. These images also suggest movement of what may have been surface material, within the same 1-hr interval.

A much smaller cloud motion was seen on two consecutive high-resolution Viking frames. The movement of the cloud and its shadow within the 4.5-s interval between frames is probably another unique observation for the Viking mission. This cloud also may have been an eruption [10] or a dust devil, although it was so small that it could not have been identified on any but the highest-resolution Viking images.

Other examples of cloud motion observed by Viking include the diurnal "bore waves" over the Tharsis area [11,12], a local dust storm in the Chryse area [13], and the much larger regional dust storm between 60° and 70°N that had been described as a moving "cold front" [14]. The Viking orbiters recorded a large number of different types of clouds, but only a small percentage of them on the same day or consecutive days, giving us only sporadic glimpses of measurable motion. However, these data on moving clouds provide graphic examples of the nature of atmospheric transport on Mars.

References: [1] Martin L. J. and Baum W. A. (1969) *Final Report B*, JPL Contract 951547, Lowell Observatory, Flagstaff, Arizona. [2] Baum W. A. et al. (1970) *Icarus*, 12, 437-439. [3] Martin L. J. and McKinney W. M. (1974) *Icarus*, 23, 380-387. [4] Martin L. J. (1974) *Icarus*, 22, 175-188. [5] Martin L. J. (1976) *Icarus*, 29, 363-380. [6] Martin L. J. et al. (1991) In *LPI Tech. Rpt. 92-02*, 99-100. [7] Martin T. Z. and Richardson M. I. (1991) In *LPI Tech. Rpt. 92-02*, 101-102. [8] Martin L. J. and Zurek R. W. (1993) *JGR*, 98, 3221-3246. [9] Martin L. J. and Baum W. A. (1978) *Bull. Am. Astron. Soc.*, 10, 551. [10] Martin L. J. (1981) *Third International Colloquium on Mars*, LPI Contribution 441, 145. [11] Hunt G. E. et al. (1980) *Nature*, 286, 352-364. [12] Kahn R. and Gierasch P. (1982) *JGR*, 87, 867-880. [13] James P. B. and Evans N. (1981) *GRL*, 8, 903-906. [14] James P. B. (1983) In *Recent Advances in Planetary Meteorology* (G. E. Hunt, ed.), 85-99, Cambridge.

EVIDENCE FOR DUST TRANSPORT IN VIKING IR THERMAL MAPPER OPACITY DATA. T. Z. Martin, Jet Propulsion Laboratory, California Institute of Technology, Pasadena CA 91109, USA.

Global maps of 9- μ m dust opacity derived from radiometric observations made by the Viking Orbiter IR Thermal Mapper instruments have revealed a wealth of new information about the distribution of airborne dust over 1.36 Mars years from 1976-1979 [1,2]. In particular, the changing dust distribution during major dust storms is of interest since the data provide a point of contact with both Earth-based observations of storm growth and with global circulation models.

The set of maps have a time resolution of 5° in L_s (areocentric solar longitude) necessitated by the need to cover a large area in a single map; they are consequently not ideal for the detailed study of dust transport. A different approach, retaining the full-time resolution of the data acquisition process, is to create a set of opacity time histories for selected sites of interest. An example of one of these histories, for a 10° × 10° area centered on latitude -40°, longitude

180°, is shown below for the L_s range 200°–350°. Crosses indicate data from the instrument on Viking Orbiter 1; triangles are from VO2. Although it is uncommon to obtain time resolution finer than about one day, and keeping in mind the effect of data coverage gaps that occur, several interesting points can be established with the set of opacity/time plots. There is a difference in the onset of the 1977b storm between northern and southern latitudes. Opacities remain high far longer at equatorial latitudes than in southern middle latitudes. Opacities at the Viking Lander sites were considerably smaller than those near the equator or to the south.

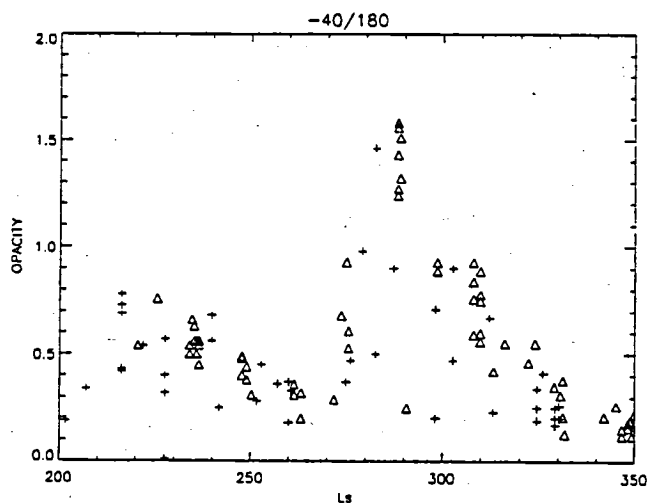


Fig. 1.

References: [1] Martin T. Z. (1986) *Icarus*, 66, 2. [2] Martin T. Z. (1993) *JGR*, in press.

RETRIEVAL OF TEMPERATURE PROFILES FROM MARTIAN INFRARED SPECTRA. W. W. McMillan¹, J. C. Pearl², and B. J. Conrath², ¹NAS/NRCNASA Goddard Space Flight Center, Code 693.2, Greenbelt MD 20771, USA, ²NASA Goddard Space Flight Center, Code 693.2, Greenbelt MD 20771, USA.

Introduction: In theory, a thermal emission spectrum of Mars (200–1600 cm^{-1}) contains a wealth of information about the composition and thermal structure of the atmosphere and surface. However, in practice, the ability to retrieve quantitative information from the spectrum is limited by a number of factors including (1) the ill-posed nature of the spectral inversion problem and the resulting nonuniqueness of all solutions; (2) assumptions built into any spectral inversion program; (3) uncertainties in surface pressure, temperature, and emissivity; and (4) uncertainties in the optical properties of atmospheric aerosols. Below, factors (1) and (2) are discussed as fundamental limitations on temperature retrievals from Mariner 9 Infrared Interferometer Spectrometer (IRIS) spectra.

In preparation for the Mars Observer mission and the return of tens of thousands of infrared spectra per day from the Thermal Emission Spectrometer (TES), we have developed a fast inversion algorithm to retrieve temperature structure and aerosol opacity from

the infrared spectra. The derived atmospheric models will be used to provide the atmospheric contribution to the TES spectra, so that the thermal emission spectra of the underlying surface can be determined for making mineralogical identifications. As a test of our algorithm we are undertaking a systematic analysis of the entire Mariner 9 Infrared Interferometric Spectrometer (IRIS) dataset of 21,000+ spectra. While portions of the IRIS dataset have been previously analyzed, the lack of a speedy and robust algorithm to invert the IRIS spectra to retrieve temperature profiles and aerosol opacities has been a major impediment to a truly comprehensive analysis.

Technique: Generally, the most prominent feature of an IRIS spectrum is the 15- μm (667- cm^{-1}) band of CO_2 (see Fig. 1). Because of our understanding of the CO_2 molecule, its optical properties can be calculated and the 15- μm band inverted to obtain an estimate of the vertical thermal structure of the martian atmosphere. Independent temperature profiles can be obtained by separately inverting the two sides of the band (P and R branches). In the absence of any other atmospheric opacity, these profiles should be identical to within the rms error resulting from measurement noise propagation (1–2 K) and uncertainties in the CO_2 absorption properties. However, in practice, additional wavenumber-dependent extinction due to absorption and scattering by atmospheric aerosols will cause the retrieved P and R branch profiles to differ. These differences will be exploited to assist in deriving information on opacity resulting from the presence of the particulates.

We use a constrained linear inversion (maximum entropy) technique in an iterative scheme to solve the radiative transfer equation to retrieve P and R branch temperature profiles for each spectrum. Given a temperature profile, the transmittances required for the radiative transfer equation are interpolated in pressure, temperature, and absorber mass from a lookup table of homogeneous path transmittances, using the Curtis-Godson approximation for the effective temperature and pressure. The homogeneous path transmittance lookup table is precomputed using an accurate line-by-line program. An iterative scheme is required because of the nonlinear relationship between temperature and measured radiances. For a spectrum taken through a clear atmosphere, a judicious choice of the

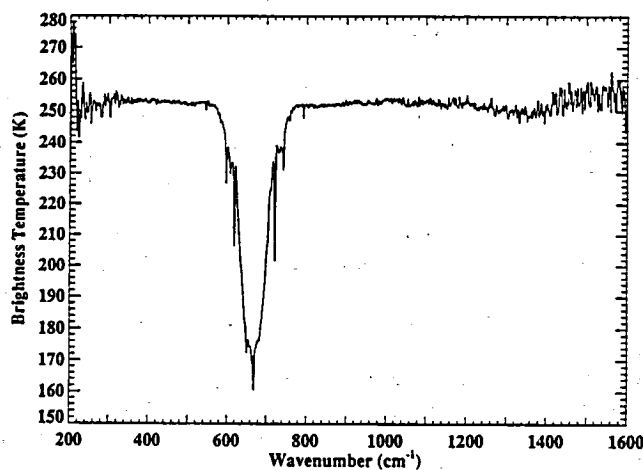


Fig. 1. Mariner 9 IRIS spectrum. DAS = 13507967.

damping factor and a "good" initial guess lead to convergence in 3-5 iterations.

Temperature Retrievals: The retrieval of a temperature profile proceeds by first selecting a set of wavenumbers for use in the inversion. The radiances measured at these wavenumbers (IRIS spectrum) are used in the iterative scheme until the computed radiances for a retrieved profile are within the noise equivalent spectral radiance ($NESR = 5 \times 10^{-8} \text{ W cm}^2 \text{ sr cm}^{-1}$) of the IRIS spectrum. The wavenumbers are chosen to provide the maximum coverage in altitude with a uniform distribution of contribution functions. An appropriate set of wavenumbers and the respective contribution functions for the P-branch are shown in Fig. 2; a similar set of contribution functions is selected for the R branch. Retrieved P- and R-branch temperature profiles for the clear IRIS spectrum of Fig. 1 are shown in Fig. 3.

At the $2.4\text{-}\mu\text{m}^{-1}$ spectral resolution of the Mariner 9 IRIS, for nadir viewing, the center of the $15\text{-}\mu\text{m}$ band of CO_2 probes near the 0.2-mb region of the martian atmosphere. This is evident from the broad peak of the contribution function for 668.45 cm^{-1} (the IRIS sample nearest the band center) shown in Fig. 2. The contribution

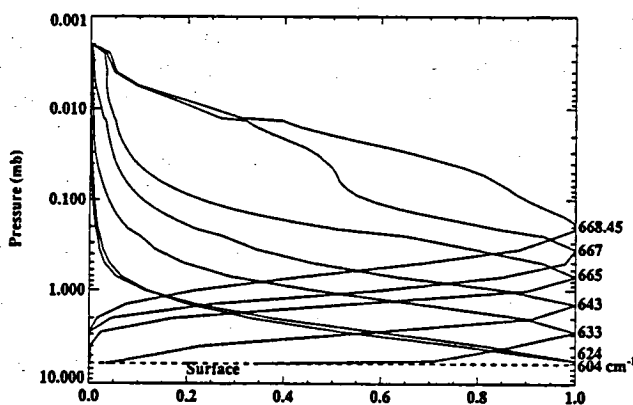


Fig. 2. Normalized contribution functions.

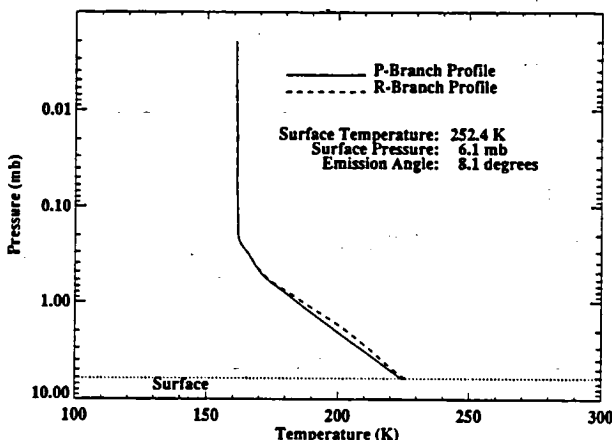


Fig. 3. P- and R- branch retrieved temperature profiles.
DAS = 13507967.

function indicates the pressures sampled at a given wavenumber for a given vertical temperature profile. Above the peak of the 668.45-cm^{-1} contribution function, the information content decreases as shown. Thus, the atmospheric temperature profile can only be accurately retrieved up to the vicinity of the pressure at the peak of the 668.4-cm^{-1} contribution function; for a 10-km scale height this is roughly 35 km .

Vertical structure that is significantly smaller than the half-width of the contribution functions (about a half scale height) is unresolvable. Thus, including additional wavenumbers to provide a denser vertical spacing of contribution functions will not substantially improve the resolution of a retrieved temperature profile.

Our inversion technique is sensitive to the initial guess at the top of the atmosphere; we take the initial temperature profile above the peak of the 668.45-cm^{-1} contribution function to be isothermal at the brightness temperature of the IRIS spectrum at 668.45-cm^{-1} . We have found that such an initial guess minimizes the spectral residuals at band center. The lower part of the initial temperature profile is estimated by assigning the brightness temperatures at selected wavenumbers to the pressures where the corresponding contribution functions peak.

Conclusion: Within the limitations discussed above, we have demonstrated the success of our inversion algorithm for the retrieval of temperature profiles for clear IRIS spectra like Fig. 1. Work continues on the modeling of aerosol extinction for the retrieval of temperatures and aerosol opacities from more dusty IRIS spectra. The simultaneous analysis of IRIS spectra of the same geographic location, but different viewing geometries, will be used in the characterization of the optical properties of airborne particulates.

DUST TRANSPORT IN THE MARTIAN ATMOSPHERE.

J. R. Murphy, NASA Ames Research Center, Moffett Field CA 94035-1000, USA.

Dust in suspension within the martian atmosphere is an important driver of the atmospheric thermal and, ultimately, dynamical states. By virtue of its presence in the atmosphere, this suspended dust is susceptible to transport by the winds and thus the location from which dust is lifted from the surface is not necessarily the location at which it will return to the surface. Such surface dust lifting and subsequent transport, when accumulated over daily, seasonal and annual time intervals define the martian dust cycle [1]. The atmospheric transport element (and equally surface lifting and redeposition) of this cycle is strongly dependent upon season and the quantity of dust in suspension. The seasonal dependence arises due to the dominance of particular components of the atmospheric circulation at particular locations (latitudes) at various times through the year. The dependence on dust abundance is due to the amount of dust available for transport, but it is also due to the influence that the dust has on the intensity of the circulation. As dust abundance and therefore its radiative influence increases, some components of the circulation intensify (Hadley circulation, thermal tides), while some components may decline in intensity (baroclinic waves, condensation flow) [2,3]. For these reasons, our ability to understand the martian dust cycle is dependent on our ability to define the contributions that various circulation components, under varying seasonal and dust-radiative forcings, play in the transport of dust around the planet.

Below we will discuss a number of components of the atmospheric circulation and what their impacts might be upon net dust transport. The points made here are based in part on observations, on numerical modeling, and on extrapolations of our understanding of transport processes in the terrestrial atmosphere. The presentation here is less quantitative than one might prefer, but it helps to frame the questions that need to be addressed to produce the quantification we desire.

The best-characterized transport mechanism, and possibly most important in a global sense, is provided by the Hadley circulation. This thermally direct cell, with its ascending branch situated near the subsolar latitude at any particular time of year, can span a wide latitudinal range and provide an efficient mechanism by which dust lifted from a confined area can be redistributed over a large fraction of the globe. This is seemingly what occurs during global dust storms. During these events, which preferably begin in the southern hemisphere, during southern spring and summer, dust fills the atmosphere to a depth of several scale heights and covers most of the globe. The cross-equatorial Hadley cell responds by intensifying and expanding meridionally, with dust raised at southern subtropical and middle latitudes spreading into the northern hemisphere at elevations one to several scale heights above the surface. This intensified circulation, which rapidly transports dust, is also probably involved in the raising of dust from the surface. Numerical modeling has shown the Hadley circulation to be quite efficient at transporting dust from a prescribed southern hemisphere subtropical/middle latitude source to northern middle latitudes in the span of only several sols [4,5]. This rate of dust spreading is consistent with observations.

Eastward-migrating mid- and high-latitude waves are present during autumn, winter, and spring. These baroclinic waves arise in response to the thermal gradient between the warm equator and cold pole at these seasons. These waves might play an important role in the transport of dust to the polar regions. The airflow within these waves exhibits poleward flow of warm air in advance of the eastward migrating wave, and the equatorward flow of cold air in the wave's lee. Since the air equatorward of the seasonal cap should in general possess a greater dust content than air over the cap, since the CO₂ cover prevents the lifting of dust, one might expect baroclinic waves to provide a net poleward transport of dust. Since the baroclinic waves have a finite latitudinal extent, as the seasonal cap grows, the northward extent to which the baroclinic waves can transport dust will migrate equatorward. Similarly, as the seasonal cap retreats in the spring, the poleward limit of the dust transport will advance toward the pole. In this way, baroclinic waves can play a major role in the incorporation of dust into the seasonal cap. They also can play a role in transporting dust to the pole for possible inclusion in the polar laminae. This dust can either come directly from much lower latitudes, or it can be dust that was previously incorporated into the seasonal cap earlier in the season, which then becomes susceptible to resuspension and transport after the seasonal cap has sublimed away.

Viking Lander 2 meteorological and visible opacity observations at a northern mid-latitude site (47°N) do suggest a correlation between the passage of baroclinic waves and variations in the overhead opacity [6]. Opacity increases during the poleward flow in advance of the wave trough, and after the trough passage opacities decrease in the equatorward flow behind the trough [7], as our conceptual model suggests. Numerical modeling of dust transport in

the martian atmosphere also shows such correlations (Fig. 1). In fact, baroclinic waves are the most important element for transporting dust to high northern latitudes during a simulated global dust storm with a specified southern subtropical dust source [8].

Baroclinic waves exist in years with and without global dust storms, and thus their effects upon net dust transport to high latitudes might well be more important than transport that might arise from the episodic global dust storms (discussed further below). Numerical modeling of dynamical processes has pointed out that baroclinic wave activity is more intense in the northern hemisphere than in the southern hemisphere [2]. These differing amplitudes might be a response to the model topography (which may be incorrect!) differences in the two hemispheres. However, another reason for hemispheric differences is probably due to the greater latitudinal extent of the southern hemisphere seasonal CO₂ cap and concurrent changes in the zonally averaged thermal and wind fields, which reduce the baroclinic instability [2]. These hemispheric differences in wave amplitude should then result in hemispheric differences in wave transport of dust to high latitudes. The persistence of a south polar residual CO₂ cap through the summer months during some years could possibly be a manifestation of this difference, dust contamination of the north cap producing a lower albedo, that prevents retention of a CO₂ cap there.

A component of the martian atmospheric circulation that distinguishes it from its terrestrial counterpart is the substantial seasonal net mass transfer between the polar regions. This "condensation" flow arises due to the condensation upon the winter pole of a significant fraction (~30%) of the atmospheric mass [9,10]. This flow is manifested by a net mass-averaged meridional flow from the hemisphere of the subliming seasonal cap to the hemisphere of the condensing seasonal cap. The hemispheric difference in the sizes of the seasonal caps, caused by Mars' large orbital eccentricity, implies differences in the magnitude of the condensation flow with season. Such differences, in conjunction with seasonal variations of dust loading during years with and also without global-scale storms, might lead to a net transfer of dust from one hemisphere to another. The condensation flow magnitude during southern autumn/winter is greater than the magnitude during northern autumn/winter. The atmospheric dust loading is generally greater during northern autumn/winter than during the same southern seasons. This leaves open the question of net transport, since the correlation between flow magnitude and dust loading variations might balance out over an annual cycle.

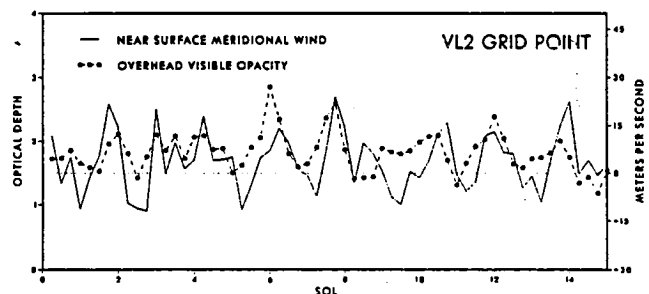


Fig. 1. The model-calculated near-surface meridional wind and column-integrated visible dust opacity at a grid point corresponding to the Viking Lander 2 northern mid-latitude site. The positive correlation between the variables represents a net poleward transport of dust by low-frequency baroclinic waves.

Dust transport induced by atmospheric tidal motions is very poorly defined. There are several scenarios in which dust transport by the tides can be envisioned. During the developing stage of a global dust storm, tidal amplitudes rapidly intensify. This amplification occurs during a time period in which the atmospheric dust load is rapidly increasing due to sources located at southern subtropical latitudes. The large meridional (and zonal) flows that accompany the tidal amplifications can produce large dust fluxes if dust is present at the appropriate vertical levels. Time-constant tidal amplitudes are less likely to produce a net transport of dust; however, dust particle sedimentation, in conjunction with nonamplifying tidal flow, can produce net dust transport. It has been shown [11] that inclusion of tidal forcing in a zonal-mean model during a simulated global dust storm (large dust loading) enables the Hadley circulation to extend to higher latitudes in the winter hemisphere, with a concurrent shift of the northward extent of dust transport. However, this expansion does not extend into polar regions. The rapid intensification of tidal amplitudes at the onset of dust storms and the very large wind speeds that result are certainly an inviting mechanism to invoke to explain the rapid growth of the observed storms. Much more work is required to better define the importance of such a process.

Regional types of flows can also produce net dust transport. East-west circulations at northern subtropical latitudes have been invoked to explain an inferred removal of dust from high-thermal-inertia, low-elevation, dark areas, and subsequent redeposition of this same dust upon low-thermal-inertia, higher-elevation, visibly brighter locations [12]. Such east-west, or Walker type, circulations could themselves be driven by the heating contrasts engendered by the surface properties outlined above.

Diurnally forced upslope/downslope flows along the numerous sloping regions on Mars are another local or regional factor that can be invoked to produce a net dust transport. The Hellas Basin, characterized by sloping faces on the order of 1000 km in length, have been observed as preferential locations for the appearance of suspended dust. The southeast flank of Tharsis is another location of apparently preferred dust raising. The factors involved in and the importance of such relatively small-scale (mesoscale) processes upon the martian dust cycle have not been theoretically dealt with at all.

A final class of motions that can be invoked as transport-capable is what I will term "special circumstances." These features are those that might be sporadic in nature but can possibly have a very large impact upon net transports over a range of timescale. The best example of such a process is the circumstances surrounding a winter polar warming similar to that observed during the second 1977 global dust storm. As [13] has pointed out, whatever dynamical process is fundamentally responsible for the warming, it must involve poleward flow at high altitude and descent over the pole (which adiabatically generates the observed warming). The persistence of the warming, ~ 30 sols [14], and its intensity suggest that substantial meridional transport of various species (dust, water) from low latitudes to the polar region could occur during such an event. This dust could then become incorporated into the polar cap due to either direct sedimentation upon the surface or its incorporation into water or CO_2 "snow flakes," which subsequently fall to the surface. The viability of this transport process depends strongly upon the vertical and latitudinal distribution of dust at low latitudes during the time period of the warming.

In this presentation I have attempted, albeit rather crudely, to describe various components of the martian atmospheric circulation and their implications for dust transport. The seasonality of various components must surely be considered when attempting to define net annual and multi-annual effects of individual components, as should the seasonality of suspended dust abundance. Quantification of these various processes, both from numerical models and the Mars Observer dataset will tremendously expand our understanding of the martian dust cycle and the relative importance of its various constituent parts.

References: [1] Kahn et al. (1993) *Mars*, 29, Univ. Arizona. [2] Haberle et al. (1993) *JGR*, 98, 3093-3123. [3] Barnes et al. (1993) *JGR*, 98, 3125-3148. [4] Haberle et al. (1982) *Icarus*, 50, 322-367. [5] Murphy et al. (1993) *JGR*, 98, 3197-3220. [6] Tilman et al. (1979) *JGR*, 82, 2947-2955. [7] Ryan and Henry (1979) *JGR*, 84, 2821-2829. [8] Murphy et al. (1993) in preparation. [9] Pollack et al. (1990) *JGR*, 95, 1447-1474. [10] Pollack et al. (1993) *JGR*, 98, 3149-3181. [11] Zurek and Haberle (1988) *JAS*, 48, 1005-1023. [12] Zurek and Christensen (1990) *Bull. AAS*, 22, 1075. [13] Barnes (1990) *JGR*, 95, 1381-1400. [14] Jakosky and Martin (1987) *Icarus*, 72, 528-534.

THREE-DIMENSIONAL NUMERICAL SIMULATION OF NEAR-SURFACE FLOWS OVER THE MARTIAN NORTH POLAR CAP. T. R. Parish¹ and A. D. Howard², ¹Department of Atmospheric Science, University of Wyoming, Laramie WY 82070, USA, ²Department of Environmental Sciences, University of Virginia, Charlottesville VA 22903, USA.

Introduction: Measurements made by Viking Lander VL-2 (48°N) have shown that the near-surface wind and temperature regime on Mars displays striking similarities to terrestrial counterparts [1]. The diurnal radiative cycle is responsible for establishment of a well-defined thermal circulation in which downslope (katabatic) flows prevail during the nighttime hours and weak upslope (anabatic) conditions prevail during the daytime. Previous work [2] has indicated that the slope flows are much like those found on Earth, particularly the katabatic winds, which show striking similarities to drainage flows observed over Antarctica. The low-level wind regime appears to be an important factor in the scouring of the martian landscape [3]. The north polar cap shows evidence of eolian features such as dunes, frost streaks, and grooves from Viking imagery. The direction of the prevailing wind can in cases be inferred from the eolian features.

Here we examine the thermally induced flows that result from the radiative heating and cooling of the martian north polar region using a comprehensive three-dimensional atmospheric mesoscale numerical model. The same model has been used previously for simulation of Antarctic katabatic winds [4]. The model equations are written in terrain-following σ coordinates to allow for irregular terrain [5]; prognostic equations include the flux forms of the horizontal momentum equations, temperature, continuity. A surface energy budget equation is also incorporated in which the surface temperature is determined. Explicit parameterization of both terrestrial (longwave) and solar (shortwave) radiation is included. Turbulent transfer of heat and momentum in the martian atmosphere is assumed to follow the similarity expressions in the surface boundary layer on Earth [6-8]. The terrain heights for the martian north polar

region have been obtained from the U.S. Geological Survey map and digitized onto a 57×57 grid with a spacing of 75 km. The resulting terrain map is shown in Fig. 1. The vertical grid consists of 15 levels ($\sigma = 0.998, 0.99, 0.98, 0.97, 0.96, 0.94, 0.92, 0.90, 0.85, 0.775, 0.70, 0.60, 0.50, 0.30, 0.10$). The high resolution in the lower atmosphere is necessary to capture details of the boundary layer flows. The lowest level corresponds to a height of approximately 20 m above the ground, the second level 100 m.

Model Results: *Katabatic wind simulations over the north polar cap.* To examine the intensity and pattern of drainage flows over the martian north polar region, a series of numerical experiments have been conducted. To isolate the drainage flows, the model is initialized about a state of rest. No ambient horizontal pressure gradients are assumed to exist in the model atmosphere at the start. The model simulation is assumed to be representative of polar night conditions; solar radiation is neglected throughout the model domain. The motions that develop are therefore the result of the long wave radiative flux divergence at the surface and in the low levels of the atmosphere. The model equations are integrated for a 24-martian-hr period, by which time near-steady drainage flows have developed.

Figure 2 depicts the streamlines and wind speeds of the katabatic drainage at the end of the 24-hr integration period at the second σ level (approximately 100 m above the surface). Note that the drainage flows move radially outward from the various ridges atop the north polar region, being deflected some 40° – 60° to the right of the fall line due to the Coriolis influences. Confluence zones, regions where the drainage streamlines converge, can be identified as well. In such areas cold, negatively buoyant air collects; katabatic wind can be significantly enhanced along the confluence axis. The wind speeds of the drainage flows are comparable to what would be observed over Antarctica. The strongest wind speeds appear to be related to the steepness of the terrain. Confluence effects account for only a minor enhancement in the simulated katabatic intensities.

Effect of solar heating of the martian north polar region. Numerical simulations have also been conducted incorporating solar insolation over the irregular terrain over the northern martian latitudes. The model terrain heights are as shown in Fig. 1. Model equations have been integrated for a period of three martian days to ensure that the wind and temperature regimes have had ample time to adjust to the cycle of solar heating (solar constant is set to 600 W m^{-2}). It was found that the second- and third-day results of the model integration were nearly identical. Here the third-day results of one

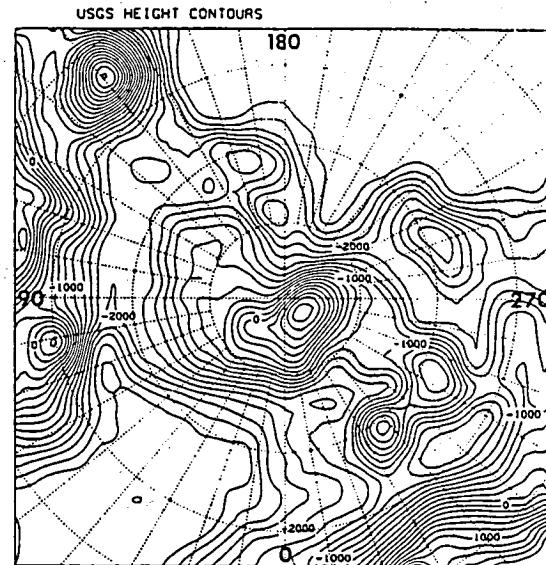


Fig. 1. Terrain contours (200-m increment) near the martian north polar region adapted from U.S.G.S. map.

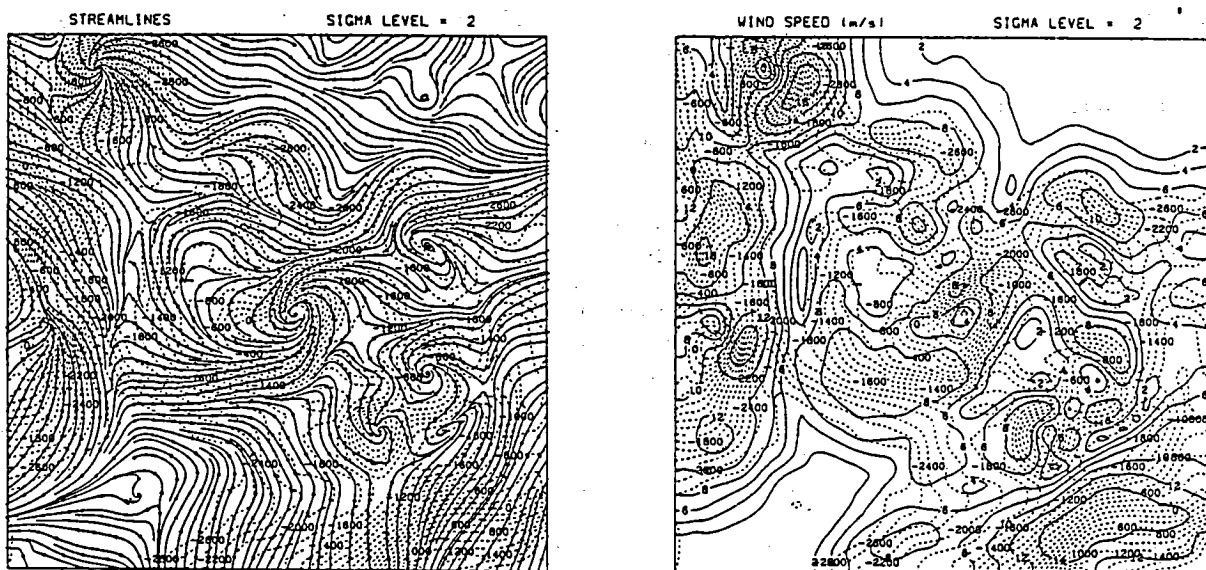


Fig. 2. Model simulations of streamlines (left) and wind speeds (right) of katabatic flows at the second σ level after 24-hr integration period.

such experiment will be presented. In this experiment, the solar declination is assumed to be 25° , representative of midsummer conditions. It is assumed that the atmosphere is dust free. As before, the model is initialized about a state of rest to isolate the thermally induced slope flows in the lower atmosphere. Values of albedo and thermal inertia were taken from Paige [9].

Figure 3 illustrates the solar insolation received at the surface and corresponding surface temperatures. Local noon at this time is along the 60° meridian in Fig. 1. Note that significant spatial variations in the intensity of solar radiation reaching the surface are found near the polar cap in response to albedo differences. Temperatures range from 260 K along the southern edge of the 60° meridian

in the model domain to around 190 K in the nighttime section of the model domain situated about the 210° meridian. Examination of the surface temperature regime shows little diurnal variation over the north polar ice cap; the largest diurnal changes are seen in the midlatitude portion of the model domain, as expected. The temperatures at the first σ level (not shown) vary from approximately 238 K along the 30° meridian to approximately 198 K in the nighttime sector of the model domain.

The thermally induced slope flows become significantly modified from the pure katabatic drainage pattern shown in Fig. 2. Anabatic motions become established in response to the intense solar heating of the sloping terrain. Figure 4 illustrates the stream-

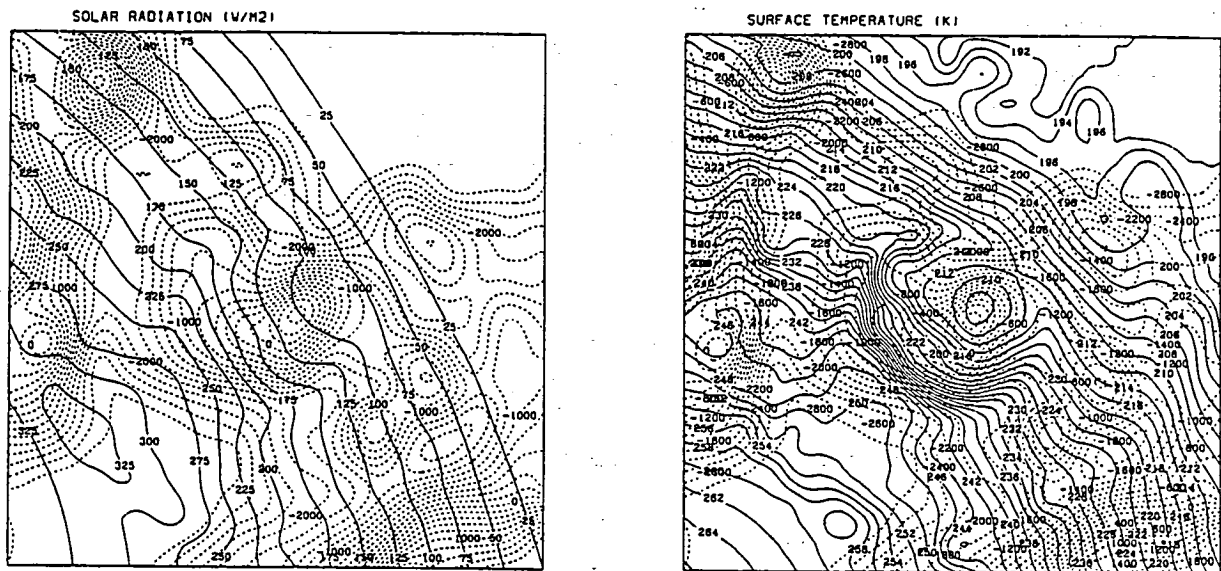


Fig. 3. The intensity of solar radiation ($W m^{-2}$) reaching the surface (left) and corresponding surface temperatures (right) from numerical simulation of diurnal cycle.

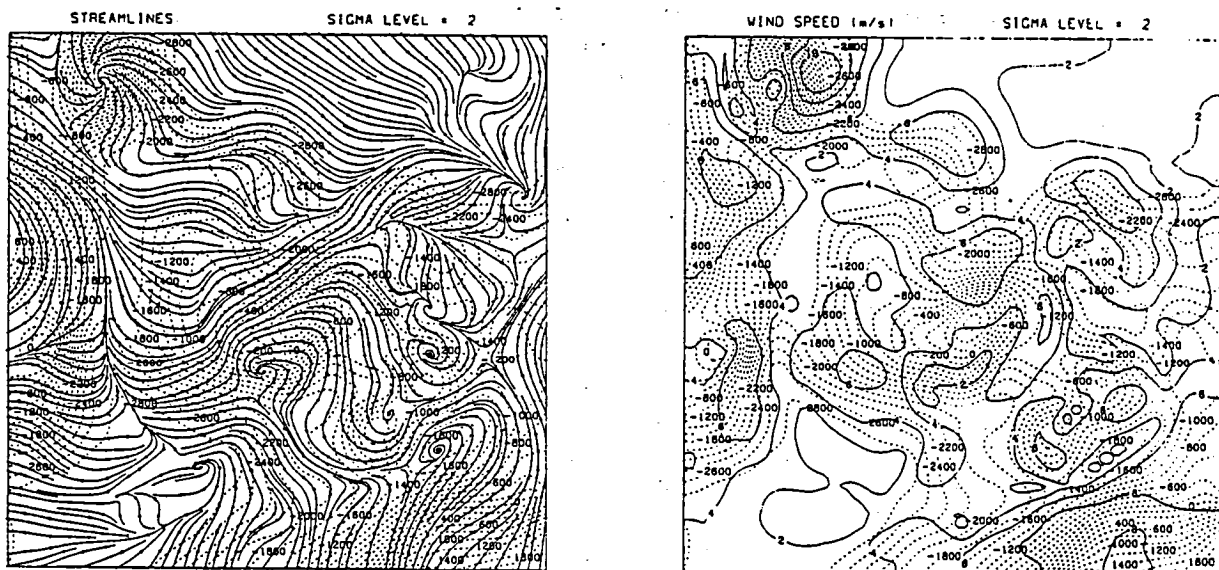


Fig. 4. Model simulations of streamlines (left) and wind speeds (right) of slope flows at the second σ level for diurnal cycle experiment.

lines and wind speeds at the second σ level for the time of the local solar forcing shown in Fig. 3. Note that especially along the 30° meridian, the streamline patterns are dramatically altered by the solar insolation as compared to Fig. 2. Upslope wind conditions are simulated at middle to high latitudes from approximately 315°–90°. As seen in the previous simulation, the strongest winds are associated with the steepest terrain. Upslope flows reach 7 m s⁻¹ along the 60° meridian. The intensity of the upslope flows appears to be weaker than their nocturnal katabatic counterparts. This is in agreement with numerous terrestrial observations such as over the Antarctic ice sheet. Note that the katabatic wind speeds simulated over the nighttime sector centered about 210° are only slightly weaker than the katabatic winds seen in Fig. 2, emphasizing the rapid response of the wind field to the radiative-induced temperature changes near the surface.

Summary: Numerical simulations of the martian near-surface wind regime using a three-dimensional atmospheric model have shown that katabatic winds prevail over the sloping terrain during nighttime hours. Such winds are forced by the strong radiative cooling of the sloping surface, which sets up a downslope-directed horizontal pressure gradient force. Both the magnitude and direction of these flows are similar to terrestrial counterparts such as those over Antarctica. Introduction of solar radiation strongly perturbs the slope flows; anabatic conditions develop in middle to high latitudes during the daytime hours due to the solar heating of the sloping terrain. Wind speeds for the upslope flows are somewhat weaker than for corresponding katabatic flows. There appears to be a rapid transition from the katabatic to the anabatic flow regimes, emphasizing the primary importance of radiative exchanges at the surface in specifying the horizontal pressure gradient force.

References: [1] Hess S. L. et al. (1977) *JGR*, 82, 4559–4574. [2] Parish T. R. and Howard A. D. (1993) *JGR*, submitted. [3] Howard A. D. (1981) *NASA TM 82385*, 333–335. [4] Parish T. R. and Waight K. T. (1987) *Mon. Wea. Rev.*, 115, 2214–2226. [5] Anthes R. A. and Warner T. T. (1978) *Mon. Wea. Rev.*, 106, 1045–1078. [6] Brost R. A. and Wyngaard J. C. (1978) *J. Atmos. Sci.*, 35, 1427–1440. [7] Busch N. E. et al. (1976) *J. Appl. Meteor.*, 15, 909–919. [8] Businger J. A. et al. (1971) *J. Atmos. Sci.*, 28, 181–189. [9] Paige D. A. (1992) *LPS XXIII*, 1013.

THE ROLE OF ATMOSPHERIC HEAT TRANSPORT IN THE SEASONAL CARBON DIOXIDE CYCLE. J. B. Pollack¹, R. M. Haberle¹, J. R. Murphy¹, J. Schaeffer², and H. Lee², ¹NASA Ames Research Center, Moffett Field CA 94035-1000, USA, ²Sterling Software, Inc., Palo Alto CA 94303, USA.

We have carried out numerical experiments with a general circulation model (GCM) and energy balance model of the martian atmosphere to define the importance of heat transported to the polar regions in determining the amount of CO₂ condensed on the surface during the fall and winter seasons and the amount sublimated during the spring and summer seasons [1,2]. In so doing, we performed both sensitivity experiments, in which the dust opacity was varied over the full range of its observed values [3], and annual simulations, in which the dust opacity varied continuously with seasonal data, in accord with measurements taken at the Viking landers [3].

Dust opacity represents the key variable for determining the contribution of atmospheric heat advection to the energy budget in

the polar regions. The amount of heat advected to the winter polar regions increases monotonically as the dust opacity at low and middle latitudes increases. However, the increase is sharpest between optical depths of 0 and 1 and tends to level off at still higher optical depths. Heat advection is more important at times of CO₂ condensation than CO₂ sublimation, since the temperature gradients are much steeper in the winter hemisphere than in the summer hemisphere. Because dust opacity is much higher during northern winter than during southern winter, atmospheric heat advection reduces the amount of CO₂ that condenses in the north by a much larger factor than it does in the south.

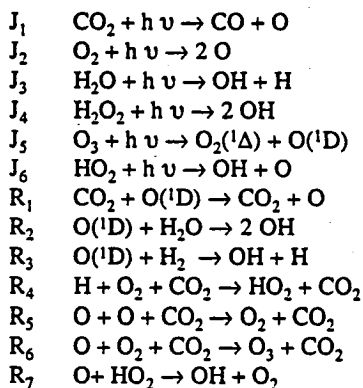
Three wind components play key roles in transporting heat to the polar regions: the zonally mean overturning circulation (Hadley cell), the transient eddies (baroclinic eddies), and the condensation flow. As the dust opacity increases, the Hadley circulation strongly expands poleward (but its poleward expansion is ultimately limited by angular momentum considerations); eddy transport shifts poleward; and the condensation flow weakens.

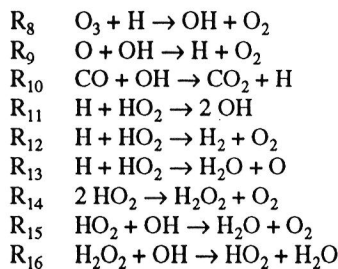
The importance of atmospheric heat advection can be illustrated by comparing an annual simulation that includes it and whose parameters have been adjusted to match the seasonal pressure variations measured at the Viking landers [4] with an identical simulation, in which atmospheric heat advection is ignored. Pressure differences of as much as 0.5 mbar are found between the two runs, i.e., heat advection is responsible for several tens of percent of the observed signal. The seasonal pressure curves show a greater degree of symmetry with heat advection removed and an even greater degree of symmetry when seasonal hemispherical shifts in the global atmospheric pressure distribution is ignored.

References: [1] Pollack J. B. et al. (1990) *JGR*, 95, 1447–1473. [2] Pollack J. B. et al. (1993) *JGR*, 98, 3149–3181. [3] Colburn D. S. et al. (1989) *Icarus*, 79, 159–189. [4] Tillman J. E. (1988) *JGR*, 93, 9433–9451.

EDDY MIXING COEFFICIENT UPPER LIMIT DERIVED FROM THE PHOTOCHEMICAL BALANCE OF O₂. J. Rosenqvist¹ and E. Chassefière², ¹DESPA, Observatoire de Paris-Meudon, 92195 Meudon, France, ²C.N.R.S., Service d'Aéronomie, B.P. No. 3, 91371 Verrières-le-Buisson Cedex, France.

The Model: This work is based on the study of the photochemical balance of molecular oxygen in the martian atmosphere by using a one-dimensional model of photochemical reactions involving species derived from CO₂ and H₂O.





The model is basically similar to the one used by [1] for the study of the regulation of CO on a global scale, but the chemical rates are taken from [2]. In the present scheme, the regulation of molecular oxygen is studied over timescales of the order of its photochemical lifetime (≈ 30 yr), which is much shorter than typical escape timescales ($[O_2]/\phi(O) \approx 10^5$ yr). Thus, the escape fluxes are fixed to the values given by [3] and [4]. We examine the calculated equilibrium abundances of O_2 for given thermal, eddy diffusion coefficients and H_2O profiles. The thermal profile is taken from [5] in the lower atmosphere. At higher levels, in order to include the diurnal and seasonal thermal profile variability, we have also used the IRTM data [6]. The pressure at the surface has been taken from [7]. In order to study the influence of both temperature and pressure profiles on the O_2 mixing ratio, we have made several tests corresponding to different martian seasons. The results show that the influence of pressure and temperature is quantitatively weak compared to the one of K and of the water vapor density $[H_2O]$. Thus, in the following we have fixed the pressure at the surface to a value of 7 mbar and we have used a unique standard thermal profile corresponding to a profile roughly averaged over the year, the season, and the day: $T = 205$ K at 0 km altitude, 175 K at 25 km, and 145 K at 50 km.

Variation of $[O_2]$ with K : Increasing K will accelerate the transport of O atoms, large amounts of which are formed above 40 km by the CO_2 photolysis, toward the lower atmosphere where, in turn, they will be destroyed by reacting with odd hydrogen radicals HO_2 (reaction R_7) and OH (reaction R_9). By taking into account only the dominant terms, the residual production rate of O_2 , when subtracting balance equations of O_3 and HO_2 , may be written

$$P_{O_2} = k_5 [O]^2 [CO_2] + k_9 [O][OH] \quad (1)$$

Reactions R_5 and R_9 are the only terms entering the production of O_2 averaged over a time larger than the O_3 and HO_2 lifetimes. They work mainly above 40 km, R_5 being maximum between 60 and 70 km, and R_9 at 50 km. As K increases, R_9 becomes more important relatively to R_5 .

At altitudes greater than 60 km, the balance of O shows that oxygen atoms reform O_2 . But when K is large, the O atoms are less abundant at these levels because some of them are transported down to lower altitudes. For a fixed water vapor vertical distribution, when K is large, the downward transport of O atoms is important. In this case, the production of molecular oxygen is inefficient. Conversely, production of O_2 by the action of O with itself becomes important for small values of K ($\approx 10^6$ $cm^2 s^{-1}$). However, for extremely low values of K ($\approx 10^5$ $cm^2 s^{-1}$), the production of O_2 again decreases. This fact can be explained by the very slow transport of O atoms produced by photodissociation in the upper atmosphere towards the 50–70-km altitude range where R_5 and R_9 occur. Thus,

for a given distribution of H_2O , the O_2 mixing ratio is globally anticorrelated with the eddy diffusion coefficient when the latter is somewhat larger than 10^6 $cm^2 s^{-1}$.

Variation of $[O_2]$ with $[H_2O]$: If the water vapor amount is large, the formation of odd hydrogen (H , HO_2 , OH , H_2O_2) radicals is also large. Then, in order to ensure the balance of odd hydrogen radicals, the destruction of H^* should increase. It shows that H atoms and HO_2 densities must globally increase. At this step, the equilibrium of H atoms over the whole atmosphere can be written as

$$\begin{aligned}
 \int k_{10} [CO][OH] dz + \int k_9 [O][OH] dz = \\
 \int k_4 [O_2][H][CO_2] dz + \int k_8 [O_3][H] dz
 \end{aligned} \quad (2)$$

Quantitative comparison of the first and second terms of the left side of the above equation shows that

$$\int k_{10} [CO][OH] dz \gg \int k_9 [O][OH] dz \quad (3)$$

whatever the input values of K and $[H_2O]/[CO_2]$. In the same manner, the comparison of the right side of this equation leads to

$$\int k_4 [O_2][H][CO_2] dz \gg \int k_8 [O_3][H] dz \quad (4)$$

Moreover, the first part of the left side of the equation is constant as shown by [1]. Consequently, the product $[H][O_2]$ is expected to be roughly constant. Thus, as the amount of water vapor increases, $[O_2]$ decreases.

Results: As has been mentioned previously by several authors [8–11], an interesting property of O_2 is that its abundance is rather sensitive to the eddy diffusion coefficient K and the amount of water vapor in the atmosphere. Thus, the knowledge of the O_2 abundance (1.1 – $1.3 \cdot 10^{-3}$) measured from Earth [12–14], allows an interesting constraint on K and H_2O . This model being a stationary one-dimensional model, these constraints correspond to eddy diffusion

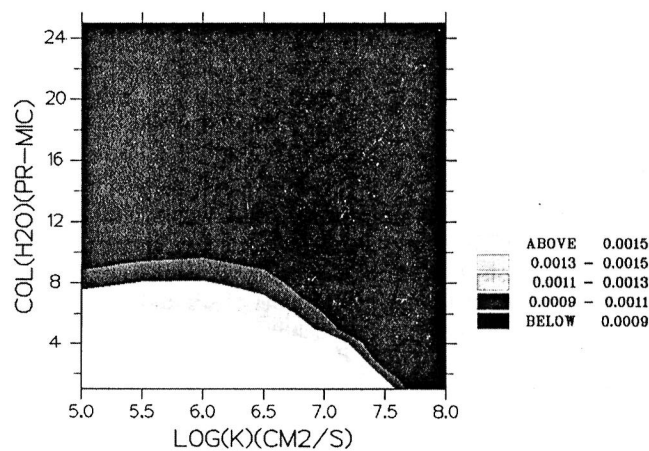


Fig. 1. Calculated O_2 mixing ratio as a function of K and the total water vapor amount in the atmosphere. The scale indicates the ranges of O_2 mixing ratios. The clear gray shaded area corresponds to expected values of the O_2 mixing ratio (1.1×10^{-3} – 1.3×10^{-3}). The white area corresponds to an O_2 mixing ratio larger than 1.5×10^{-3} and the dark one to a O_2 mixing ratio lower than 9×10^{-4} .

sional model, these constraints correspond to eddy diffusion coefficients and water vapor amounts averaged over time (several decades) and over space (whole planet). Figure 1 shows the range of the molecular oxygen mixing ratio as a function of the eddy diffusion coefficient and water vapor total amount. The clear gray area corresponds to the O_2 mixing ratios, which are consistent with the observations ($O_2 = 1.1\text{--}1.3 \cdot 10^{-3}$). An upper limit of $9\mu\text{m}$ for H_2O may be derived from this figure. This limit (which is an average over the night and day) is in agreement with expected abundances of H_2O [15]. On the other hand, from Fig. 1, the absolute upper limit on the eddy mixing coefficient is $3 \cdot 10^7 \text{ cm}^2 \text{ s}^{-1}$ in the lower atmosphere (20–80 km). This value is consistent with recent estimates of K derived from observations [16,17]. If the water vapor amount is lower than $4 \text{ pr } \mu\text{m}$, K should be larger than $10^7 \text{ cm}^2 \text{ s}^{-1}$. Conversely, if the water vapor amount is larger than $6\mu\text{m}$, K should be lower than $10^7 \text{ cm}^2 \text{ s}^{-1}$. This last result shows that, if compared with the observations [16,17], the mean diurnal H_2O amount must be larger than $4\mu\text{m}$.

References: [1] Chassefière E. (1991) *GRL*, 18, 1055–1058. [2] Moreau D. et al. (1991) *JGR*, 96, 7933–7945. [3] Krasnopolsky V. A. (1986) *Photochemistry of the Atmospheres of Mars and Venus* (U. Von Zahn, ed.), 41–45, Springer Verlag, Berlin. [4] Liu S. C. and Donahue T. M. (1976) *Icarus*, 28, 231–246. [5] Seiff A. (1982) *Adv. Space Res.*, 2, 3–17. [6] Martin T. Z et al. (1979) *JGR*, 84, 2830–2842. [7] Hess S. L. et al. (1980) *GRL*, 7, 197–200. [8] Parkinson T. D. and Hunten D. M. (1972) *JAS*, 29, 1380–1390. [9] McElroy M. B. and Donahue T. M. (1972) *Science*, 177, 986–988. [10] McElroy M. B. and Kong T. Y. (1976) *GRL*, 3, 569–572. [11] Shimazaki T. (1989) *J. Geomag. Geoelectr.*, 41, 273–295. [12] Barker E. S. (1972) *Nature*, 238, 447–448. [13] Carleton N. B. and Traub W. A. (1972) *Science*, 177, 988–990. [14] Trauger J. T. and Lunine J. L. (1983) *Icarus*, 55, 272–281. [15] Jakosky B. M. and Barker E. S. (1984) *Icarus*, 57, 322–334. [16] Kahn R. (1990) *JGR*, 95, 14677–14693. [17] Chassefière E. et al. (1992) *Icarus*, 97, 46–69.

DIAGNOSTIC CALCULATIONS OF THE CIRCULATION IN THE MARTIAN ATMOSPHERE. M. Santee and D. Crisp, Earth and Space Sciences Division, Jet Propulsion Laboratory, California Institute of Technology, Pasadena CA 91109, USA.

The circulation of the martian atmosphere during late southern summer is inferred from observed atmospheric temperature and dust distributions. We use global maps of temperature and dust optical depth (–0–60 km) retrieved from a subset of the Mariner 9 IRIS thermal emission spectra spanning $L_s = 343^\circ\text{--}348^\circ$ [1]. This thermal structure is characterized by a reversed meridional temperature gradient at altitudes above about 40 km, and temperatures that decrease from equator to pole at lower altitudes. Zonal-mean zonal winds are derived from the zonally averaged temperatures assuming gradient wind balance and zero surface zonal wind (Fig. 1). Both hemispheres have intense midlatitude westerly jets with velocities of $80\text{--}90 \text{ m s}^{-1}$ near 50 km; in the southern tropics the winds are easterly with velocities of 40 m s^{-1} near 50 km. The north-south atmospheric transport includes contributions from both the zonal-mean meridional circulation and large-scale waves.

Their net effect can be approximated by the diabatic circulation, which can be derived from the atmospheric thermal structure and

the net radiative heating rates. A radiative transfer model [2] that accounts for absorption, emission, and multiple scattering by particles and nongray gases is used to compute the solar heating and thermal cooling rates from diurnal averages of the retrieved IRIS temperature and dust distributions (Fig. 2). At pressures below 4 mbar, there are large net radiative heating rates (up to 8 K d^{-1}) in the equatorial region and large net radiative cooling rates (up to 20 K d^{-1}) in the polar regions. These net radiative heating rates are used in a diagnostic stream function model that solves for the meridional and vertical components of the diabatic circulation simultaneously. We find a two-cell circulation, with rising motion over the equator, poleward flow in both hemispheres, sinking motion over both polar regions, and return flow in the lowest atmospheric levels (Fig. 3). The maximum meridional velocity is 4 m s^{-1} in the tropics at $\sim 55 \text{ km}$ altitude, and the maximum vertical velocity is 4 cm s^{-1} downward over the north pole at about 60 km altitude. This circulation is sufficiently vigorous that the meridional transport timescale is about 28 days. The assumption that the advective and diffusive transport timescales should be roughly comparable leads to a vertical eddy diffusion coefficient of about 30

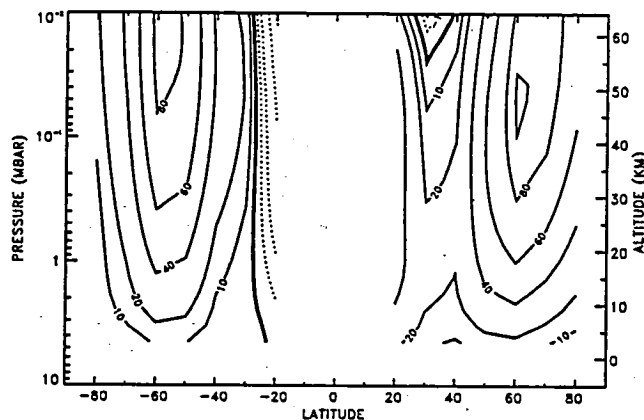


Fig. 1. Zonal-mean zonal winds, in m s^{-1} , calculated from the gradient thermal wind equation. Positive values represent eastward winds, negative contours are dashed, the zero contour is thicker, and the contour interval is nonuniform.

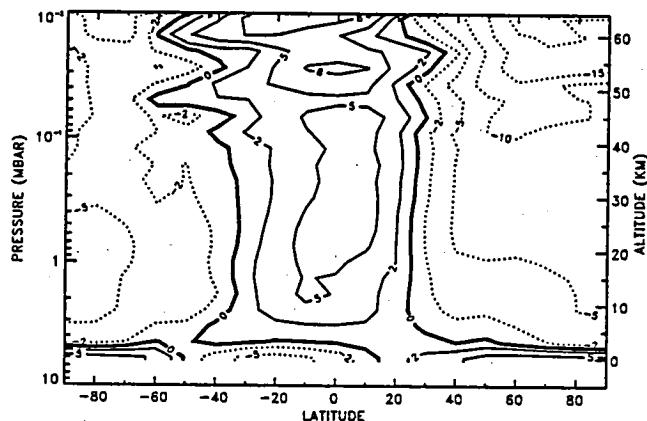


Fig. 2. Net radiative heating rates (K d^{-1}) for the nominal IRIS temperatures and dust abundances, calculated by summing the solar heating and thermal cooling rates. Negative contours are dashed, the zero contour is thicker, and the contour interval is nonuniform.

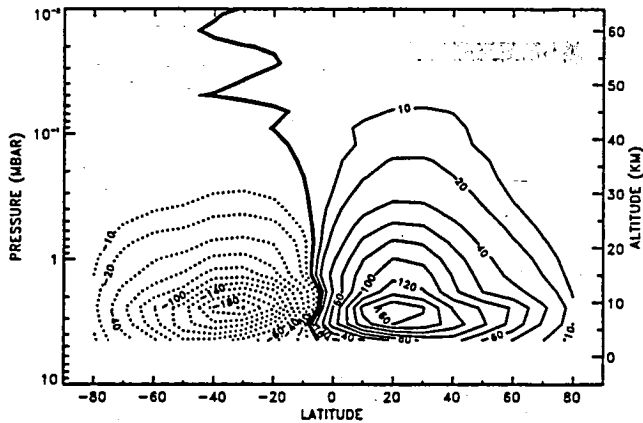


Fig. 3. Mass-weighted stream function, Ψ_m in units of 10^7 kg s^{-1} . Positive values represent clockwise flow, negative contours are dashed, the zero contour is thicker, and the contour interval is nonuniform.

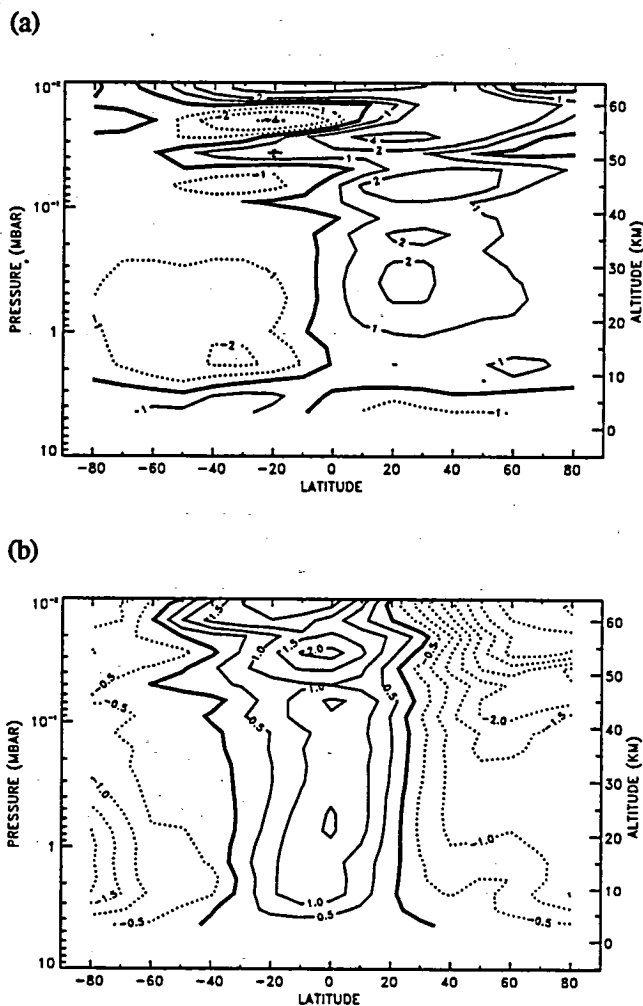


Fig. 4. (a) Diabatic meridional velocity, in m s^{-1} . Positive values represent northward winds, negative contours are dashed, the zero contour is thicker, and the contour interval is nonuniform. (b) Diabatic vertical velocity, in cm s^{-1} . Positive values represent upward winds, negative contours are dashed, and the zero contour is thicker.

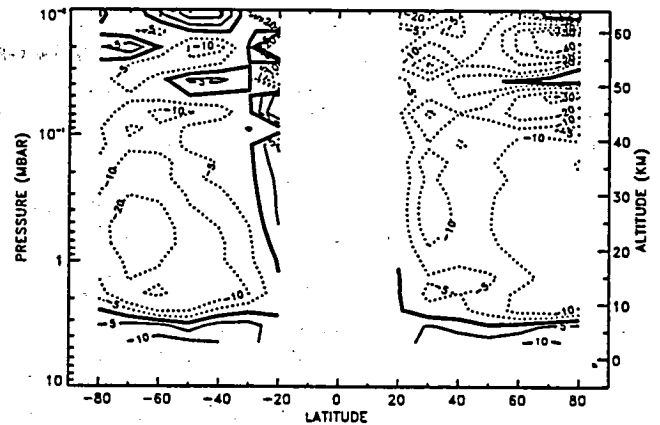


Fig. 5. Eliassen-Palm flux divergence $((\rho \cos \phi)^{-1} \nabla \cdot \mathcal{F})$ in units of $\text{ms}^{-1} \text{ d}^1$. Negative contours are dashed, and the zero contour is thicker.

$\text{m}^2 \text{ s}^{-1}$, two orders of magnitude smaller than the commonly used value. The EP flux divergence is found to have the largest values at high latitudes in the winter hemisphere at altitudes above $\sim 40 \text{ km}$, which coincides with the region of anomalously warm temperatures described in [1].

The diabatic meridional circulation during non-dust-storm conditions can transport a $1\text{-}\mu\text{m}$ dust particle over global scales, but is not intense enough to support $5\text{-}\mu\text{m}$ particles over a large altitude range. The strong meridional circulation also has important implications for the role of atmospheric transport in the seasonal cycle of water on Mars. At lower atmospheric levels, the meridional circulation carries water vapor into the equatorial regions, where the prevailing winds blow upward. The rising motion leads to ice-cloud formation and eventual precipitation of the largest particles, increasing the water abundance at low latitudes. The water that does not precipitate out is transported poleward (as either small ice particles or vapor) by the high-altitude meridional winds. This process could provide a high-altitude source of water vapor for the formation and maintenance of the north polar hood.

References: [1] Santee M. and Crisp D. (1993) *JGR*, 98, 3261–3279. [2] Crisp D. (1990) *JGR*, 95, 14577–14588.

MARTIAN MESOSCALE CIRCULATIONS INDUCED BY VARIATIONS IN SURFACE OPTICAL AND THERMAL CHARACTERISTICS: A NUMERICAL STUDY. T. Siili¹ and H. Savijarvi², ¹Finnish Meteorological Institute (FMI), Department of Geophysics, P.O. Box 503, 00101 Helsinki, Finland, ²University of Helsinki, Department of Meteorology (DMUH), P.O. Box 4, 00101 Helsinki, Finland.

Introduction: According to Mariner 9 and Viking observations the surface albedo and the thermal inertia of Mars' surface vary substantially, and fairly large gradients also occur [1]. The Syrtis Major region is bounded in the west by high-albedo cratered terrain and in the east by Isidis Planitia, a high-albedo plateau. Sinus Meridiani, centered at $0^\circ\text{W } 5^\circ\text{S}$, is almost surrounded by higher albedo regions with sharp boundaries, and Acidalia Planitia, between 10° and 50°W and north of 35°N , has sharp albedo boundaries to the east and west.

Observational and modeling studies, e.g., on Australian dry salt lake coasts, have shown that discontinuities and gradients in surface properties can induce mesoscale circulations [2]. We have used a version of the DMUH mesoscale model to simulate atmospheric circulations induced by variations in the reflectivity and in the thermal inertia of the martian surface.

The Model: A two-dimensional hydrostatic σ -coordinate model is described in detail in [3] and elsewhere. The terrestrial version of the model has been used for studies of sea-breezes [e.g., 4] and the one-dimensional and two-dimensional Mars versions for summer PBL [5] and slope wind [6] studies respectively. The optical depth of the atmosphere is spatially and temporally constant and has typically been given the value $\tau=0.4$ corresponding to martian clear conditions. The soil temperature is predicted with the force-restore method, forced by the model's radiative and turbulent surface fluxes. The soil and surface variations are incorporated as profiles of topography, albedo, thermal inertia, and surface roughness. Profiles are created off line and given as input to the model; both idealized profiles as well as those based on Planetary Data System data (see Fig. 1) have been used. The Coriolis parameter is constant and in our simulations corresponds to 45°N . The season is $L_s = 135^\circ$ (northern midsummer). Vertical and horizontal mesh extents have been $\approx 6\text{--}8\text{ km}$ and $600\text{--}1000\text{ km}$ respectively.

Circulations Due to Albedo Variations: In our ideal-case simulations we have used albedo profiles consisting of two plateaus connected with a spline curve. The results show that a reasonable albedo gradient of $\Delta a/\Delta x = 0.1/300\text{ km}$ (see Fig. 1) creates a soil temperature differential, which is at its largest in the early afternoon and is of the order of $5\text{--}10\text{ K}$, depending on the latitude and season.

This temperature variation induces an afternoon and evening circulation cell superficially resembling the terrestrial sea-breeze circulation cells. Clear upward motion of several centimeters per second is observed above the low-albedo/high-temperature region and sinking motion above the high-albedo/low temperature region. Daytime and evening horizontal wind from the high-albedo region to the low-albedo region can be several meters per second and a weaker return flow higher up is also observed. In the early evening the cell is decoupled from the stable surface layer and stays until after midnight. A nocturnal flow near the surface opposite to the daytime flow (but slightly smaller in magnitude) is also observed. The near-surface winds are fairly light (typically less than 2 m s^{-1}), increasing with height and reaching a maximum at a few hundred meters of altitude. With no large-scale wind the cell appears to

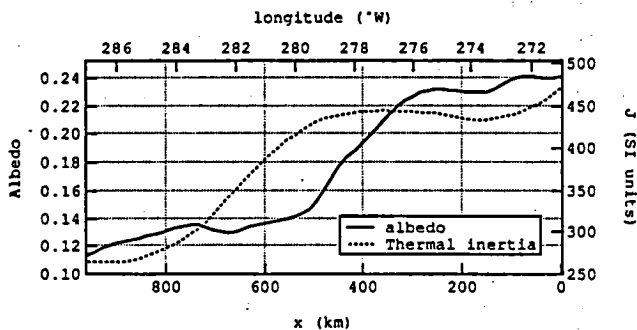


Fig. 1. Albedo and thermal inertia along the latitude circle 7°N between 271° and 287°W (Syrtis Major region) based on PDS data.

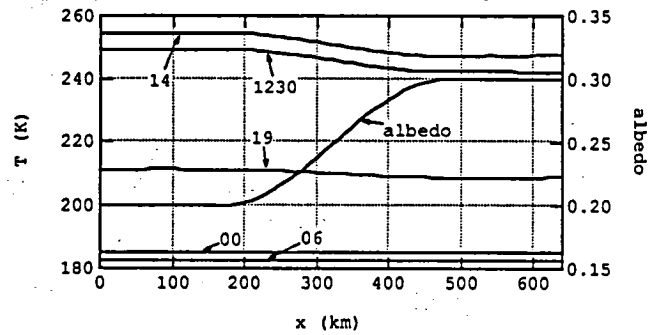


Fig. 2. Surface temperatures during the sol and the surface albedo profile. Horizontal step length $\Delta x = 10\text{ km}$.

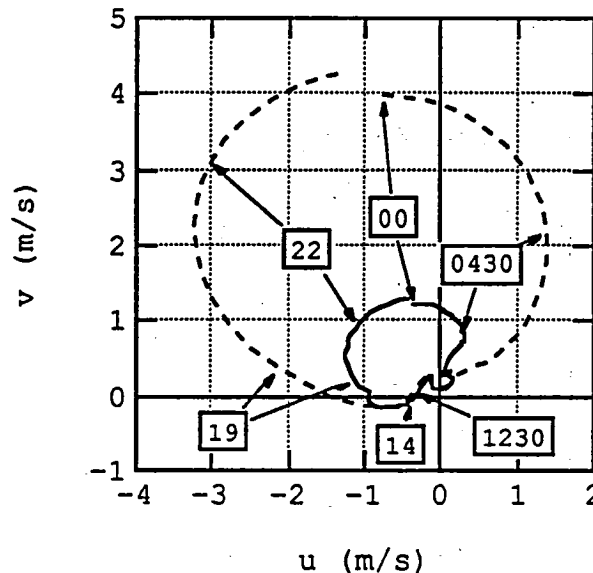
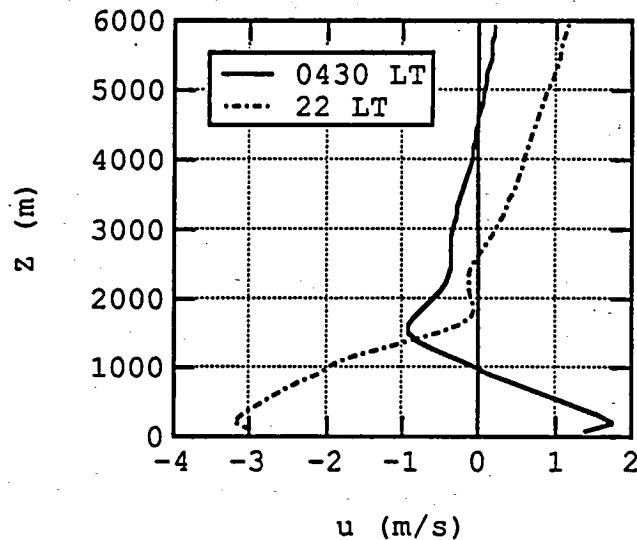


Fig. 3. Vertical profile of the wind across the albedo gradient (top) and the 1.6-m (solid) and 60-m (dashed) altitude hodographs (both at horizontal mesh midpoint).

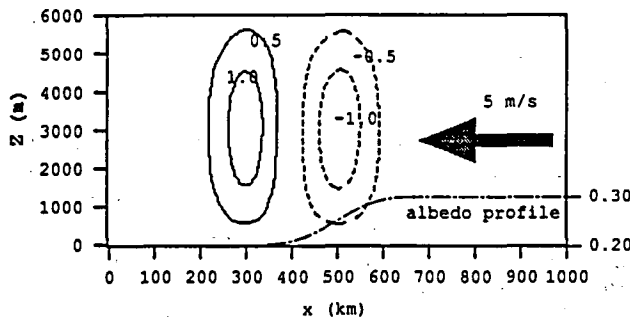


Fig. 4. Locations of the vertical motion areas at 1930 LT. The contour values are in cm s^{-1} .

remain—unlike a terrestrial sea-breeze cell—stationary above the albedo gradient region. If large-scale wind is present, the cell is advected by it; the displacement of the cell can be some hundreds of kilometers before collapse.

As observed in terrestrial sea-breeze situations, increasing prevailing wind attenuates the vertical motion and the cell strength [7]. The cell is weakened by increased optical thickness due to reduced short-wave heating. The horizontal wind maximum is approximately halved when optical thickness is increased from 0.3 to 1.2; vertical flow is also attenuated.

Conclusions and Future Prospects: Our simulations show indications of the occurrence of surface-induced mesoscale circulations in the martian atmosphere. Especially albedo variations appear to generate regular and clear circulation cells with smaller effects due to thermal inertia variations. The cell characteristics depend on the albedo profile, season, large-scale wind and the atmospheric optical thickness. Possible observational verification methods are, e.g., surface wind measurements and identification of the vertical motion regions by cloud formation from orbital imagery. As at some regions on Mars the albedo gradients occur probably due to adjacent dust-covered and clear bedrock areas, the horizontal winds due to the albedo differentials may play a role in dust raising at those areas. Dust thus raised would modify the circulation itself. To study the interaction between the surface dust and the albedo-induced circulations, a future avenue of study is inclusion of dust lifting and dynamics into the model.

References: [1] Kieffer H. H. et al. (1977) *JGR*, 82, 4249–4291. [2] Physick W. L. and Tapper N. J. (1990) *Monthly Wea. Rev.*, 118, 1029–1042. [3] Alestalo M. and Savijarvi H. (1985) *Tellus*, 37A, 156–162. [4] Savijarvi H. and Alestalo M. (1988) *Contrib. Atmos. Phys.*, 61, 98–104. [5] Savijarvi H. (1992) *Contrib. Atmos. Phys.*, 64, 219–229. [6] Savijarvi H. and Siili T. (1993) *JAS*, 50, 77–88. [7] Pielke R.A. (1984) *Mesoscale Meteorological Modeling*, Academic.

TWO-DIMENSIONAL MODELING OF THERMAL INVERSION LAYERS IN THE MIDDLE ATMOSPHERE OF MARS. B. Théodore and E. Chassefière, Service d'Aéronomie du CNRS, BP 3, 91371 Verrières-le-Buisson Cedex, France.

There is some evidence that the thermal structure of the martian middle atmosphere may be altered in a significant way by the general circulation motions. Indeed, while it is well known that the

circulation in the meridional plane is responsible for the reversal of the latitudinal thermal gradient at the solstice through the adiabatic heating due to sinking motions above the winter pole, here we want to emphasize that a likely by-product effect could be the formation of warm layers, mainly located in the winter hemisphere, and exhibiting an inversion of the vertical thermal gradient.

Observations: A noteworthy result was obtained from heterodyne measurements using the IRAM 30-m telescope: A mapping of the CO($J = 2 - 1$) line was performed during the 1988 opposition, while Mars was under northern winter solstice conditions. It allowed the retrieval of the vertical thermal profile as a function of the position on the martian disk, with a spatial resolution of one half hemisphere. The winter profiles definitely exhibit a bump near 50 km altitude, i.e., a relative warming of about 5 K compared to the southern profiles. This may be interpreted as the presence of a warm layer above the high winter latitudes, implying an inversion of the vertical thermal gradient of about 30 K [1]. Such inversions were inferred, but with a weaker amplitude, from the presence at the equinox and near the equator of water ice clouds detected by solar occultations performed aboard the Phobos 2 spacecraft [2].

It must be pointed out that this phenomenon is distinct from the polar warming reported by Martin and Kieffer [3] from the Viking lander data, which is believed to be quite similar to the terrestrial sudden stratospheric warming (SSW) and may be linked to the planetary waves activity [4]. The warming we observed is probably analogous to the terrestrial mesospheric inversions detected below the mesopause by lidar [5] or from space [6], and it was shown [5] that their presence is a response to the dynamical forcing provided by the breaking of internal gravity waves.

It is well accepted that gravity waves play a key role in atmospheric dynamics. The energy budget of the atmosphere requires the presence of a strong dynamical forcing in order to be balanced. The breaking of gravity waves could play this role: the momentum deposition drags the flow and generates turbulence. The former closes the zonal jets near the mesopause and leads to the formation (or the persistence) of a meridional circulation cell because of the Coriolis torque, while the latter leads to a local turbulent heating and creates a jump in the eddy diffusion coefficient vertical profile that seems to be realistic [7]. Yet the main effect on the thermal structure of the atmosphere is due to vertical motions in the meridional cell that produce adiabatic warming or cooling; it is how the latitudinal temperature gradient is inverted. This phenomenon is well known in the terrestrial mesosphere and it seems likely in the case of Mars. Indeed, Deming et al. [8] observed that the middle atmosphere is far from radiative equilibrium above polar regions, unlike equatorial ones. The formation of inversion of the vertical temperature gradient is believed to follow the same mechanism, but implies the momentum deposition to occur in a narrow layer instead of the whole atmosphere, leading to local heating.

Modeling: In order to assess the relative importance of the various processes involved in this phenomenon, we adapted a two-dimensional model of the terrestrial mesosphere, initially devoted to the study of gravity waves-mean flow interactions in the middle atmosphere of the Earth and developed by Hauchecorne and Maillard [9]. We improved this code by the addition of the vertical and meridional advection terms and by optimizing the filtering [10]. This work may be considered as following the exploratory work of Barnes [11], who showed that gravity wave activity could lead to a strong warming in the middle martian atmosphere.

Our code solves the zonally averaged primitive equations in spherical coordinates. Gravity wave effects appear in terms of friction in the zonal momentum equation (the waves are assumed to be purely zonally propagating), turbulent heating in the thermodynamic equation, and vertical diffusion of all the components. Molecular diffusion is neglected and filtering plays the role of the horizontal diffusion. Radiative processes are parametrized with a Newtonian cooling that relaxes permanently the thermal field toward the initial "radiative" field.

The gravity wave effect parameterization is basically the same as formulated by Lindzen [12], using the saturation hypothesis: waves propagate upward until they reach a level where they become unstable. Above this level, up to the critical level (determined as the level where the wave phase speed is equal to mean flow velocity), the wave amplitude is assumed to remain constant; just enough turbulence is produced to prevent the growth of the wave. We assume the wave to be not damped by the radiative processes or by the eventual background turbulence below the breaking level. Holton and Zhu [13] and Barnes [11] showed that this has little influence,

but it is perhaps a crude assumption. In order to simulate a spectrum of waves we use three phase velocities associated with three wave amplitudes, and we make the assumption that the wave generation is latitudinally uniform.

As the program runs, the breaking of gravity waves leads to the closure of the zonal wind jets through the drag exerted near the mesopause (Fig. 1). The strong meridional winds induce a deep penetration of the summer jet in the northern hemisphere (up to 20°N), as suggested by wind measurements in the middle martian atmosphere [14]. Furthermore, a warm layer develops above the winter polar regions, leading to an inversion of the vertical thermal gradient of about 30 K. This inversion occurs by adiabatic heating in the sinking branch of the meridional cell. A noteworthy result was obtained: for some wave characteristics, a warming occurs above the equatorial regions. Its amplitude depends on several parameters, like the wave characteristics as well as the value of the Newtonian cooling coefficient (which may be related to the optical depth of the atmosphere). It is due to the action of gravity waves on the tongue of retrograde winds entering the winter hemisphere; indeed, they

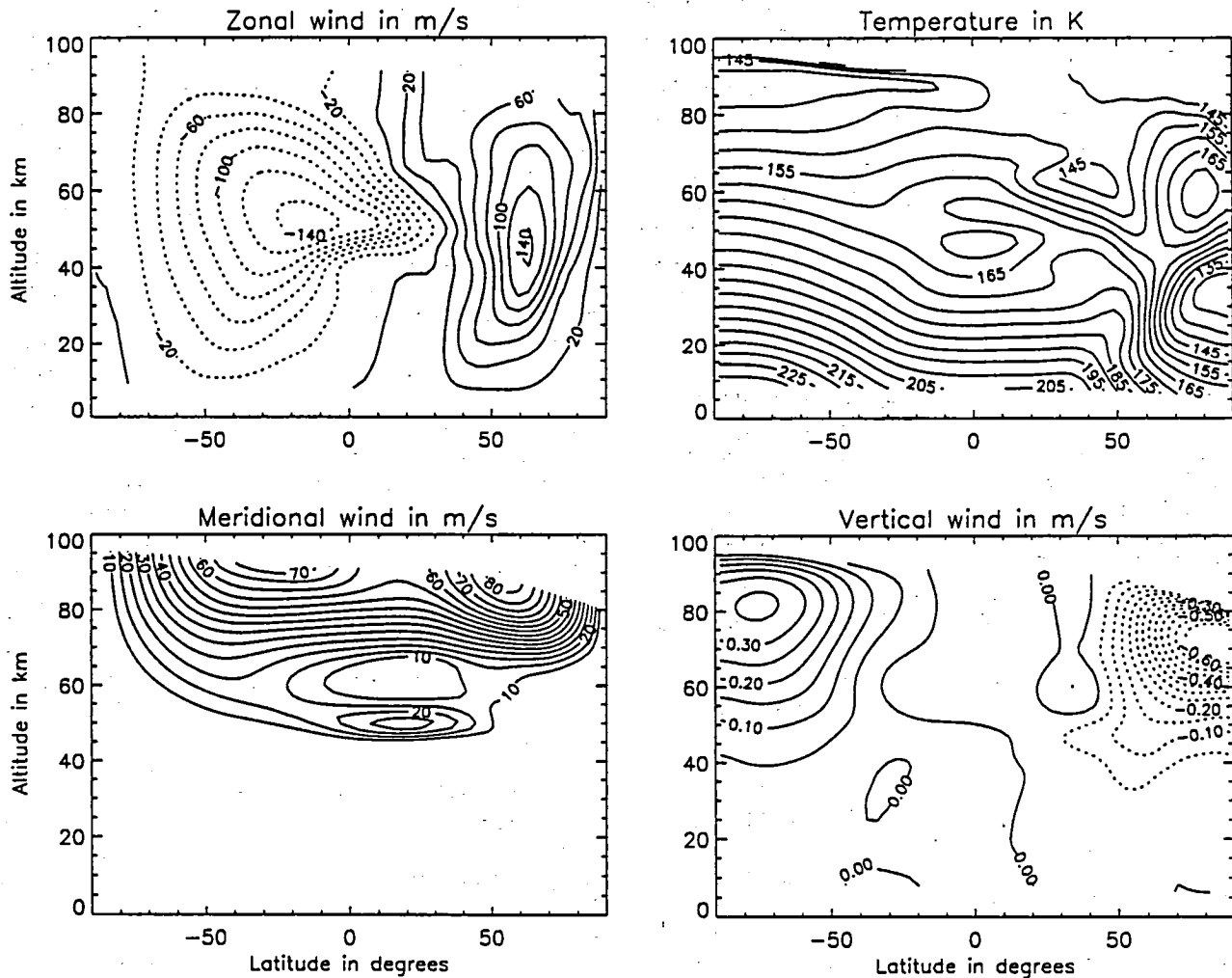


Fig. 1. A latitude-altitude cross section of the zonal, meridional, and vertical wind and temperature.

tend to counteract the meridional circulation locally. The amplitude of the inversions strongly depends on the wave parameters and they can vanish if the wave amplitude is too weak.

Conclusions: This work reinforces the belief in favor of a strong wave activity in the middle atmosphere of Mars at planetary scales. Using a simple numerical simulation of the interaction between internal gravity waves and general circulation, which must be considered at the present stage as a heuristic model dedicated to the understanding of new phenomena, still poorly observed and constrained, it has been possible to successfully interpret global-scale millimeter-wave observations of wind velocities and thermal structure in the martian middle atmosphere. The strong retrograde winds observed in the whole summer hemisphere up to the low latitudes of the winter hemisphere [14], and the relative atmospheric warming above the winter hemisphere near 50 km can be simultaneously explained by the effect of breaking gravity waves.

It is noteworthy that global-scale observations of temperature and wind fields in the middle atmosphere of Mars may be explained by using our schematic two-dimensional model. In spite of the crude initialization and other simplifying assumptions relative to the modeling of wave propagation and breaking, a consistent picture may be found. This shows that, as originally suspected by Barnes [11], gravity waves could play a major role in the setting of the dynamical regime of the martian middle atmosphere. In addition, new phenomena, like equatorial temperature inversions, are predicted. It must be noted that such inversions are observed in the Earth's mesosphere [6], but still not understood, suggesting that the study of this phenomenon might help modelers of the Earth's mesosphere. The martian atmosphere, simpler than the terrestrial atmosphere and expected to be dynamically and thermally more contrasted, could turn out to be a good natural laboratory for the study of wave activity.

New millimeter-wave observations, obtained in December 1992, will provide additional information on the dynamics of the middle atmosphere of Mars near the equinox. The Mars Observer mission will bring substantial information on the thermal structure of the middle martian atmosphere at all seasons, mainly through PMIRR and Radio Science experiments. The use of the present model for the interpretation of PMIRR data will constitute a unique opportunity to test in a detailed way and to improve it, for example, by introducing more realistic initialization of the wind and thermal fields. Implications for the vertical distribution of some photochemically active constituents like ozone will be tested by using the results of experiments mounted onboard Mars 94/96 missions, like the SPICAM experiment.

References: [1] Théodore B. et al. (1993) *Icarus*, submitted. [2] Chassefière E. and Blamont J. E. (1992) *GRL*, 19, 945-948. [3] Martin T. Z. and Kieffer H. H. (1979) *JGR*, 84, 2843-2852. [4] Haberle R.M. et al. (1982) *Icarus*, 50, 322-367. [5] Hauchecorne A. et al. (1987) *GRL*, 14, 933-936. [6] Clancy R. T. and Rush D. W. (1989) *JGR*, 94, 3377-3393. [7] Blamont J. E. and Chassefière E. (1993) *Icarus*, revised March 1993. [8] Deming D. et al. (1986) *Icarus*, 66, 366-379. [9] Hauchecorne A. and Maillard A. (1990) *GRL*, 17, 2197-2200. [10] Théodore B. et al. (1993) *J. Atmos. Sci.*, submitted. [11] Barnes J. R. (1990) *JGR*, 95, 1401-1421. [12] Lindzen R. S. (1981) *JGR*, 86, 9707-9714. [13] Holton J. R. and Zhu X. (1984) *J. Atmos. Sci.*, 41, 2653-2662. [14] Lellouch E. et al. (1991) *Ap. J.*, 383, 401-406.

THREE-DIMENSIONAL NUMERICAL SIMULATION OF THERMAL TIDES IN THE MARTIAN ATMOSPHERE.

R. J. Wilson, Geophysical Fluid Dynamics Laboratory/NOAA, Princeton University, P.O. Box 308, Princeton NJ 08542, USA.

Analysis of the Mariner 9 IRIS and Viking Orbiter IRTM temperature data and of the time series of surface pressure from the Viking landers has indicated that atmospheric thermal tides are a significant component of the martian general circulation. Classical tidal theory, considering only the Sun synchronous components, has been shown to at least roughly account for the amplitudes of the observed diurnal and semidiurnal surface pressure oscillations. In particular, Zurek and Leovy [1] have demonstrated that classical tidal theory can reproduce the observed dependence of the strength of the semidiurnal tide on aerosol optical depth. The high-amplitude topography of Mars, however, can cause longitudinal distortions in the thermotidal forcing, leading to additional tidal modes that are not Sun synchronous. In particular, observation [2] and theory [3] have suggested the likely presence of a diurnal, zonal wavenumber-1 K wave. Hamilton and Garcia [4] noted that the wavenumber-1 K normal mode has a period of close to 24 hr and may be detectable in surface pressure observations. Zurek [5] has discussed the possibility of this mode being resonantly excited for various atmospheric temperature structures. The semidiurnal wavenumber-2 K mode, with roughly a 12-hr period, could also be resonantly excited. A numerical model with finite amplitude topography and a self-consistent thermotidal forcing resulting from the daily heat flux at the surface and atmospheric absorption of solar radiation by aerosols is used here to explore the influence of topography on martian thermal tides and to examine the possibility of Kelvin wave resonance.

A fully nonlinear, three-dimensional, global primitive equation model has been constructed to address some of the limitations of linear theory. In order to obtain realistic thermotidal forcing, the model physics include a three-level soil model, a Monin-Obukhov surface drag formulation, Richardson number-dependent vertical diffusion, and convective adjustment of heat (but not momentum). The model does not yet provide for the CO₂ condensation circulation. Experiments with the NASA Ames martian GCM [6] suggest that this omission is not important in determining the zonal mean wind and temperature fields except at the surface in the vicinity of the polar caps and, hence, is not of great significance for tidal studies. Atmospheric heating by solar radiation is due to absorption in the NIR bands of CO₂ and by aerosols. Heating by aerosols is calculated using a delta-Eddington approximation for aerosol scattering. The optical parameters are those suggested by Pollack et al. [7]. Cooling by dust at longwave frequencies is accounted for in the same fashion as in Haberle et al. [8] using an emissivity formulation for the region outside the 15- μ m band. The IR effects of CO₂ are based on the simple 15- μ m CO₂ band model of Goody and Belton [9]. At present the model is usually run with a uniform surface thermal inertia and albedo except where the surface temperatures imply the formation of CO₂ ice. The model has been run with 25 or 40 levels (typically 40) in the vertical, with the domain extending to roughly 45 or 90 km in height. To date, all runs have used a 5° × 6° horizontal resolution.

In each of the experiments described here, the aerosol has a horizontally uniform distribution with visible optical depth chosen to be 0.3, 1.0, or 2.0. The zonally averaged winds and temperatures

agree quite well with those from the NASA Ames GCM [6]. In particular, the circulations have a similar dependence on the season and on dust optical depth. The two models exhibit comparable amplitudes of diurnal temperature variability up to 40 km.

The first experiments employed an idealized wavenumber-2 topography with a cosine dependence in latitude. A series of simulations was carried out, varying the topographic amplitude from 0.5–3 km and using different dust optical depths. Figure 1 displays the results of a harmonic analysis of the model surface pressure for 2-km amplitude topography. The eastward and westward propagating components of the zonal wavenumber-1 diurnal tide are shown, as well as the corresponding wavenumber-2 components of the semidiurnal tide. The figure clearly shows the presence of an eastward propagating wavenumber-1 K wave with diurnal frequency. The strength of this Kelvin wave response varies approximately linearly with topographic amplitude over the range of amplitudes considered, and is fairly insensitive to atmospheric tempera-

ture variations associated with variable dust loading. As expected, the westward (Sun-synchronous) tides show a pronounced sensitivity to increased dust, with the semidiurnal tide having relatively greater sensitivity. The strength of the semidiurnal wavenumber-2 K wave is apparently highly dependent on atmospheric thermal structure as well as topographic amplitude. With only wavenumber-2 topography present, this presumably resonant mode must have been forced by nonlinear interactions.

A latitude-height plot of the amplitude of the wavenumber-1, eastward-propagating, diurnal component of zonal velocity has a classical Kelvin wave signature in the lower atmosphere, but displays a pronounced tilt with height towards the westerly jet in the winter hemisphere.

Simulations with highly smoothed versions of realistic topography bear out the results of the idealized topography cases. Again, the zonal wavenumber-2 component is crucial for the Kelvin wave excitation. Figure 2 shows the spatial variability of the amplitude of

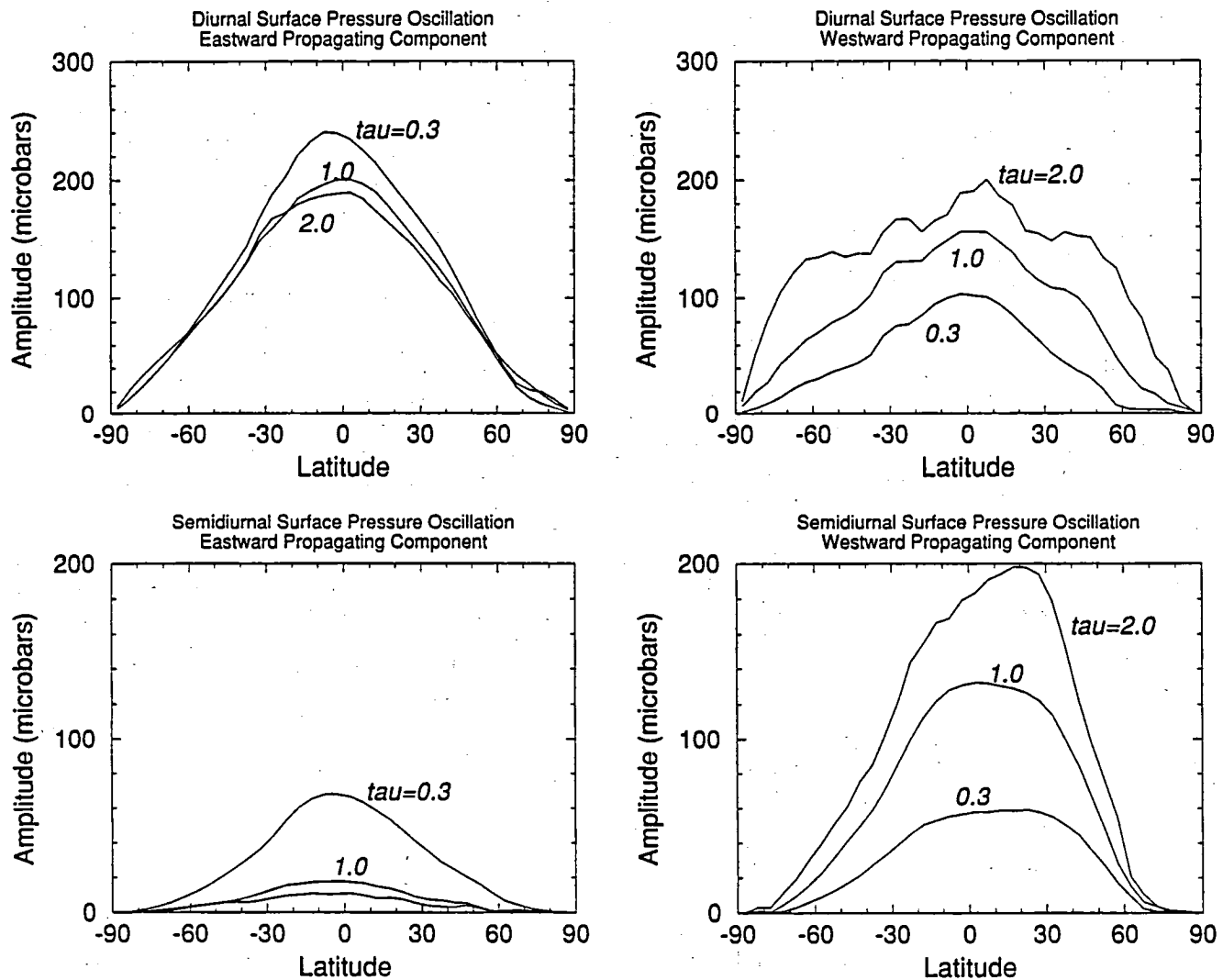


Fig. 1. Harmonic analysis of the surface oscillations for the case of 2.0-km idealized topography at the time of southern hemisphere solstice.

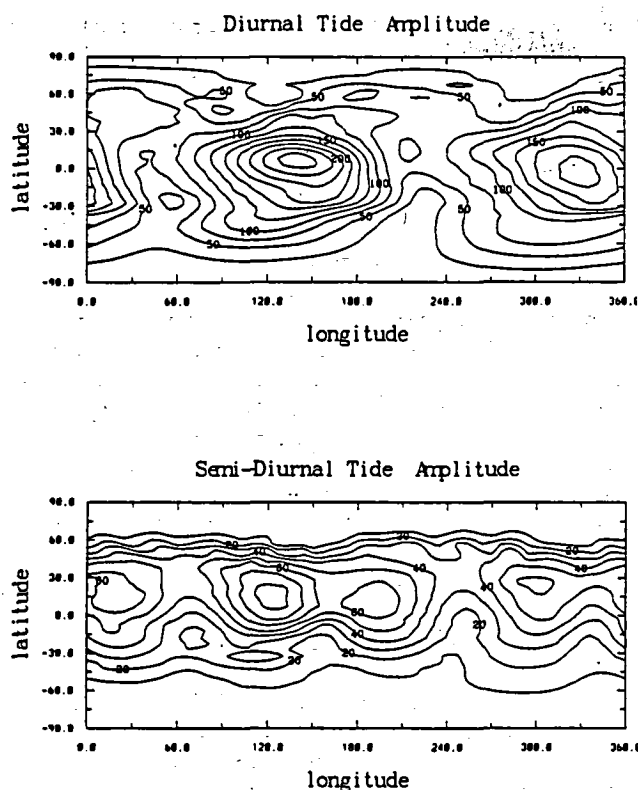


Fig. 2. Diurnal and semidiurnal pressure amplitudes as simulated with smoothed realistic topography at the time of southern hemisphere solstice. Dust optical depth is 0.3; amplitude is in microbars.

the diurnal and semidiurnal surface-pressure oscillations for a case with dust optical depth of 0.3. There is a considerable degree of topographic modulation in the diurnal tide and a fair degree in the semidiurnal tide, which clearly is a departure from the longitudinally uniform amplitudes of classical tidal theory. An experiment with wavenumber-2 variation in the thermotidal forcing due to surface albedo variation (0.15–0.35) produced only a rather weak Kelvin wave response relative to that with topography. A series of simulations with a varying gas constant (which should change the resonant frequency of the Kelvin mode) suggests that the solar tides in the martian atmosphere are indeed within a resonance regime.

Work is in progress to examine the structure of linear tidal modes in the presence of strongly varying basic states and to determine the effects of the diurnal cycle on the simulated general circulation.

References: [1] Zurek R. W. and Leovy C. B. (1981) *Science*, 213, 437–439. [2] Conrath B. J. (1976) *JAS*, 33, 2430–2439. [3] Zurek R. W. (1976) *JAS*, 33, 321–337. [4] Hamilton K. and Garcia R. R. (1986) *JGR*, 91, 11867–11875. [5] Zurek R. W. (1988) *JGR*, 93, 9452–9462. [6] Haberle R. M. et al. (1993) *JGR*, 98, 3093–3123. [7] Pollack J. B. et al. (1979) *JGR*, 84, 2929–2946. [8] Haberle R. M. et al. (1982) *Icarus*, 50, 322–367. [9] Goody R. M. and Belton M. J. S. (1967) *Planet. Space Sci.*, 15, 247–256.

VERTICAL TRANSPORT OF WATER IN THE MARTIAN BOUNDARY LAYER. A. P. Zent¹, R. M. Haberle², and H. C. Houben³, ¹SETI Institute and NASA Ames Research Center, Moffett Field CA 94035, USA, ²NASA Ames Research Center, Moffett Field CA 94035, USA, ³Space Physics Research Institute and NASA Ames Research Center, Moffett Field CA 94035, USA.

We are continuing our examination of the transport of H₂O through the martian boundary layer, and we have written a one-dimensional numerical model of the exchange of H₂O between the atmosphere and subsurface of Mars through the planetary boundary layer (PBL) [1]. Our goal is to explore the mechanisms of H₂O exchange, and to elucidate the role played by the regolith in the local H₂O budget. The atmospheric model includes effects of Coriolis, pressure gradient, and frictional forces for momentum, as well as radiation, sensible heat flux, and advection for heat. The model differs from Flasar and Goody by use of appropriate Viking-based physical constants and inclusion of the radiative effects of atmospheric dust. We specify the pressure gradient force or compute it from a simple slope model. The subsurface model accounts for conduction of heat and diffusion of H₂O through a porous adsorbing medium in response to diurnal forcing. The model is initialized with depth-independent H₂O concentrations (2 kg m⁻³) in the regolith, and a dry atmosphere. The model terminates when the atmospheric H₂O column abundance stabilizes to 0.1% per sol.

Results suggest that in most cases the flux through the martian surface reverses twice in the course of each sol. In the midmorning, the regolith begins to release H₂O to the atmosphere, and continues to do so until midafternoon, when it once more becomes a sink. It remains an H₂O sink throughout the martian night. In the early morning and late afternoon, while the atmosphere is convective, the atmosphere supplies H₂O to the ground at a rapid rate, occasionally resulting in strong pulses of H₂O into the ground. The model also predicts that for typical conditions, perhaps 15–20 sols are required for the regolith to supply an initially dry atmosphere with its equilibrium load, although more than half of the equilibrium load typically appears in the atmosphere on the first sol.

The effects of surface albedo, thermal inertia, solar declination, atmospheric optical depth, and regolith pore structure have been explored. Increased albedo cools the regolith, so less H₂O appears in the atmospheric column above a bright surface. The friction velocity is higher above a dark surface, so there is more diurnal H₂O exchange; relative humidities are much higher above a bright surface. Thermal inertia (I) affects the propagation of energy through a periodically heated homogeneous surface. Our results suggest that higher thermal inertia forces more H₂O into the atmosphere because the regolith is warmer at depth. Surface stresses are higher above a low I surface, but there is less diurnal exchange because the atmosphere is dry. The latitude experiment predicts that the total diurnal insolation is more important to the adsorptively controlled H₂O column abundance than the peak daytime surface temperature. Fogs and high relative humidity will be far more prevalent in the winter hemisphere. The dust opacity of the atmosphere plays a very significant role; the PBL height, column abundances, relative humidity, and surface stresses all increase very strongly as the optical depth approaches zero. The dust opacity of the atmosphere must be considered in subsequent PBL models.

Current plans for upgrades include making the thermal properties of the regolith temperature dependent, and including the latent heat of phase change for atmospheric and subsurface H_2O . While all previous simulations terminated after equilibration between the atmosphere and subsurface, we are currently allowing the model to time-march through several degrees of L_s in order to track seasonal changes in the vertical distribution of atmospheric and subsurface H_2O . We are also exploring the effects of changes in atmospheric opacity. The equilibrium column abundance of H_2O in a clear atmosphere is much higher than in a dusty atmosphere. However, it is not clear that an increase in optical depth, such as due to the arrival of a dust storm, could remove water from the atmosphere, since the diurnal boundary layer collapses as the optical depth increases. This may be analogous to the late afternoon collapse of the boundary layer due to increased static stability, which effectively strands a considerable amount of water at altitude, even though it is out of adsorptive equilibrium with the cold surface.

References: [1] Zent A. P. et al. (1993) *JGR*, 98, 3319–3338.

THE MARS AERIAL PLATFORM (MAP) MISSION. R. Zubrin¹, S. Price¹, T. Gamber¹, B. Clark¹, R. Haberle², and J. Cantrell³, ¹Martin Marietta Astronautics, P.O. Box 179, Denver CO, 80201, USA, ²NASA Ames Research Center, Moffett Field CA, 94035, USA, ³Space Dynamics Lab, Utah State University, Logan UT 84322, USA.

The Mars Aerial Platform (MAP) mission is a conceptual design for a low-cost, Discovery-class mission whose purpose would be to generate tens of thousands of very-high-resolution (20 cm/pixel) pictures of the martian surface, map the global circulation of the martian atmosphere, and examine the surface and subsurface with ground-penetrating radar, infrared spectroscopy, neutron spectroscopy, and other remote sensing techniques. The data would be acquired by instruments that are carried by balloons flying at a nominal altitude of about 7 km over the martian surface. Because new balloon and microspacecraft technology is now available, the balloon probes could be quite long-lived, lasting hundreds or even thousands of days, producing an immense science harvest in the process. Together with the Mars Environmental Survey (MESUR) surface network science mission, MAP would revolutionize our knowledge of the Red Planet.

Mission Description: The MAP mission will be carried out as follows: A low-cost launch vehicle such as a Delta 7925 (1000 kg TMI) is used to propel a small spacecraft carrying eight entry capsules onto trans-Mars injection. Approaching Mars, a spinner is used 10 days prior to arrival to release the capsules outward so that they enter Mars' atmosphere at widely dispersed locations. Each capsule then enters the atmosphere, and deploys a parachute that slows it down to the point where a balloon can be inflated. The inflation is accomplished during descent, so that no landing system is required (the practicality of accomplishing this has been demonstrated on Earth at altitudes of up to 150,000 ft, where atmospheric density is similar to Mars). After the balloon is inflated, the parachute, capsule, and inflation equipment is jettisoned, and used to land a meteorology package consisting of pressure and temperature sensors, battery, and transmitter on the surface. Each of the balloon probes will then commence their float around Mars at an altitude of about 7 km (23,000 ft) above the mean surface level. The probes,

which will never land in the course of their long-duration aerial cruise, will carry a gondola payload of 8 kg, which includes 2 cameras, 1 kg of atmospheric science and additional instruments, data recording and transmitting equipment, a rechargeable battery, and solar array.

When it is daylight two pictures are taken simultaneously every 15 minutes. One is taken with a high-resolution CCD black and white camera with a nominal resolution of 20 cm per pixel; with a 1024 × 1024 pixel field, this gives a field of view 204 m on a side. The other is taken with a color camera at a moderate resolution of 10 m per pixel; this gives a field of view 10.2 km on a side. The two cameras are aligned so that the high-resolution image is located at the center of the medium-resolution picture, whose features in turn can be used to locate the region studied on a map of the planet. The cameras are mounted on a vertical pan, so that either vertical, horizontal, or oblique pictures can be taken. The data is compressed and stored and then is periodically uplinked to an orbiting satellite, which could either be Mars Observer or the MESUR comsat, and is then transmitted back to Earth. Under typical conditions, each aerostat will be able to transmit 40 picture pairs per day. It is anticipated that the science return of this mission will be large, with 32,000 high-resolution pictures returned to Earth for each 100 days of operation of an eight balloon fleet, plus an equal number of pictures at resolutions superior to the best Viking images. The high-resolution pictures will have a factor of 7 greater resolution than the best pictures returned from Mars Observer. Additional science return will result from use of other instruments, such as a ground-penetrating electromagnetic sounder. Tracking the balloons will yield knowledge of Mars' global atmospheric circulation. The cost of the mission is anticipated to be low, falling below the \$150 million (without launch) ceiling of the Discovery-class guidelines.

Science Return: Some of the science areas that will be benefited by the MAP mission will include the following:

1. *Geologic science.* The greatest benefit from high-resolution images is the information that could be gained on surface processes. In contrast to Mars Observer, whose highest-resolution images will show objects as small as a mid-sized car, the cameras on the MAP gondola will be able to reveal surface features the size of a cat. Such images will give us submeter surface morphology, block size distributions, and surface textures, all of which provide insight into volcanic processes, sedimentary deposits, fluvial history, and aspects of impact cratering. In addition, eolian features such as ripple fields, individual dunes, small channels, etc., will be visible, providing direct evidence for the link between the atmosphere and the surface. The scale of some of these is below Mars Observer resolution. Assessment of these and other features that are submeter in size will provide a whole new suite of information on surface/atmosphere interactions.

2. *Atmospheric science.* The MAP mission provides a unique *in situ* platform for atmospheric science. Each balloon will float at a fixed density level (0.008 kg m⁻³, or about 7 km above the mean surface) for at least 100 days. If the balloons were to average 10 m s⁻¹, a conservative value, then thousands of kilometers will be traversed. Depending on the circulation, it is possible that some of the balloons will circumnavigate the planet several times. Thus global sampling of the atmosphere is possible.

Measurements that can be taken aboard the MAP balloons include temperature, pressure, horizontal wind speed and direction (via tracking), dust size and composition, and water vapor concen-

tration. Atmospheric science goals that could then be addressed include the critically important surface boundary layer and its diurnal variability, atmospheric dynamics, circulation systematics, aerosol composition and properties, and the seasonal cycles of dust and water. Tracking of the balloons would give information on winds and circulation systems that could be used to test the computational global circulation models currently being developed by NASA. Slope wind systems may be particularly important on Mars and the MAP balloons should be able to help characterize their structure and dynamics. Aerosols, dust in particular, are known to be ubiquitous in the martian atmosphere, yet their composition, size, and shape are uncertain. MAP balloons could measure these properties directly and thereby greatly increase our understanding of these climatically significant particles. Water vapor concentrations could be measured, furthering our understanding of the nature and distribution of near surface water reservoirs.

3. *Exploratory science.* Infrared detectors on the balloons would be able to detect local geothermally heated hot-spots on the martian surface, should any exist and fall within several kilometers of the probe's ground track. Neutronic devices would be able to detect local concentrations of ice, hydrated minerals, or deposits of carbonates. Ice layers 10 m or more below the surface may also be revealed by electromagnetic sounding using the radar altimeter, which can function as a simple ground-penetrating radar.

The discovery of such features would be of very high value for exobiological investigations.

4. *Development of Mars engineering models.* Numerous U.S. and international groups have a high interest in developing engineering models of the martian surface. A recurring theme is the need for imaging of the surface at the scale that could be provided by MAP. In particular, knowledge of size-block distributions, slopes, surface discontinuities, etc., at a scale important to landers, roving vehicles, and other landed mission operations is of high interest. The advantage of MAP is that a wide variety of terrains could be sampled to provide input to engineering models. The Mars Observer camera has a resolution of about 1.5 m/pixel, allowing it to resolve features about 4 m across. Such resolution is too gross for use in assessment or avoidance of landing hazards facing Mars surface science missions. Submeter scale imaging is also needed to provide context for the activities of a landed rover mission. This context would permit significantly richer surface operations activities, and a concurrent improvement in the caliber of science conducted. The results from the MAP aerostats will be obtained concurrently with data returned by the meteorology packages delivered to the surface by the entry probe parachutes. This will enhance the potential science return by the synergy that will result from concurrent measurements from the surface network with the balloon drift measurements. This will provide more information on the atmospheric structure than could be obtained by either a balloon or surface network acting alone. The large array of potential science instruments that could be carried by MAP are summarized in Table 1. There are far too many to be all carried in the same gondola; however, if the probes sent to Mars are divided into four "science sets" (which we label "A,B,C, D") with two probes per set for a Delta launch, then the full range of potential investigations could be carried out. To minimize power consumption, all instruments would be cycled on and off in coordination with the camera.

Balloon Flight Profile: At the time of entry, the balloons may be targeted to widely dispersed locations, typically spread over 130°

of latitude. The balloons will then commence to float at the velocity of the martian winds at their altitude. Current models suggest that the wind will carry the balloons primarily in the west-east direction with typical velocities on the order of 30–60 km hr⁻¹. At such speeds each aerostat could be expected to circumnavigate the planet every 10–30 days. There will also be some north-south migration, which will probably cause some balloons to wander into and out of Mars' polar regions during portions of the mission. This may afford an opportunity to examine regions of the planet that cannot be targeted for direct probe entry during a given launch opportunity. If an aerostat should wander into a polar region during the Arctic night, gondola operations will be curtailed until it leaves. Characteristic aerial velocities of the balloons suggest that such a shutdown should last no more than a few days at most. Since the thermal protection power needed by the MAP gondola is provided by three Radioisotope Heating Units (RHUs), which require no electric power, the gondola is survivable even if solar incidence should drop far below anticipated levels for an extended period.

The balloons have a nominal float altitude during the northern summer of 7 km, with a diurnal altitude variation of a few hundred meters. However, because of the evaporation of CO₂ from Mars' south polar cap, the average atmosphere during the course of the year is thicker than that of the northern summer, and so the balloons on the average will actually float at a typical altitude of about 8.5 km, clearing over 97% of all martian terrain. Having such a large fraction of the planet safe for travel gives each balloon fair odds for a long-duration flight. Although an eventual crash is certainly possible, chances for balloon loss through collision with obstacles is diminished by the tendency of balloons to follow the streamlines of air which must, of necessity, go around all obstacles the airflow encounters.

Probe Navigation: Latitude of the MAP aerostats can be determined by the time of comsat overpass, which will occur 2–5 times each sol. In addition, the perpendicular distance of the probe from the comsat groundtrack can be determined by the Doppler

TABLE 1. Candidate MAP instruments.

Instrument	Mass (kg)	Power (W-h/sol)	Data (Mbar/sol)	Science Set (example)
Camera (BW or 3-color)	0.6	10	26.0	A, B, C, D
Temperature and pressure	0.1	0.01	0.02	A, B, C, D
Sun sensor	0.1	0.01	0.02	A, B, C, D
Accelerometer	0.1	0.1	0.2	A, C
Neutron spectrometer	0.2	0.03	0.06	A, B, C
Gamma ray spectrometer	1.0	2.0	5.0	B
Electromagnetic sounder	0.4	8.0	1.0	A, C
Microwave radiometer	0.3	0.1	0.02	A
Magnetometer	0.2	2.0	0.02	A, D
Infrared radiometer	0.1	0.01	0.02	A, C, D
Infrared spectrometer	0.5	2.0	5.0	C
Nephelometer	0.2	0.5	1.0	D
Hygrometer	0.2	0.02	0.02	D
Dust composition analyzer	0.4	0.1	0.02	D

shifting of the signal the comsat receives from the Probe. In addition, longitude can be determined twice a day by noting the time of sunrise and sunset. If longitude is known, then a Sun sensor can be used to determine latitude and gondola orientation. The aerostat location can also be determined by comparing its 10×10 -km medium-resolution images with Mars Observer and Viking surface imagery. Since the position of the probe is periodically known precisely, the position of the probe at all times can be known if overlap can be maintained between the areas captured by the medium-resolution images. Since the probe can know its own location using such techniques, probes can be preprogrammed to take horizontal photographs when they find themselves in a certain region and pointing (the balloons are expected to slowly rotate) in a given direction. Thus it will be possible to obtain horizontal or oblique panoramic images of many of the major sights on Mars, such as Olympus Mons or the Valles Marineris.

Conclusion: We conclude that the MAP mission offers the potential for a very high science return mission at modest cost, and recommend that appropriate steps be taken to implement it at an early date.

MARS OBSERVER: APPLICATIONS TO ATMOSPHERIC TRANSPORT. R. W. Zurek and D. J. McCleese, Jet Propulsion Laboratory, California Institute of Technology, Pasadena CA 91109, USA.

The Pressure Modulator Infrared Radiometer (PMIRR) is an atmospheric sounder designed to observe temporal and spatial variations of water vapor and of dust suspended in the Mars atmosphere, to characterize the planetary-scale thermal structure and circulation of the atmosphere, and to quantify the polar radiative balance [1]. These measurements are fundamental to understanding the seasonal cycles of dust, of water, and of CO_2 on Mars and, in particular, to determining the role of atmospheric transport. Using

measurements in eight narrow-band infrared spectral regions and one broadband visible channel, the PMIRR investigation teams at JPL and Oxford University will derive vertical profiles of atmospheric temperature, extinction due to suspended dust, and water vapor concentration, as well as locations of CO_2 and H_2O ice clouds. These data will be used in a variety of ways to address issues of atmospheric dynamics and transport.

Three topics will be emphasized here: (1) the expected precision of the retrieved profiles of temperature, dust extinction, and water vapor, including plans for validating the profiles; (2) the observational strategy, designed to best use PMIRR's two-axis scan mirror, as deployed in the Mars Observer mapping orbit; and (3) approaches to mapping the atmospheric fields globally and the derivation of key meteorological fields related to estimating atmospheric transport.

The underlying philosophy of the observing strategy is to map the atmospheric fields as continuously and as systematically as possible, since much of what we want to learn comes from observing variations with both space and time. Changes in the mapping strategy as a function of season (with a planet-encircling dust storm counted as a "seasonal" event) will be discussed. The individual vertical profiles will be mapped using different algorithms to provide synoptic global fields of temperature, of dust, and, where possible, of water vapor. These mapped fields can be used to directly derive estimates of wind shear and of radiative forcing; they and/or the retrieved vertical profiles will also be provided to several groups for assimilation of the retrieved fields into data-model blends that will provide estimates of the meteorological fields, including fields that cannot be derived directly (e.g., reference-level winds and vertical velocities). While such data assimilation techniques can, in principle, provide "optimal" estimates of the fields, there are many issues yet to be resolved, including proper characterization of observational errors and of deficiencies in the dynamical models.

References: [1] McCleese D. J. et al. (1992) *JGR*, 97, 7735-7757.

List of Workshop Participants

Michael Allison

NASA Goddard Institute of Space Studies
2880 Broadway
New York NY 10025
Phone: 212-678-5554
E-mail: bitnet.pcmda@nasagiss

F. Scott Anderson

Department of Geology
Arizona State University
Tempe AZ 85287-1404
Phone: 602-965-7129
E-mail: anderson@asuacad

Don Banfield

Mail Stop 170-25
California Institute of Technology
Pasadena CA 91125
Phone: 818-356-6448

J. Barnes

Department of Atmospheric Science
Oregon State University
Corvallis OR 97331
Phone: 503-737-5685
Fax: 503-737-2540
E-mail: barnes@eddy.ats.orst.edu

Stephen Bougher

Lunar and Planetary Laboratory
Space Science Building
University of Arizona
Tucson AZ 85721
Phone: 602-621-4900
Fax: 602-621-4933
E-mail: sbougher@hindmost.lpl.arizona.edu

E. Chassefière

CNRS Astronomy and Astrophysics
Observatoire de Meudon
F-92195
Meudon Cedex
FRANCE

R. T. Clancy

Laboratory for Atmospheric and Space Physics
Box 10
University of Colorado
Boulder CO 80309
Phone: 303-492-6998
Fax: 303-492-6946
E-mail: clancy@isidis.colorado.edu

Benton Clark

Martin Marietta
Mail Stop B0560
P.O. Box 179
Denver CO 80201
Phone: 303-971-9007
Fax: 303-971-9141

Matthew Collins

Department of Meteorology
University of Reading
Reading RG1 3PW
UNITED KINGDOM
Phone: 0734-875123, ext. 7618
Fax: 0734-352604
E-mail: swrcolin@uk.ac.rdg

Barney J. Conrath

Mail Code 693.2
NASA Goddard Space Flight Center
Greenbelt MD 20771
Phone: 301-286-9529
E-mail: LEPVAX::U3BJC

Armin Drescher

DLR Institut für Planetary Research
D-8031 Oberpfaffenhofen
GERMANY
Phone: 49-8153-28793
Fax: 49-8153-2476

Eric Fetzer

Jet Propulsion Laboratory
4800 Oak Grove Drive
Pasadena CA 91109
Phone: 818-354-0649

Francois Forget

Mail Stop 245-3
NASA Ames Research Center
Moffett Field CA 94035-1000
Phone: 415-604-3784
Fax: 415-604-6779
E-mail: forget@pan.arc.nasa.gov

R. M. Haberle

Space Science Division
Mail Stop 245-3
NASA Ames Research Center
Moffett Field CA 94035
Phone: 415-604-5491
Fax: 415-604-6779
E-mail: haberle@humbabe.arc.nasa.gov

Robert Haskins

*Jet Propulsion Laboratory
4800 Oak Grove Drive
Pasadena CA 91109
Phone: 818-354-6893
E-mail: rdh@airs.ljpl.nasa.gov*

David Hinson

*Center for Radar Astronomy
219 Durand Building
Stanford University
Stanford CA 94305-4055
Phone: 415-723-3534
Fax: 415-723-9251
E-mail: hinson@nova.standard.edu*

Jeffrey L. Hollingsworth

*NRC Research Associate
Mail Stop 245-3
NASA Ames Research Center
Moffett Field CA 94035
Fax: 415-604-6779
E-mail: jeffh@humbabe.arc.nasa.gov*

Howard Houben

*Space Physics Research Institute
Mail Stop 245-3
NASA Ames Research Center
Moffett Field CA 94035
Phone: 415-604-3381*

Frederic Hourdin

*Laboratory de Meteoritics Dynamique
Ecole Normale Supérieure
24 rue Lhomond
75231 Paris Cedex 05
FRANCE
Phone: 43291225, ext. 3479
Fax: 33-143-36-8392*

Bruce Jakosky

*Laboratory for Atmospheric and Space Physics
Campus Box 392
University of Colorado
Boulder CO 80309-0392
Phone: 303-492-8004
Fax: 303-492-6946
E-mail: ZODIAC::JAKOSKY*

P. B. James

*Physics and Astronomy Department
University of Toledo
Toledo OH 43606
Phone: 419-537-4906
Fax: 419-537-2723
E-mail: pbj@utphysa.phya.utoledo.edu*

Manoj Joshi

*Department of Physics
Atmospheric Physics
Clarendon Laboratory
Oxford University
Parks Road
Oxford OX1 3PU
UNITED KINGDOM
Phone: 44-865-272258
Fax: 44-865-272923
E-mail: atmnmj@vax.ox.ac.uk*

Kyle Kotwica

*Department of Atmospheric Science
Oregon State University
Corvallis OR 97331*

S. W. Lee

*Laboratory for Atmospheric and Space Physics
Campus Box 392
University of Colorado
Boulder CO 80309
Phone: 303-492-5348
Fax: 303-492-6949
E-mail: lee@syrtis.colorado.edu*

Conway Leovy

*Department of Atmospheric Sciences
Mail Code AK-40
University of Washington
Seattle WA 98195
Phone: 206-543-4952
Fax: 206-543-0308
E-mail: conway@atmos.washington.edu*

Stephen Lewis

*Department of Physics
Atmospheric Physics
Clarendon Laboratory
Oxford University
Parks Road
Oxford OX1 3PU
UNITED KINGDOM
Phone: 44-865-272086*

Sanjay S. Limaye

*Space Science and Engineering Center
University of Wisconsin
1225 West Dayton Street
Madison WI 53706
Phone: 608-262-9541
Fax: 608-262-5974
E-mail: limaye@lacc.wisc.edu*

Leonard Martin

*Lowell Observatory
1400 West Mars Hill Road
Flagstaff AZ 86001
Phone: 602-774-3358
Fax: 602-774-6296
E-mail: ljm@lowell.edu*

Terry Z. Martin

*Mail Stop 169-237
Jet Propulsion Laboratory
4800 Oak Grove Drive
Pasadena CA 91109
Phone: 818-354-2178
Fax: 818-393-4619
E-mail: tzmartin@jpl-pds.jpl.nasa.gov*

Cole McCandlish

*Department of Atmospheric Sciences
Oregon State University
Corvallis OR 97331*

Daniel J. McCleese

*Mail Stop 183-335
Jet Propulsion Laboratory
4800 Oak Grove Drive
Pasadena CA 91109
Phone: 818-354-2317
Fax: 818-393-6546
E-mail: djmcc@scn1.jpl.nasa.gov*

W. Wallace McMillan

*Mail Code 693.2
NASA Goddard Space Flight Center
Greenbelt MD 20771
Phone: 301-286-1388
E-mail: yswwm@lepva.gsfc.nasa.gov*

A. E. Metzger

*Mail Stop 183-501
Jet Propulsion Laboratory
4800 Oak Grove Drive
Pasadena CA 91109
Phone: 818-354-4017
Fax: 818-354-0966*

Jim Murphy

*Mail Stop 245-3
NASA Ames Research Center
Moffett Field CA 94035
Phone: 415-604-3119
Fax: 415-604-6779
E-mail: murphy@anarchy.arc.nasa.gov*

Thomas R. Parish

*Department of Atmospheric Science
University of Wyoming
P.O. Box 3038
Laramie WY 82071-3038
Phone: 307-766-5153
Fax: 307-766-2635
E-mail: parish@lynx.uwyo.edu*

John Pearl

*Mail Code 693.2
NASA Goddard Space Flight Center
Greenbelt MD 20771
Phone: 301-286-8487
Fax: 301-286-3271
E-mail: john@chryse.gsfc.nasa.gov*

John Pinder

*3414 Jasmine
Apartment #3
Los Angeles CA 90034*

James B. Pollack

*Space Science Division
Mail Stop 245-3
NASA Ames Research Center
Moffett Field CA 94035
Phone: 415-694-5530
Fax: 415-604-6779
E-mail: GAL::POLLACK*

Peter L. Read

*Department of Physics
Clarendon Laboratory
University of Oxford
Parks Road
Oxford OX1 3PU
UNITED KINGDOM
Phone: 44-865-272082*

Mark Richardson

*3414 Jasmine
Apartment # 3
Los Angeles CA 90034
Phone: 310-838-2471
E-mail: mark@thesun.ess.ucla.edu*

Don Sandstrom

*Mail Stop 87-08
Boeing Company
P.O. Box 3999
Seattle WA 98124
Phone: 206-773-9098
Fax: 206-773-4946
E-mail: sandstrd@atc.boeing.com*

Michelle Santee

*Mail Stop 183-701
Jet Propulsion Laboratory
Pasadena CA 91109
Phone: 818-354-9424
Fax: 818-393-5065
E-mail: mls@jplrac.jpl.nasa.gov*

John Schofield

*1225 Hastings Ranch Drive
Pasadena CA 91107
Phone: 818-354-2517*

Adam Showman

*Geological and Planetary Sciences Division
Mail Code 170-25
California Institute of Technology
Pasadena CA 91125
Phone: 818-356-6448*

Tero Siili

*Department of Geophysics
Finnish Meteorological Institute
P.O. Box 503
SF-00101 Helsinki
FINLAND
Phone: 358-0-192-0676
Fax: 358-0-192-9533
E-mail: tero.siili@fmi.fi*

Peter Smith

*Lunar and Planetary Laboratory
University of Arizona
Tucson AZ 85721
Phone: 602-621-2725
Fax: 602-621-9876
E-mail: psmith@lpl.arizona.edu*

Jim Tillman

*Department of Atmospheric Sciences
Mail Stop AK-40
University of Washington
Seattle WA 98195
Phone: 206-543-4586
Fax: 206-543-0308*

Dean Vickers

*Department of Atmospheric Sciences
Oregon State University
Corvallis OR 97331
E-mail: vickers@ats.orst.edu*

Thomas D. Walsh

*College of Oceanic and Atmospheric Sciences
Oregon State University
Strand Ag Hall, Room 326
Corvallis OR 97331
Phone: 503-737-2531
Fax: 503-737-2540
E-mail: walsh@ats.orst.edu*

R. John Wilson

*Geophysical Fluid Dynamics Laboratory
P.O. Box 308
Princeton NJ 08542
Phone: 609-452-6592
E-mail: rjw@gfdl.gov*

Aaron Zent

*Mail Stop 245-3
NASA Ames Research Center
Moffett Field CA 94035
Phone: 415-604-5517
Fax: 415-604-6779
E-mail: zent@pan.arc.nasa.gov*

Richard Zurek

*Mail Stop 169-237
Jet Propulsion Laboratory
4800 Oak Grove Drive
Pasadena CA 91109
Phone: 818-354-3725
Fax: 818-393-4619
E-mail: rwz@rich.jpl.nasa.gov*

2
1
1

1
1
1

NASA Technical Library



3 1176 01403 6777